Technical Report Documentation Page

1. Report No. FHWA/TX-16/0-6719-1	2. Government Accession No.	3. Recipient's Catalog No.
4. Title and Subtitle Strengthening Existing Continuous Non-Composite Steel Girder Bridges Using Post-Installed Shear Connectors		5. Report Date October 2015; Published June 2016 6. Performing Organization Code
7. Author(s) Kerry Kreitman, Amir Reza Ghiami Azad, Hemal Patel, Michael Engelhardt, Todd Helwig, Eric Williamson, Richard Klingner		8. Performing Organization Report No. 0-6719-1
9. Performing Organization Name and Address Center for Transportation Research The University of Texas at Austin 1616 Guadalupe Street, Suite 4.202 Austin, TX 78701		10. Work Unit No. (TRAIS) 11. Contract or Grant No. 0-6719
12. Sponsoring Agency Name and Address Texas Department of Transportation Research and Technology Implementation Office P.O. Box 5080 Austin, TX 78763-5080		13. Type of Report and Period Covered Technical Report (9/11-8/15) 14. Sponsoring Agency Code

15. Supplementary Notes
Project performed in cooperation with the Texas Department of Transportation and the Federal Highway Administration.

16. Abstract

This study investigated the use of post-installed shear connectors for strengthening existing non-composite continuous steel girder bridges. The existing bridges considered in this study have strength deficiencies in both the positive and the negative moment regions. The type of post-installed shear connector investigated in this study was an adhesive anchor, which is installed from underneath the bridge deck. The strengthening approach involves installing adhesive anchors to increase girder flexural capacity in positive moment regions, and allowing inelastic moment redistribution in negative moment regions. A variety of theoretical, computational, and experimental studies were completed as part of this investigation.

The findings of this research indicate that strengthening non-composite continuous steel girder bridges with post-installed shear connectors and moment redistribution is a feasible and efficient method of extending the useful service life of a bridge. Increases of more than 60% in the load rating of bridges considered in this study were attained by strengthening to a composite ratio of only 30%. Design recommendations are provided in this report.

17. Key Words Continuous steel bridges, composite action, shear connectors, strengthening, shakedown, moment redistribution, fatigue		18. Distribution Statement No restrictions. This document is available to the public through the National Technical Information Service, Springfield, Virginia 22161; www.ntis.gov.	
19. Security Classif. (of report) Unclassified	20. Security Classif. (of this page) Unclassified	21. No. of pages 158	22. Price

Form DOT F 1700.7 (8-72) Reproduction of completed page authorized

THE UNIVERSITY OF TEXAS AT AUSTIN
CENTER FOR TRANSPORTATION RESEARCH

Strengthening Existing Continuous Non-Composite Steel Girder Bridges Using Post-Installed Shear Connectors

Kerry Kreitman
Amir Reza Ghiami Azad
Hemal Patel
Michael Engelhardt
Todd Helwig
Eric Williamson
Richard Klingner

CTR Technical Report:	0-6719-1
Report Date:	October 2015
Project:	0-6719
Project Title:	Strengthening Continuous Steel Girders with Post-Installed Shear Connectors
Sponsoring Agency:	Texas Department of Transportation
Performing Agency:	Center for Transportation Research at The University of Texas at Austin

Project performed in cooperation with the Texas Department of Transportation and the Federal Highway Administration.

Center for Transportation Research
The University of Texas at Austin
1616 Guadalupe, Suite 4.202
Austin, TX 78701

http://ctr.utexas.edu/

Disclaimers

Author's Disclaimer: The contents of this report reflect the views of the authors, who are responsible for the facts and the accuracy of the data presented herein. The contents do not necessarily reflect the official view or policies of the Federal Highway Administration or the Texas Department of Transportation (TxDOT). This report does not constitute a standard, specification, or regulation.

Patent Disclaimer: There was no invention or discovery conceived or first actually reduced to practice in the course of or under this contract, including any art, method, process, machine manufacture, design or composition of matter, or any new useful improvement thereof, or any variety of plant, which is or may be patentable under the patent laws of the United States of America or any foreign country.

Notice: The United States Government and the State of Texas do not endorse products or manufacturers. If trade or manufacturers' names appear herein, it is solely because they are considered essential to the object of this report.

Engineering Disclaimer

NOT INTENDED FOR CONSTRUCTION, BIDDING, OR PERMIT PURPOSES.

Project Engineer: Michael D. Engelhardt
Professional Engineer License State and Number: Texas No. 88934
P. E. Designation: Research Supervisor

Acknowledgments

The authors extend their appreciation to the Texas Department of Transportation for providing the funding for this research. The authors thank Yuan Zhao, the initial project director, and the entire project monitoring committee for their assistance and guidance. The authors also thank the Project Manager, Darrin Jensen, for oversight and coordination of this project.

Table of Contents

List of Figures

List of Tables

Chapter 1. Introduction

1.1 Overview

Many older bridges in the state of Texas were constructed with floor systems consisting of a non-composite concrete deck over steel girders. While the individual elements in these bridges tend to still be in good condition, the structures often do not satisfy current load requirements and thus may need to be strengthened or replaced. A potentially economical method for strengthening is to develop composite action by attaching the existing concrete deck to the steel beams using post-installed shear connectors.

Composite action allows for the transfer of shear forces between the concrete deck and the steel beam, causing the deck and the steel beam to bend together as one element. This can significantly increase the strength and stiffness of the section as compared to a non-composite beam in which the two elements bend separately because there is no shear transfer at the interface. Figure 1.1 illustrates the difference between composite and non-composite behavior.

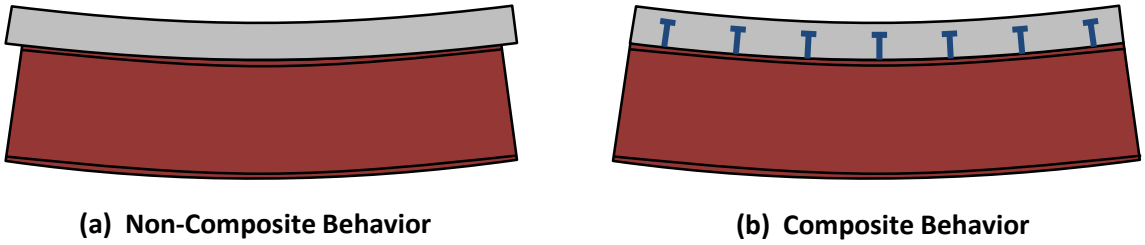

Figure 1.1 Behavior of (a) Non-composite beams and (b) Composite beams

A previous TxDOT project (0-4124), completed in 2007 by researchers at The University of Texas at Austin, developed and tested several different types of post-installed shear connectors under static and fatigue loading conditions. They recommended three connectors, illustrated in Figure 1.2, for potential use in the strengthening of positive moment regions of bridges (Kwon et al. 2007). Additionally, large-scale testing was carried out on simple-span, partially composite girders with post-installed shear connectors. Partial-composite design was recommended as an economical strengthening technique because the post-installed shear connectors have very good fatigue behavior, so fatigue strength will likely not control the design. Finally, a TxDOT implementation project (5-4124) was conducted to strengthen an existing non-composite simple-span bridge with post-installed shear connectors (Kwon et al. 2009).

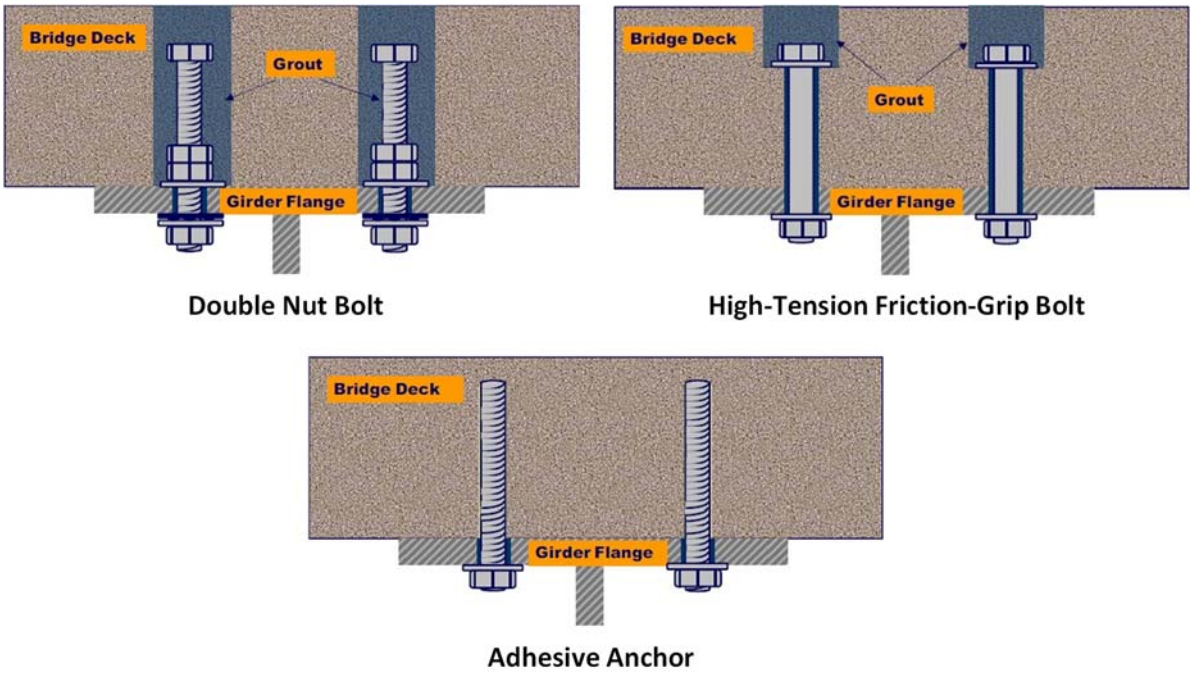

Figure 1.2 Post-Installed Shear Connectors Recommended by Kwon et al. (2009)

The goal of TxDOT project 0-6719 was to expand these strengthening concepts involving post-installed shear connectors for use in continuous bridges, where the strength of the negative moment regions over the piers is also deficient. Composite action is less effective under negative bending when the concrete in the deck is cracked in tension. The following two methods for strengthening continuous bridge girders were considered:

1. Strengthen all regions of the bridge by post-installing shear connectors. In the negative moment regions, engage the deck reinforcement in composite action with the steel beams.
2. Strengthen only the positive moment regions using post-installed shear connectors. Allow yielding to occur in the steel beams in the negative moment regions over the interior piers, and let excess moments redistribute to the surrounding strengthened positive moment regions as necessary.

While the first strengthening method attempts to directly increase the capacity of the negative moment regions, the second method utilizes the ductility of steel and the redundancy of continuous girder systems to redistribute the internal forces along the bridge in a more efficient manner. Because the second method allows for yielding of the steel beams over the interior supports, the shakedown behavior of strengthened bridges is of particular interest. Shakedown refers to a limit state of accumulating inelastic deformations under repeated yielding in statically indeterminate systems.

1.2 Project Objectives and Report Outline

The main goal of this research project was to develop procedures to strengthen continuous non-composite steel girder bridges using post-installed shear connectors and inelastic moment redistribution. To accomplish this objective, both experimental and analytic work were

conducted at the Ferguson Structural Engineering Laboratory at The University of Texas at Austin. The following major tasks, each of which are discussed in separate chapters in this report, were included in Project 0-6719:

- Perform a comprehensive literature review that includes the topics of composite and partial-composite design and behavior, fatigue testing and fatigue behavior of shear connectors, inelastic moment redistribution, and shakedown behavior (Chapter 2).
- Complete a survey of continuous non-composite steel girder bridges in the state of Texas to determine typical characteristics of bridges that may be candidates for strengthening in the proposed manner (Chapter 3).
- Perform preliminary concept studies for strengthening typical bridges from the survey using the proposed strengthening methods to determine which is more feasible for use in strengthening a typical non-composite bridge (Chapter 4).
- Conduct additional fatigue testing on adhesive anchor post-installed shear connectors as recommended by Project 0-4124 to propose improved recommendations for the strengthening design (Chapter 5).
- Perform large-scale laboratory testing of two-span continuous girders strengthened with post-installed shear connectors to study the structural performance of the system (Chapter 6).
- Conduct parametric studies to evaluate various post-installed shear connector configurations (Chapter 7).
- Develop design recommendations for strengthening continuous non-composite bridges with post-installed shear connectors (Chapter 8).

More details on these topics can be found in the theses and dissertations written by the researchers. For information about the bridge survey in Chapter 3 and the fatigue testing in Chapter 5, refer to Patel (2013). The remaining information will be covered in more detail in future publications (Ghiami Azad 2016, Kreitman 2016).

Chapter 2. Background

2.1 Overview

The proposed strengthening methods combine several aspects of bridge design and structural behavior to create an efficient strengthening solution. This chapter presents the relevant background information pertaining to the general behavior of composite girders under static and fatigue loading, previous research on post-installed shear connectors, principles of inelastic moment redistribution for bridges, and a summary of applicable AASHTO bridge design provisions.

2.2 Composite Behavior under Static Loading

A composite steel bridge has a floor system in which the concrete deck is mechanically attached to the steel girders so that the two elements bend together (Oehlers and Bradford 1995). This was illustrated in Figure 1.1. The shear connectors that provide the mechanical attachment must transfer the horizontal shear force at the interface between the concrete deck and the steel beam. The connectors are typically headed studs that are welded onto the top flange of the steel section and embedded into the concrete deck during casting. Historically, short channel sections and other shapes welded to the top flange have also been used as shear connectors. Composite girders are significantly stiffer and stronger than non-composite beams because more material is effective in the section. This is especially true for composite girders in positive bending where the concrete deck is in compression and the steel is in tension.

2.2.1 Full- and Partial-Composite Behavior

A fully composite girder has enough shear connectors to transfer the required horizontal interface shear to develop the full plastic moment of the composite cross section. Although a completely rigid connection is impossible to attain, the horizontal slip between the deck and the steel beam in a fully composite girder is negligible. This means that a continuous strain distribution can be assumed throughout the entire composite section, as shown in Figure 2.1(a). On the other hand, a partially composite girder does not have enough shear connectors to transfer the horizontal shear required to develop the full plastic moment of the composite section. Instead, the strength of the section is controlled by the shear connection. A significant amount of slip occurs between the deck and the girder so that the strain distribution is discontinuous at the interface, as depicted in Figure 2.1(b). A typical strain distribution in a non-composite girder is also shown in Figure 2.1(c). Although the slope of the strain profiles, or the curvatures, of the steel and concrete sections are generally assumed to be the same, each element bends separately about its own neutral axis in a non-composite section.

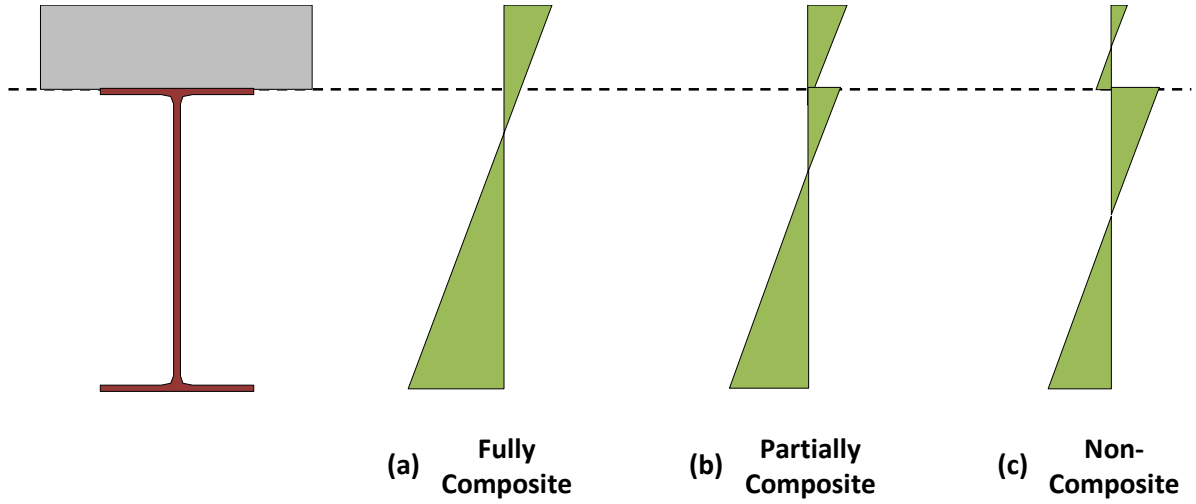

Figure 2.1 Strain Distribution in Fully, Partially, and Non-Composite Girders

At the plastic moment in a fully composite girder, the maximum horizontal interface shear that must be transferred by the shear connection is the smaller of the maximum axial forces that can be developed above and below the interface, or in the deck and in the steel, respectively. The maximum compressive force that can be developed in the deck is usually assumed to take the form of the Whitney stress block, which is composed of a constant stress distribution of 85% of the compressive strength over the entire cross-sectional area of the deck. This conservatively ignores the deck reinforcement in compression. The maximum tensile force in the deck is typically taken as the full yield strength of the longitudinal reinforcement, ignoring the concrete in tension. The maximum compressive or tensile force that can be developed in the steel beam is the maximum plastic force if all fibers are yielded. This assumes that the section is compact and well braced so that no premature local or lateral torsional buckling will occur.

For partially composite girders, the maximum interface shear that can be transferred is controlled by the shear connectors, and is thus lower than both the maximum forces that can be developed in the deck and in the steel. The maximum horizontal interface shear that can be transferred in a partially composite girder is the sum of the ultimate strengths of all shear connectors located between the points of zero and maximum moment. Thus, the horizontal interface shear force (C_f) is:

For positive moment regions:

$$C_f = min\begin{cases} 0.85\, f_c'\, A_c \\ \left(A_s\, F_y\right)_{girder} \\ \Sigma Q_n \end{cases} \qquad \textit{Equation 2.1}$$

For negative moment regions:

$$C_f = min\begin{cases} \left(A_s\, F_y\right)_{rebar} \\ \left(A_s\, F_y\right)_{girder} \\ \Sigma Q_n \end{cases} \qquad \textit{Equation 2.2}$$

where A_s is the area of the steel section or of the longitudinal reinforcement having a yield strength of F_y, A_c is the area of the concrete deck within the effective width having a 28-day

compressive strength of f_c', and ΣQ_n is the sum of the static shear strength of all shear connectors between the points of zero and maximum moment.

If the top expression in Equation 2.1 or Equation 2.2 is the smallest, the plastic neutral axis is located in the steel beam. If the middle expression is the smallest, the plastic neutral axis is in the deck. In both cases, however, the girder is considered to be fully composite. If the bottom expression is the smallest so that the shear connectors control the strength of the section, the neutral axis is in the steel beam, and the section is considered to be partially composite.

The value of the interface shear force is used to determine the required number of shear connectors (N_{full}) to be placed between points of zero and maximum moment for a fully composite girder:

$$N_{full} = \frac{C_f}{Q_n} \qquad \textit{Equation 2.3}$$

where Q_n is the static shear strength of a single connector.

The composite ratio (η) is defined as the ratio between the number of shear connectors provided (N) and the number of connectors required to develop full composite action:

$$\eta = \frac{N}{N_{full}} \qquad \textit{Equation 2.4}$$

The composite ratio is often expressed as a percentage. A girder with a composite ratio less than unity (less than 100%) is partially composite, while a girder with a composite ratio equal to or greater than unity is fully composite.

2.2.2 Strength of Composite Beams

The plastic flexural strength of a compact, well-braced, fully or partially composite girder is calculated using the assumed plastic stress distribution shown in Figure 2.2 (AISC 2010). For fully composite girders, the plastic neutral axis can be located either in the concrete deck (Figure 2.2a) or in the steel beam (b), while the plastic neutral axis in a partially composite girder will always be located in the steel section (c). All portions of the steel beam are assumed to be fully yielded in either compression or tension, depending on the neutral axis location. A compressive stress block with a resultant force equal to the horizontal interface shear force (C_f) extends down from the top of the deck through a depth that satisfies force equilibrium. The deck is assumed to resist no tensile forces. The flexural capacity is determined by the summation of moments in this stress distribution. Several experimental studies have confirmed that this results in a lower-bound estimate of the actual strength of fully and partially composite girders (Culver and Coston 1961, Slutter and Driscoll 1963, Chapman and Balakrishnan 1964).

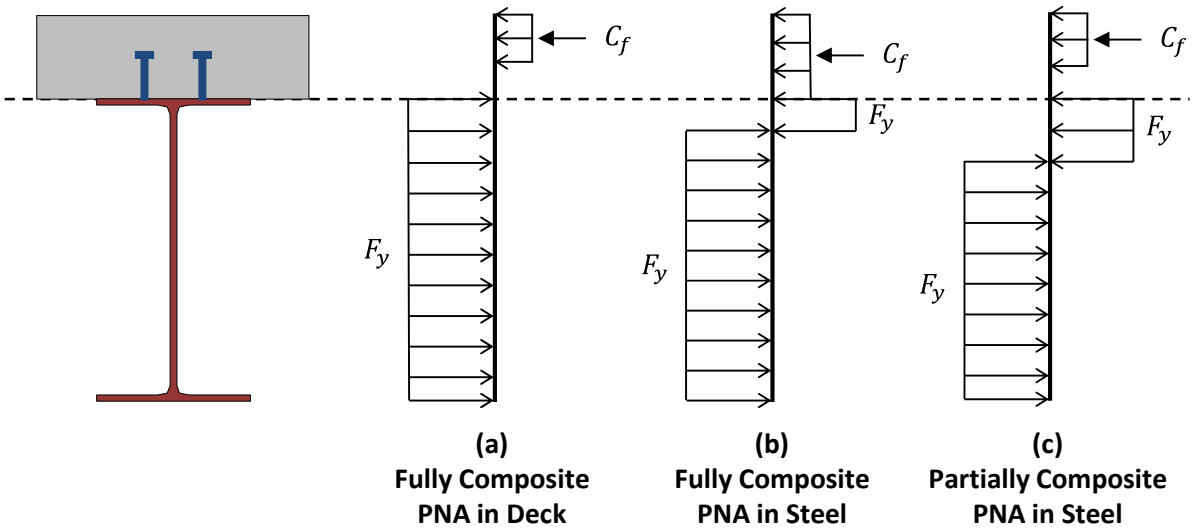

Figure 2.2 Plastic Stress Distributions in Composite Girders

While a partially composite girder has a reduced flexural strength as compared to a fully composite girder, the relationship between strength and the composite ratio is not linear. In fact, partial composite action very efficient, as small composite ratios can provide significant strength increases. This is illustrated in Figure 2.3, which shows the ultimate load-carrying capacity of a 38-foot long simple span girder with a point load at midspan as a function of the composite ratio, which is sometimes referred to as the shear connection ratio. The geometry of this girder is equivalent to the large-scale tests performed in TxDOT project 0-4124, as discussed in Section 2.5.3 (Kwon et al. 2007).

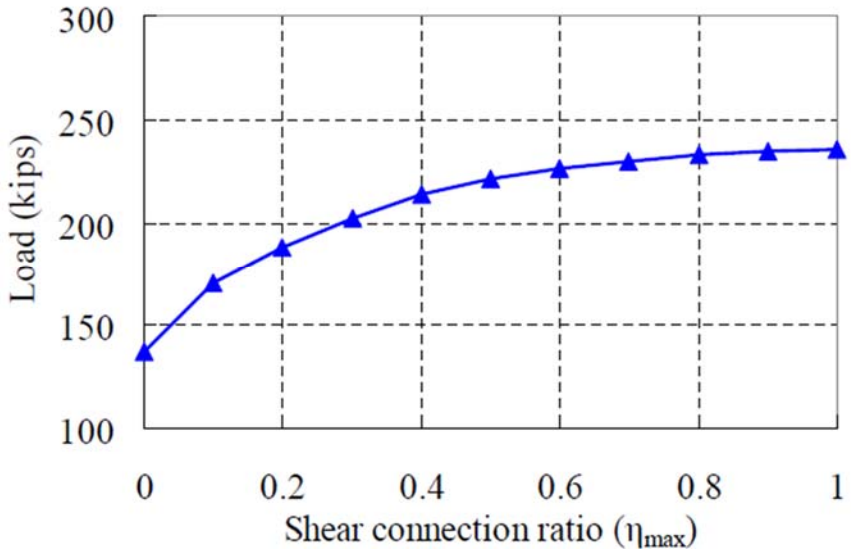

Figure 2.3 Effect of Shear Connection Ratio on Strength (Kwon et al. 2007)

Because of the efficiency of partial composite action, many building structures are designed economically using partially composite girders. However, in bridge design, the fatigue strength of conventional welded shear studs tends to control the design, rather than the static

strength requirements. Fatigue design usually requires enough shear connectors for fully composite action to develop in a bridge. The Association of American State Highway and Transportation Officials (AASHTO) bridge design specifications do not currently allow for partial-composite action (AASHTO 2010).

2.2.3 Stiffness of Composite Beams

The stiffness of fully composite beams with negligible interface slip is computed by statics as the transformed moment of inertia of the composite cross section. However, the interface slip present in partially composite beams reduces the effective stiffness of the section. The American Institute for Steel Construction (AISC) *Commentary to the Specification for Structural Steel Buildings* provides an equation to estimate the effective moment of inertia (I_{eff}) of a partially composite beam (AISC 2010):

$$I_{eff} = I_s + \sqrt{\eta}\,(I_{tr} - I_s) \qquad \textit{Equation 2.5}$$

where I_s and I_{tr} are the moments of inertia of the steel section and of the fully composite uncracked transformed section, respectively. The effective elastic section modulus (S_{eff}) can be estimated in the same manner. These equations are based on empirical testing of partially and fully composite beams in the elastic range (Grant et al. 1977).

2.3 Fatigue Behavior of Shear Connectors

Many researchers have studied the fatigue behavior of shear connectors for bridge applications, particularly in the 1950s and 1960s. The typical fatigue failure mode for conventional welded stud shear connectors is fracture at the base of the weld on top of the steel flange, although concrete crushing and stud pullout have also been observed. For this reason, the direct results of the multitude of previous experimental studies on the fatigue behavior of welded stud connectors are not applicable to the case of the non-welded post-installed connectors considered in this research. Regardless, this section gives a brief summary of the different types of testing methods that have been used, followed by a discussion of the effects of stress reversal on the fatigue performance.

2.3.1 Types of Fatigue Tests

The pushout test, depicted in Figure 2.4, is the most common test method and has been used in many studies (Thurlimann 1959, Slutter and Fisher 1966, Mainstone and Menzies 1967a). In a pushout test, shear connectors attach a concrete slab to each flange of an I-shaped steel section, which is usually loaded in a vertical manner, although many variations of this test have been developed. The majority of the current design codes around the world, including the AASHTO bridge design specifications, are based on results from pushout tests (AASHTO 2010).

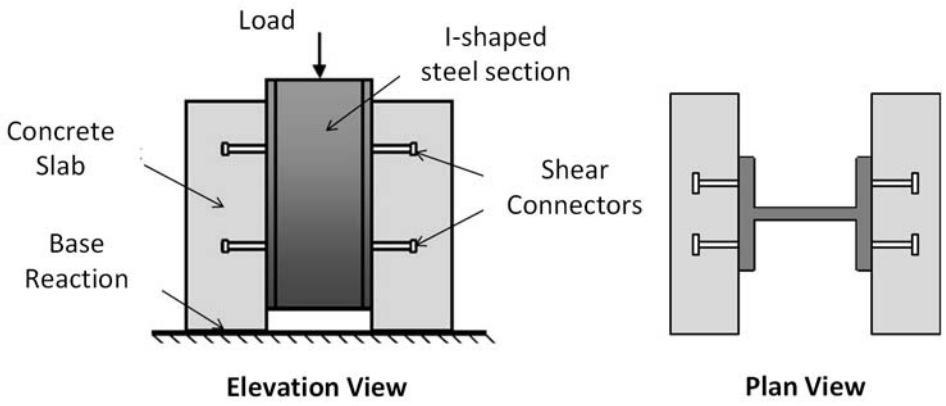

Figure 2.4 Pushout Test Setup for Fatigue Testing of Shear Connectors

The direct-shear test, shown in Figure 2.5, was developed to address some shortcomings of the pushout test, namely the likelihood of unequal loading on the multiple connectors in the two slabs and the eccentricity of the load application on the shear connectors (Gattesco and Giuriani 1996). In a direct-shear test, one or more shear connectors attach the single concrete slab to the steel plate, which is usually loaded in a horizontal manner and delivers primarily a shear force to the connector(s). Variations of the direct-shear test setup have been used by a few researchers in more recent studies (Seracino et al. 1999, Kayir 2006).

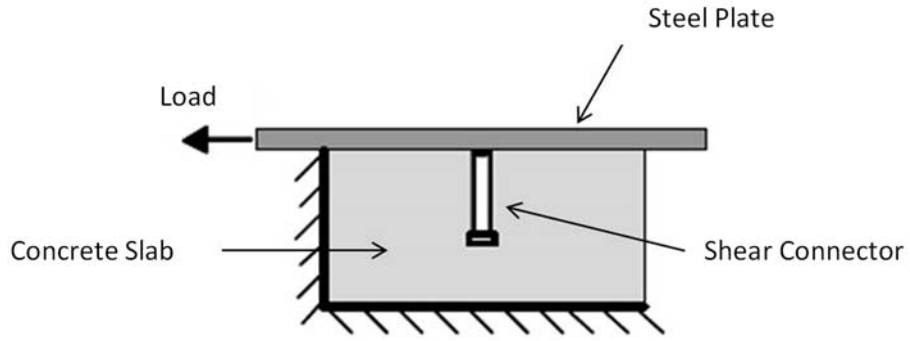

Figure 2.5 Direct-Shear Test Setup for Fatigue Testing of Shear Connectors

Some researchers have investigated the fatigue behavior of shear connectors by testing simply supported and continuous composite girders under a variety of loading conditions, composite ratios, and connector layouts (King et al. 1965, Toprac 1965, Mainstone and Menzies 1967b, Daniels and Fisher 1968). While this type of testing is the least economical and most labor intensive, it is the most realistic representation of the actual load demands that a shear connector would be exposed to in a structure.

2.3.2 Stress Reversal

Many shear connectors in continuous bridges undergo stress reversal, meaning that the connector experiences load cycles in two opposite directions as shown in Figure 2.6. However, this issue has rarely been addressed in the literature due to the difficulty of performing reversed loading tests using the conventional pushout test setup for shear connectors. While a few studies

indicate that stress reversal is not detrimental to the fatigue life, these tests were all performed on conventional welded studs at low stress ranges that would be generated in fully composite beams (Slutter and Fisher 1966, Mainstone and Menzies 1967a, Seracino et al. 1999). A more recent study indicates that consideration of stress reversal may be important at high stress ranges, which could be experienced in partial-composite design (Nakajima et al. 2003). Due to lack of testing, it is unclear how stress reversal could affect the fatigue behavior of post-installed shear connectors.

Figure 2.6 Stress Reversal on a Shear Connector

2.4 AASHTO Shear Connector Design Provisions

The following sections summarize the provisions for shear connector design in composite I-girder bridges in the United States contained in Section 6.10.10 of the AASHTO *LRFD Bridge Design Specifications* (AASHTO 2010). Generally, the design starts with the fatigue provisions, because that limit state usually governs the number of connectors required, and then a strength check is performed. Partially composite design is not allowed in these specifications, primarily because the demands of the fatigue provisions usually result in fully composite girders. A short discussion of the applicability of the current provisions to partially composite design is provided later in this section.

2.4.1 Fatigue Design

The pitch (p), or longitudinal spacing, of the shear connectors is determined using the following equation (AASHTO LRFD Equation 6.10.10.1.2-1):

$$p = \frac{n\,Z_r}{v} \qquad \textit{Equation 2.6}$$

where n is the number of connectors placed transversely in the cross section, Z_r is the fatigue resistance of a single connector, and v is the elastic shear flow at the steel-concrete interface. The fatigue resistance depends on the single-lane average daily truck traffic ($(ADTT)_{SL}$), which also determines which of the two fatigue load combinations is used for design. For $(ADTT)_{SL}$ values greater than or equal to 960 trucks per day, the Fatigue I load combination is used to design for infinite fatigue life. Otherwise, the Fatigue II load combination is used to design for a finite fatigue life for a particular number of truck passages (N) over an assumed 75-year design life. The only difference between the two load combinations is the live load factor, which is 1.50 for infinite life for Fatigue I and 0.75 for finite life for Fatigue II. The fatigue shear resistance (Z_r) for infinite and finite life are:

For infinite life and the Fatigue I load combination (AASHTO LRFD Equation 6.10.10.2-1):

$$Z_r = 5.5d^2 \qquad \textit{Equation 2.7}$$

For finite life and the Fatigue II load combination (combination of AASHTO LRFD Equations 6.10.10.2-2 and 6.10.10.2-3; 6.6.1.2.5-3):

$$Z_r = (34.5 - 4.28\log(N))d^2 \qquad \textit{Equation 2.8}$$

$$N = (365)(75)n(ADTT_{SL}) \qquad \textit{Equation 2.9}$$

where d is the diameter of the shear connector and n is the number of stress cycles on the connector for a single truck passage. For continuous bridges with span lengths greater than 40 feet, n is taken as 1.0 for all connectors located more than one-tenth of the span length away from an interior support. For connectors located within one-tenth of the span length from an interior support, n is taken as 1.5.

The shear flow is calculated as (AASHTO LRFD Equation 6.10.10.1.2-3):

$$v = \frac{V_f\, Q}{I} \qquad \textit{Equation 2.10}$$

where V_f is the range of vertical shear force at a particular section due to fatigue loading, Q is the first moment of the transformed area of the concrete deck, and I is the transformed moment of inertia of the composite cross section. This procedure inherently assumes that any slip at the interface is negligible so that the section is effectively fully composite.

The minimum and maximum longitudinal spacing allowed for shear connectors are 6 and 24 inches, respectively. The connectors are expected to be distributed with equal spacing along the length of the girders. The minimum transverse spacing of connectors is 4 inches, while the minimum clear edge distance is specified as 1 inch. Each connector must penetrate at least 2 inches into the deck and must have a clear top cover of concrete of at least 2 inches.

2.4.2 Strength Design

For strength limit states, the number of connectors required is determined through plastic analysis of the cross-section, as discussed in Section 2.2.2. The minimum number of connectors (N) to be provided between the points of zero and maximum moment is (AASHTO Equation 6.10.10.4.1-2):

$$N = \frac{P_n}{Q_n} \qquad \textit{Equation 2.11}$$

where P_n is the total longitudinal shear force in the deck at the point of maximum moment, and Q_n is the factored ultimate shear strength of a single connector, as defined in the specification. Note that P_n is equivalent to the variable C_f defined in Section 2.2.1. However, since partial-composite design is not currently allowed by the specifications, the third line of Equation 2.1 and Equation 2.2 are not included.

2.4.3 Applicability of the AASHTO Provisions to Partial-Composite Design

The current AASHTO strength design provisions are easily adaptable to incorporating partially composite girders into the specifications. The simple modification of including the third line of Equation 2.1 and Equation 2.2 in the definition of the deck force (P_n) will conservatively estimate the ultimate strength of a partially composite bridge girder.

However, the use of the current fatigue design provisions for partially composite sections will generally lead to very conservative estimates of the shear force demands on the connectors (Seracino 1999). The slip that occurs at the steel-concrete interface of partially composite girders

reduces the overall stiffness of the response, leading to a reduction of the force that the connectors are required to transfer at the interface for a given load.

In terms of structural mechanics, the major limitation in using this approach for partially composite beams is that the section properties Q and I are defined based on the assumption that plane sections remain plane, meaning that the strain profile is continuous through the depth of the composite section, as illustrated in Figure 2.1(a). For the case of partial interaction, plane sections do not remain plane due to the strain discontinuity that exists at the interface. It is impossible to define a unique value of Q and I for a partially composite section because there are an infinite number of strain profiles that can satisfy equilibrium under a given moment and axial force on the section, depending on the magnitude of the strain discontinuity (Seracino et al. 2001). In simple terms, cross-sectional analysis is very difficult for partially composite girders because plane sections do not remain plane.

An analytical procedure that accounts for the slip at the steel-concrete interface was first introduced by Newmark et al. (1951) and further developed by many others, including Proctor (1963). This procedure is based on elastic theory and considers the steel beam and concrete deck as separate entities attached by the shear connectors, leading to a differential equation describing the behavior. Newmark et al. assumed a continuous shear connection with a constant stiffness along the entire length of the girder to achieve closed form solutions for simple cases. Proctor proposed a modification that discretely models the individual connectors and uses an iterative numerical solution process. This process is documented in Appendix A of this report. While these procedures are complex and not suitable for hand calculations, they are well suited for spreadsheet calculations. Additionally, simple 3-D models can be developed to more accurately investigate the behavior of partially composite girders including interface slip.

2.5 Previous Research on Post-Installed Shear Connectors

Creating composite action in existing non-composite bridges has been investigated previously in only a few studies. Klaiber et al. (1983) performed static pushout and girder tests on two types of post-installed connectors, shown in Figure 2.7. Before insertion, the shaft of the epoxied bolt connector (see Figure 2.7(b)) was coated in a concrete-steel epoxy to fill voids and create a solid bond between the connector and the deck. Both post-installed connectors exhibited higher ultimate strengths than conventional welded studs of the same diameter, and the double-nutted connector, which was simpler to install, was successfully used in the field.

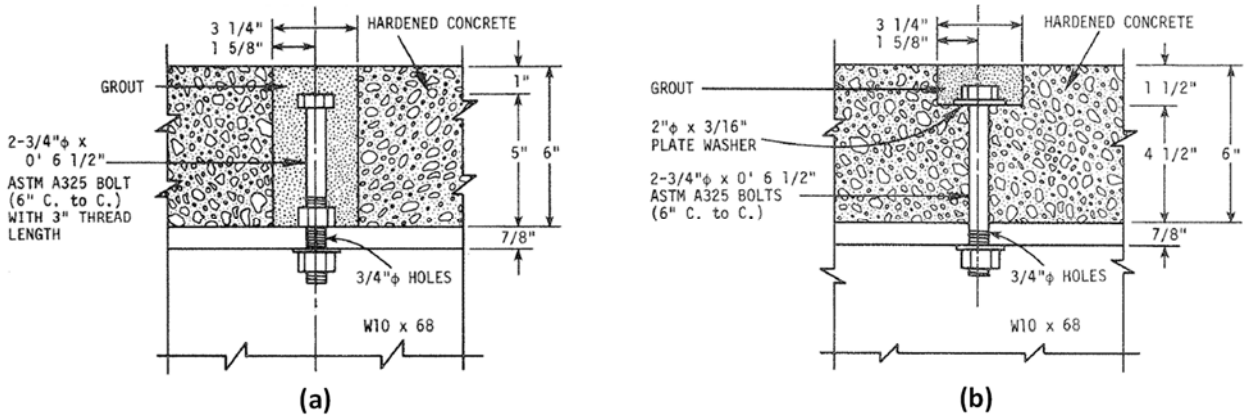

Figure 2.7 Post-Installed Connectors Tested by Klaiber et al. (1983) – (a) Double-nutted connector and (b) Epoxied bolt connector

Dionne et al. (1997) investigated the use of post-installed shear connectors by conducting small-scale direct-shear static and fatigue tests on seven different types of mechanical anchors and three types of epoxied anchors. They suggested that anchors combining both mechanical and epoxied connections, shown in Figure 2.8, were most efficient in resisting slip and providing the necessary strength and ductility.

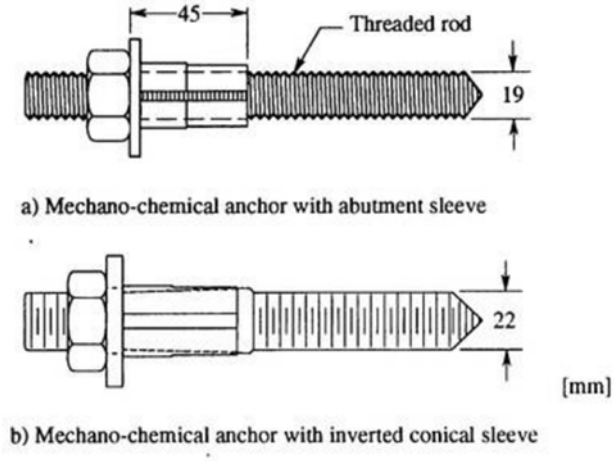

Figure 2.8 Post-Installed Connectors Recommended by Dionne et al. (1997)

Research on post-installed shear connectors funded by the Texas Department of Transportation has been ongoing at The University of Texas at Austin for the past decade, starting with a laboratory-based research project (0-4124) and continuing with an implementation project (5-4124) (Kwon et al. 2007, Kwon et al. 2009). Several theses and dissertations contain additional details on this research. Hungerford (2004) and Schaap (2004) conducted static direct-shear tests on 22 types of post-installed shear connectors, recommending 6 with good static behavior. Kayir (2006) performed fatigue tests on these six connection methods using 3/4-inch diameter connectors, along with additional static tests, narrowing it down to the three recommended connectors shown in Figure 1.2. Kwon (2008) studied larger diameter (7/8-inch) connectors under static and fatigue loading before conducting large-scale beam tests

on simple-span girders strengthened to a composite ratio of 30%. Following the lab testing, Kwon designed and implemented a strengthening scheme for an existing bridge using all three recommended connectors and conducted load tests before and after connector installation. Key findings from these studies are presented in the following sections.

2.5.1 Static Testing

Several types of post-installed shear connectors were tested under static loads in the direct-shear setup shown in Figure 2.9. Additionally, conventional cast-in-place welded studs were tested for comparison. Connectors exhibiting good stiffness, strength, and ductility were recommended for further investigation.

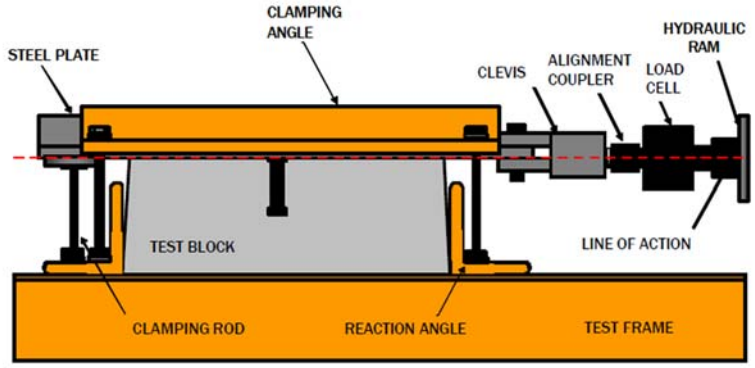

Figure 2.9 Direct-Shear Test Setup from TxDOT Project 0-4124 (Kayir 2006)

For the three connectors shown in Figure 1.2, the following equation was recommended for the ultimate static strength of a single connector (Q_n):

$$Q_n = 0.5 A_{sc} F_u \qquad \textit{Equation 2.12}$$

where A_{sc} is the cross-sectional area of the connector, taken as 80% of the gross area for threaded connectors, and F_u is the ultimate tensile strength of the connector material. Throughout all of the static testing, high-strength threaded rods (ASTM A193 B7) and structural bolts (ASTM A325) were used for the connectors.

2.5.2 Fatigue Testing

The same direct-shear test setup was adopted for the fatigue tests conducted on individual post-installed connectors in project 0-4124. The results from this fatigue testing for the three recommended connectors are shown in Figure 2.10. All three types of connectors show significantly better fatigue behavior than conventional welded studs, although the adhesive anchor exhibited the worst performance of the three. Because of this, most of the tests were completed on the adhesive anchor, and an S-N curve (stress range versus cycles to failure) was developed as a preliminary design recommendation, ignoring the two outlying data points. The majority of the double-nut bolt and high-tension friction-grip bolt specimens did not fail after 5 million cycles in fatigue, as indicated by the arrows underneath the data points in the figure, so an S-N curve could not be developed. Instead, an endurance limit of 35 ksi was proposed for these two connector types.

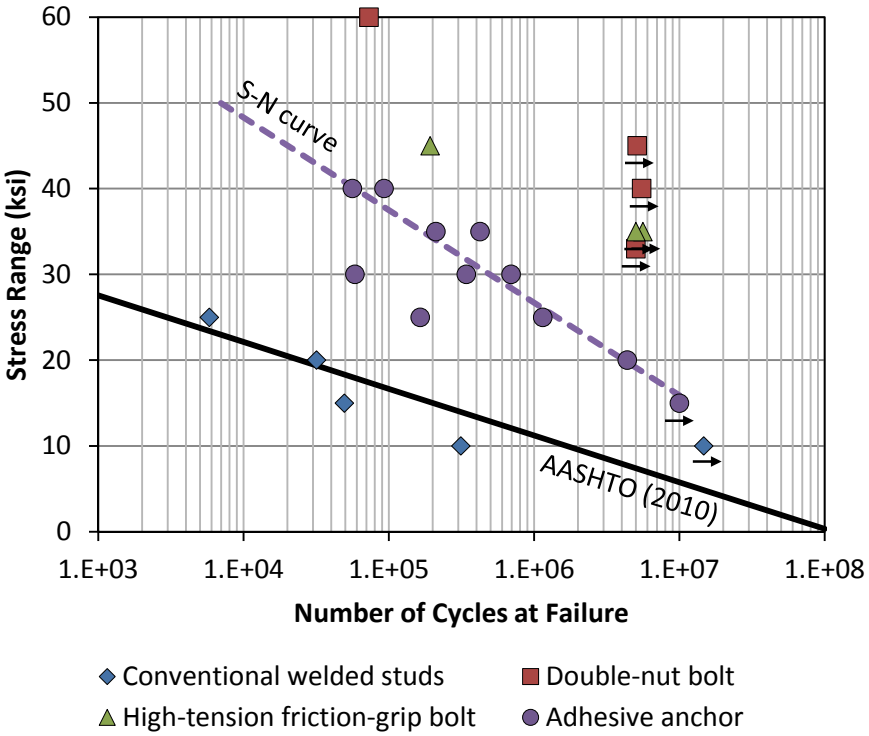

Figure 2.10 Direct-Shear Fatigue Results from TxDOT Project 0-4124 (adapted from Kwon et al. 2007, Kwon 2008)

2.5.3 Large-Scale Testing

The large-scale testing conducted in project 0-4124 consisted of 38-foot simple span girders loaded monotonically to failure by a point load at midspan (Kwon 2008). The geometry of the specimens is shown in Figure 2.11. After conducting one test on a non-composite girder, three additional girders were tested after strengthening with each of the three types of post-installed shear connectors shown in Figure 1.2. Eight pairs of connectors were installed at a uniform spacing on either side of the point load, giving the girders a composite ratio of 30%. Finally, a fifth beam was tested with the post-installed connectors concentrated near the ends of the beam to reduce the slip demand. This beam was strengthened to a composite ratio of 30% with adhesive anchors.

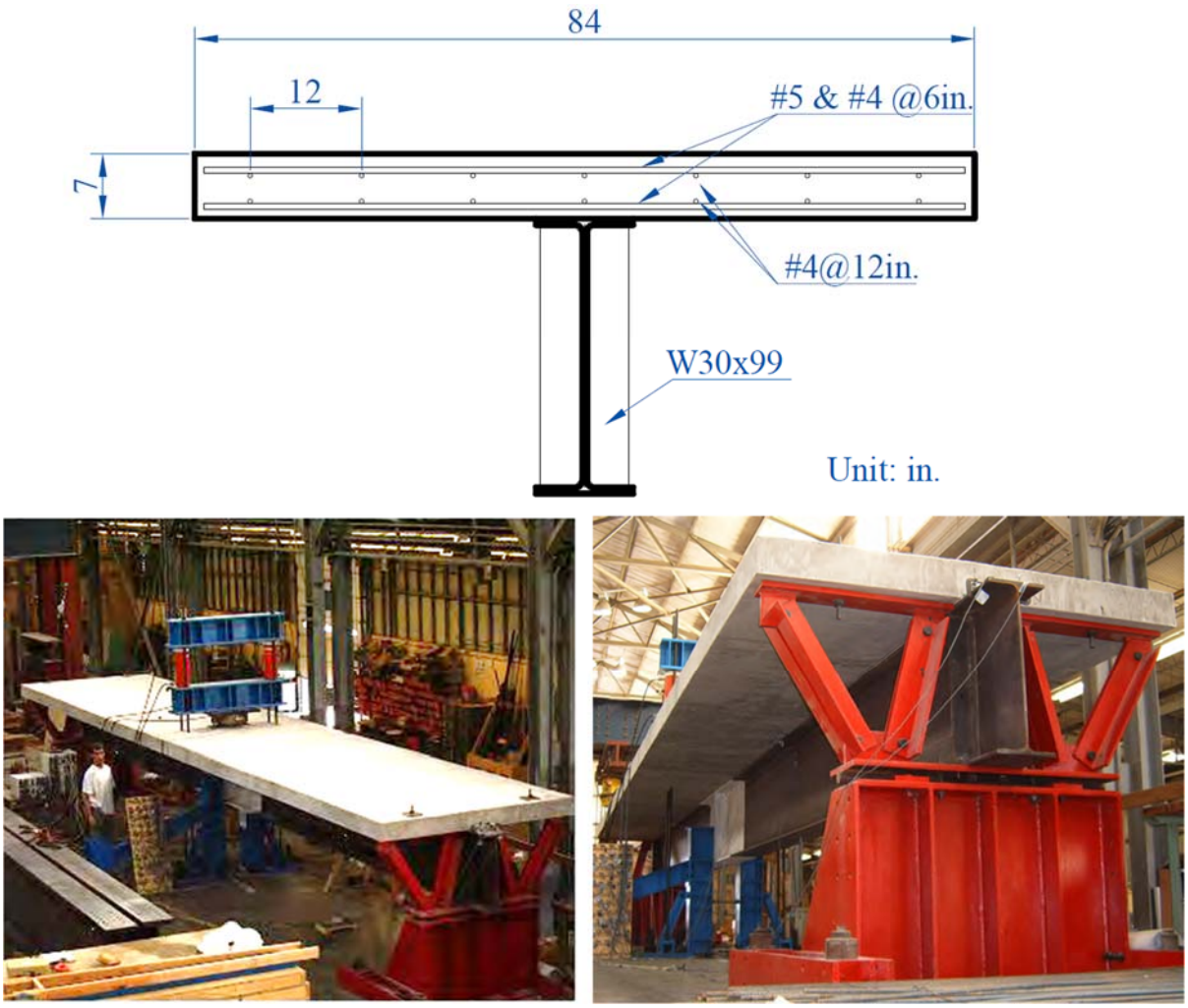

Figure 2.11 Large-Scale Test Setup in TxDOT Project 0-4124 (Kwon 2008)

The results from the large-scale testing in project 0-4124 are summarized in the load-deflection plot of Figure 2.12. The behavior of all five girders is included in the figure. The dashed black lines indicate the expected load-deflection curve for non-composite and 30% composite girders using simple plastic analysis. The ultimate strengths of all five girders agreed well with the simple plastic analysis, which was generally slightly conservative.

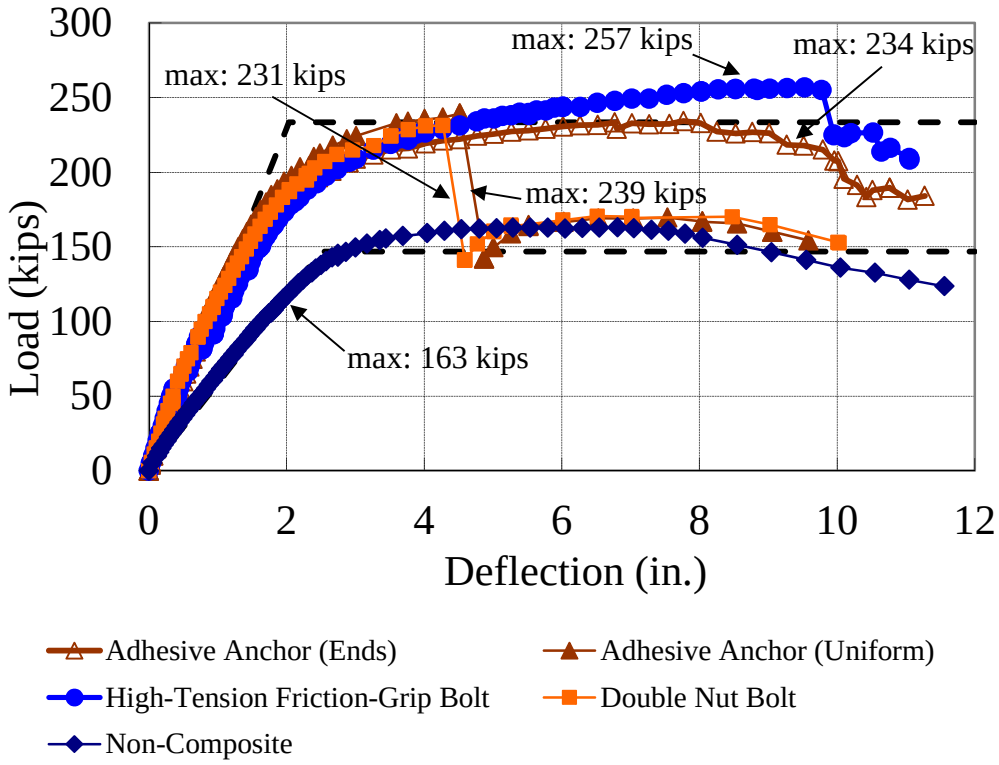

Figure 2.12 Large-Scale Test Results in TxDOT Project 0-4124 (Kwon 2008)

While the girder strengthened with high-tension friction-grip bolt connectors in a uniform distribution exhibited very good ductility, the girders strengthened with double nut bolts and adhesive anchors in a uniform distribution did not. These two specimens dropped a significant amount of load at approximately 4.5 inches of deflection, and then continued to follow the non-composite curve thereafter. This drop in load coincided with the simultaneous failure of essentially all of the post-installed connectors, leaving only a non-composite girder to resist load. However, the girder strengthened with adhesive anchors concentrated near the ends of the beam showed significantly more deformation capacity, indicating that the ductility can be improved by concentrating connectors near regions of zero moment.

Generally, these tests showed that strengthening the positive moment regions of non-composite girders by post-installing shear connectors is feasible. Additionally, partial composite construction was shown to be a viable option, as the specimens exhibited good structural performance well into the inelastic range.

2.5.4 Implementation

Following the laboratory work, a strengthening scheme was designed and implemented on a simply supported three-span bridge near San Antonio, Texas. The bridge, originally constructed in 1950, is shown in Figure 2.13. Each simply supported span was strengthened with one of the three different types of post-installed connectors from Figure 1.2. A composite ratio of 50% was used for the spans containing high-tension friction-grip bolt and double-nut bolt connectors, while significantly more adhesive anchor connectors were used due to uncertainties

in the fatigue performance. The connectors were concentrated near the ends of each simple span with a 12-inch longitudinal spacing.

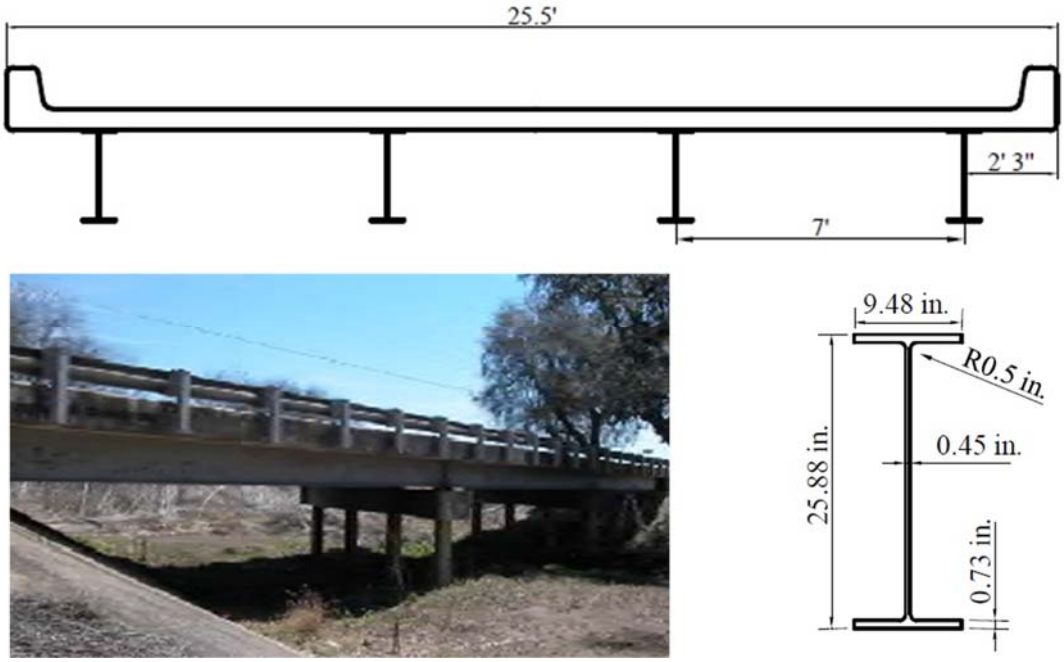

Figure 2.13 Bridge Strengthened in Implementation Project (Kwon et al. 2009)

Live load tests were carried out before and after the connectors were installed using dump trucks filled with gravel. Deflections were measured during the tests to evaluate the increase in stiffness of the bridge response before and after connector installation. Additionally, strain gages were installed at select locations to monitor the neutral axis depth, which is an indicator of composite behavior. Although it was not possible to conduct strength testing, it was concluded that the post-installed connectors were effective in developing a significant amount of composite action under service-level loads.

2.6 Moment Redistribution and Shakedown

Using inelastic procedures to design new steel bridges can result in a reduction of member sizes, particularly by eliminating the need for cover plates or multiple flange transitions in the negative moment regions over the piers. The AASHTO bridge design specifications have included some form of inelastic design procedures since 1973, including the allowance of inelastic moment redistribution from interior pier sections (Barth et al. 2004). When evaluating and strengthening existing bridges, accounting for the ductile, post-yielding behavior of steel by performing an inelastic analysis can be even more advantageous. Significant increases in load-carrying capacity can be obtained by recognizing the strength of steel beyond the elastic limit, which can minimize the amount of rehabilitation necessary for older structures. However, yielding of a bridge under repeated large truck loads could lead to an undesirable accumulation of permanent deflections in a structure over time. This section describes the phenomenon of shakedown, which addresses this type of behavior.

2.6.1 Shakedown Behavior

Shakedown is the appropriate limit state to consider for a statically indeterminate structure subjected to repeated cycles of a load pattern that causes yielding. For continuous bridges, yielding can often be allowed at the interior pier sections so that excess moments are redistributed to the adjacent span regions. The main concern with this type of behavior is that the inelastic rotations sustained at the piers may increase with every cycle of load. Eventually, this may create serviceability problems if deflections increase without bound. However, if the magnitude of the large loads crossing the bridge is high enough to cause yielding at the piers but not too high, the bridge will "shake down" after several cycles, and all future loads of equal or lesser magnitude will be resisted elastically. This is accomplished by the formation of residual moments in the continuous girders, as a result of the permanent rotations at the interior piers. These residual moments counteract the moments from the applied traffic loads and thus delay additional yielding during future cycles of load, preventing additional inelastic rotations. Note that a structure must be statically indeterminate to be able to carry residual moments and exhibit this behavior. For loads that are higher than this "shakedown load," the inelastic rotations will continue to increase with additional cycles, leading to "incremental collapse," under eventual excessive deformations. In this case, the residual moments are not capable of counteracting the moments from the applied loads to an extent that would prevent yielding and inelastic rotation from occurring at all sections along the girder during future cycles. Figure 2.14 illustrates the general behavior of shakedown and incremental collapse.

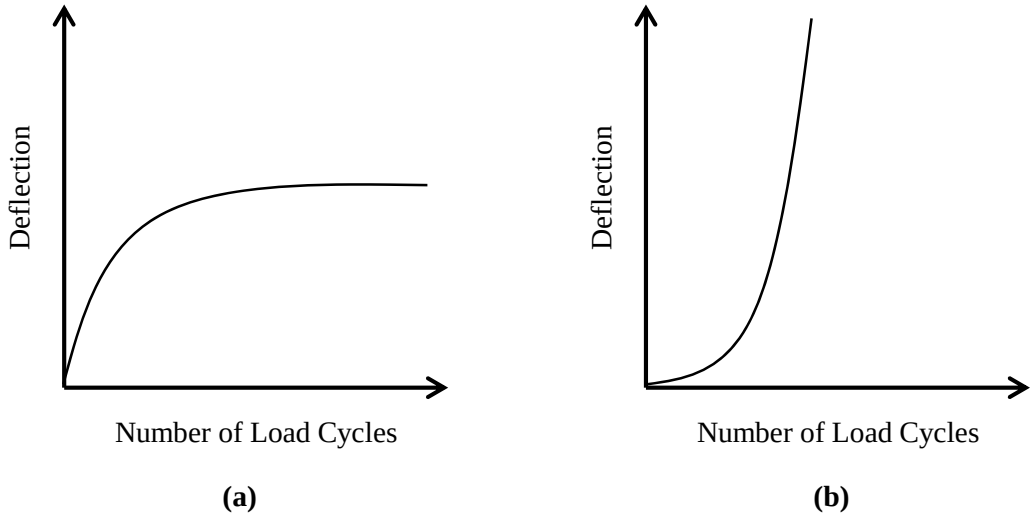

Figure 2.14 Illustration of (a) Shakedown Behavior and (b) Incremental Collapse

Note that shakedown is not the same as low-cycle fatigue, also called alternating plasticity, in which fracture occurs as a result of a loading cycle that causes alternating yielding in tension and compression (ASCE-WRC 1971). Instead, the shakedown limit state refers to progressively increasing plastic rotations and permanent deformations associated with repeated yielding in either tension or compression, but not both, at particular sections. For this reason, the shakedown limit state is often referred to as "deflection stability."

Illustrative Example

To further illustrate the shakedown behavior of a bridge girder, a simple example of a propped cantilever beam with a moving point load is presented here. This example has been adopted from Fukumoto and Yoshida (1969). Refer to Figure 2.15, which depicts the response of a beam to two cycles of a point load moving from left to right across the beam. The following analysis makes a few simplifying assumptions. First, yielding is assumed to occur instantaneously through the entire cross section when the moment reaches the plastic moment. No yielding is considered before the plastic moment has been reached. Second, the material is assumed to be elastic-perfectly plastic such that no strain hardening occurs. Thus, the plastic moment is the maximum moment that can be carried by the section. Finally, for simplicity it is assumed that the positive and negative moments are equal in magnitude ($\pm M_p$).

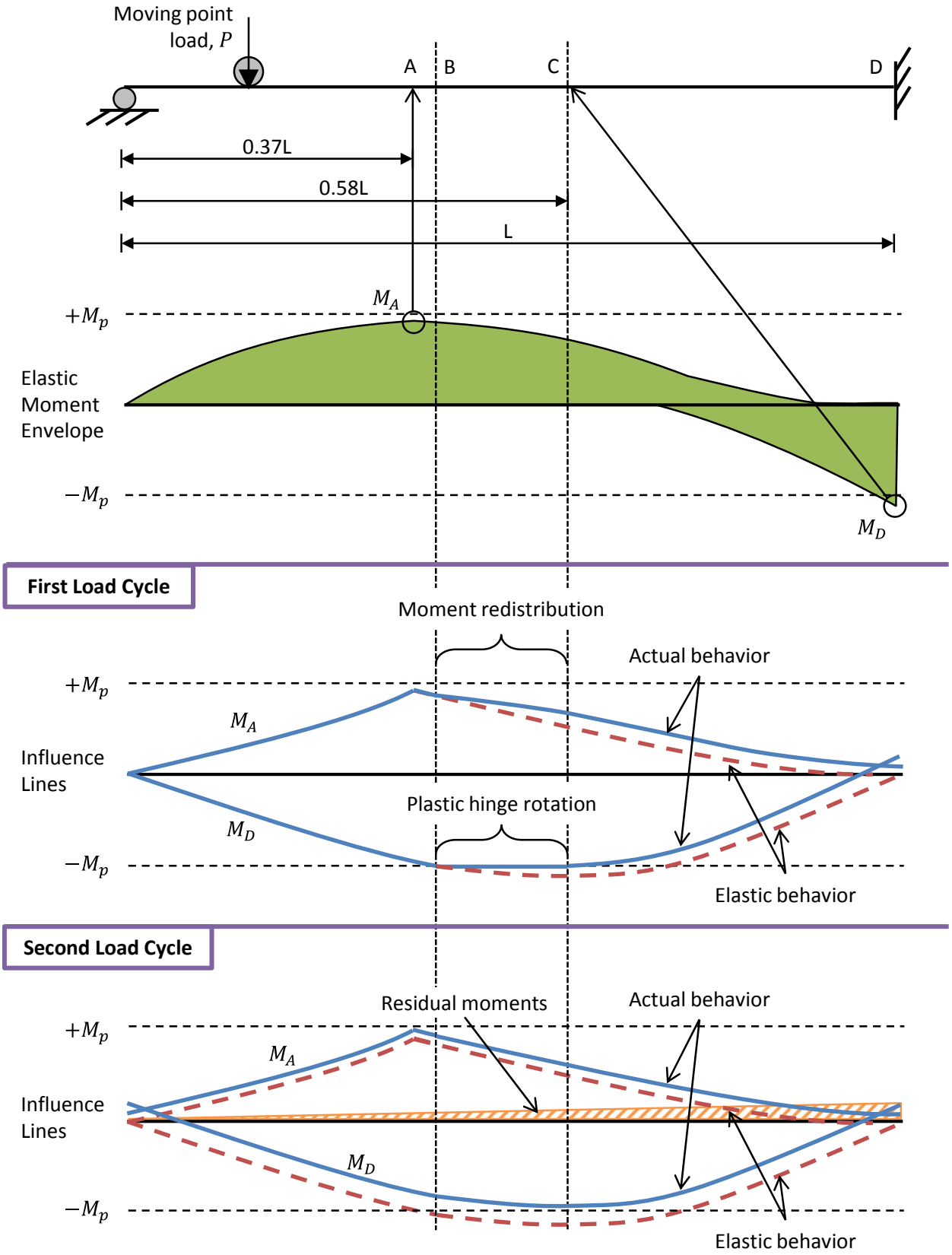

Figure 2.15 Shakedown of a Propped Cantilever with Moving Point Load – First Two Cycles

The elastic moment envelope in the top frame of Figure 2.15 plots the maximum positive and negative moment experienced by each section along the beam as the load moves across the beam. The maximum positive moment in the beam occurs at point A when the load is also located at point A. The maximum negative moment occurs at the fixed end, or point D, when the load is located near midspan at point C. For a constant magnitude of load moving across the beam, the moment at D is larger than the moment at A, indicating that yielding will occur first at D. For the purposes of this example, the magnitude of the applied load is greater than the load required to form a plastic hinge at D but smaller than the shakedown load.

The bottom two frames in Figure 2.15 show the influence lines for the moment at points A and D for the first and second loading cycles. An influence line plots the variation of a particular force quantity at a single section of the beam as a function of the position of the moving load on the beam. The elastic influence lines are shown as dotted lines, while the solid lines trace the actual influence lines. These actual influence lines differ from the elastic lines during the first cycle because yielding occurs at point D and moments are redistributed to the remaining portions of the beam. This redistribution alters the moment at both points A and D.

As the load moves from left to right across the beam during the first cycle, the initial behavior is fully elastic. When the load reaches point A, the maximum positive moment is attained, but the beam remains elastic because the moment has not exceeded the plastic capacity. Once the load reaches point B, the moment at point D is equal to the plastic moment, and a plastic hinge forms at point D. At this point in the analysis, the section at D cannot carry any additional moment. However, as the load continues to move to the right, the elastic moment demand at point D increases. Because the section cannot resist the additional demand, the excess moments are redistributed away from point D and out into the span. The result of this can be seen in the influence line for the moment at point A, which increases in magnitude as compared to the elastic influence line as the load moves to the right of point B. As the load continues to move to the right, the plastic hinge at point D rotates freely.

The maximum negative elastic moment demand at the fixed end occurs when the load reaches point C. After the load moves past this location, point D begins to unload elastically because the moment demand is now decreasing at that location. Plastic deformation and moment redistribution cease, and the beam responds elastically as the load moves off the right end of the beam. However, once the load has been completely removed from the beam, residual moments remain in the system as a result of the permanent plastic hinge rotation at point D, which prevents the beam from returning to its original straight configuration. Because only the reaction forces can act on the beam in the unloaded state, the residual moment diagram must have a triangular shape, as shown in the bottom frame of Figure 2.15 shaded with diagonal lines.

The influence lines from points A and D for the second load cycle are shown in the bottom frame of Figure 2.15. Again, the dashed lines represent the elastic influence lines, while the solid lines indicated the actual behavior. Because of the residual moments present in the system before the start of the second cycle, the initial moment at points A and D are equal to the value of the residual moment at those locations, instead of zero as they were at the start of the first cycle. After this initial offset, the trend of the elastic influence line is followed as the moving load transverses the entire length of the beam. Since the moment at points A and D does not exceed the plastic moment capacity for any locaton of the point load, no additional yielding or moment redistribution occurs. This is indicated in the figure by the actual influence lines remaining within the bounds of the capacities. Thus, the residual moments that remain in the beam when the load moves off of the right end are unchanged from the first cycle. All future

cycles of the same or lesser load will result in the same behavior as shown for the second load cycle, and no additional yielding or inelastic rotations will occur. In other words, this beam has "shaken down" for the particular magnitude of applied load.

Although the stabilization occurs after only a single cycle in this case, a more complex structure may take more than one loading cycle to shake down. If at any point during the second cycle in this example had the moment demand exceeded the plastic moment capacity at any location along the beam, additional plastic rotation and moment redistribution would have occurred in that location. This would have resulted in a different residual moment distribution at the end of the second cycle, which would then be the starting point for the third cycle. Several cycles may be necessary before a state of shakedown is reached, especially in a structure with more than two possible hinge locations

It may also be the case that the structure undergoes plastic rotation during every cycle and never comes to the stable condition shown in the second load cycle of Figure 2.15. As additional cycles are applied to such a structure, incremental collapse would eventually occur, as more and more permanent inelastic deformations accumulate with additional cycles. Any load causing this type of behavior is greater than the shakedown load and is associated with incremental collapse.

Shakedown Theorems

Shakedown was first recognized in Germany in the 1920s in statically indeterminate trusses (Grüning 1926). Much of the early theoretical work was completed in Europe during the following decade. The first mathematical representation of shakedown behavior was given by Bleich (1932) for a truss with one degree of static indeterminacy. Melan (1936) extended the mathematical framework for structures with more than one degree of indeterminacy. Since the mid-1900s, general theorems of shakedown and different methods of computing the shakedown load for beams and frames have been developed. There are three theorems that determine whether or not a structure will shake down (Neal 1977). These are the lower bound, upper bound, and uniqueness theorems, which are analogous to the well-known theorems regarding plastic limit loads for structures under static loading cases.

The lower bound theorem requires the satisfaction of equilibrium and yield conditions. This theorem states that if a set of statically admissible residual moments exists such that the sum of those residual moments and the elastic moments from a particular applied loading pattern does not produce moments exceeding the plastic moment capacity anywhere along the beam, that applied load must be less than or equal to the shakedown load. Thus, all loading conditions satisfying the lower bound theorem will result in a structure that will shake down to elastic behavior after some number of cycles.

The upper bound theorem requires the determination of a plastic mechanism that satisfies equilibrium. The theorem states that the applied load required to form this mechanism must be greater than or equal to the shakedown load. Thus, all loading conditions leading to all possible plastic mechanisms are greater than or equal to the shakedown load and will result in incremental collapse for all cases except for the true shakedown load. The true shakedown load is the smallest load resulting from all possible mechanisms.

The uniqueness theorem simply states that only the exact and unique shakedown load can satisfy both the lower and upper bound theorems.

The upper bound theorem often provides an easier method to compute the shakedown load for a particular loading pattern for simple structures, as illustrated in the example in the next

section. However, concepts based on the lower bound theorem are often used to develop simplified design procedures for complex structures. This is illustrated in Section 2.7, which discusses the AASHTO provisions for inelastic moment redistribution.

Upper Bound Method Example

This example illustrates the calculation of the shakedown load for the same propped cantilever beam from the previous example. Figure 2.16 shows the necessary diagrams for the calculations. The previous assumptions that the entire section yields simultaneously, that the material is elastic-perfectly plastic with no strain hardening, and that the positive and negative plastic moments are equivalent ($\pm M_p$) remain in effect for this example.

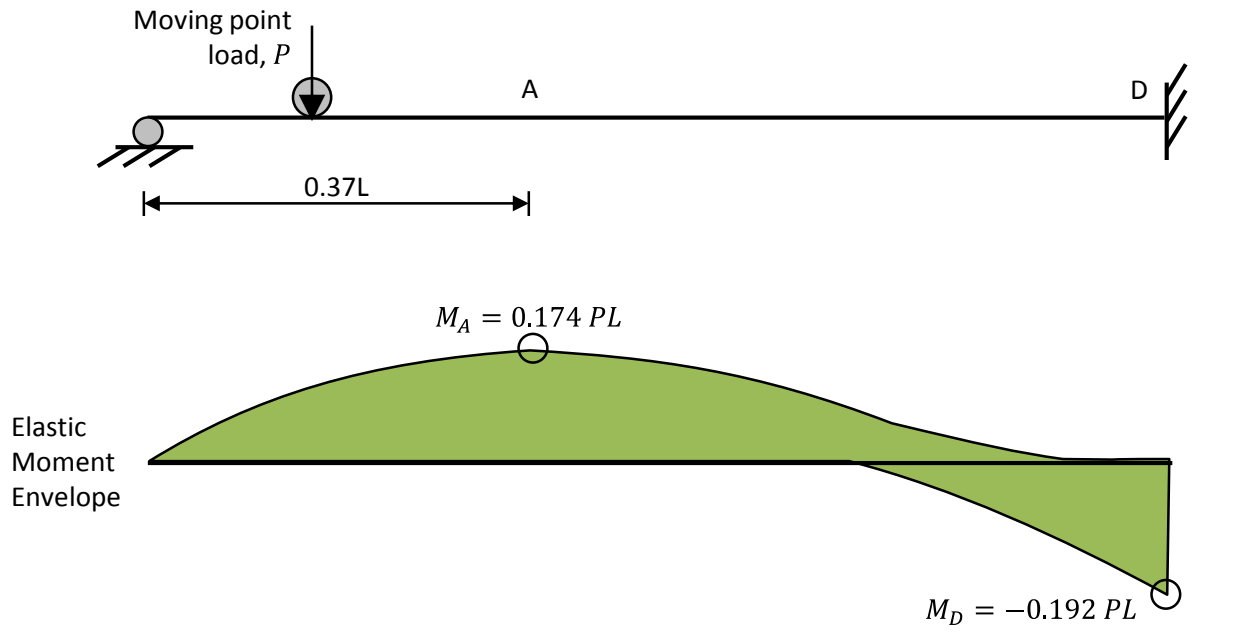

Failure Mechanism

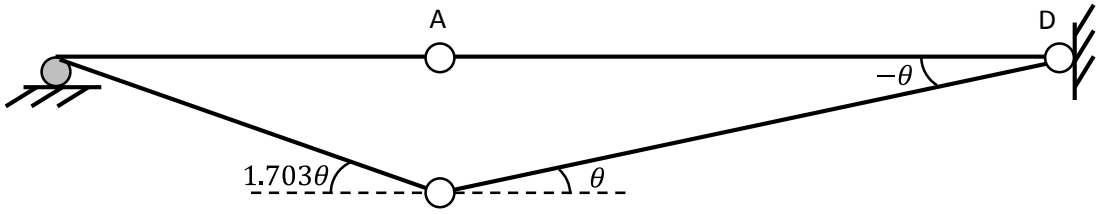

Virtual Work Calculations

$$\delta W_{internal} = (+M_p)\,(1.703\theta + \theta) + (-M_p)\,(-\theta)$$

$$\delta W_{external} = (0.174\ PL)(1.703\theta + \theta) + (-0.192\theta)(-\theta)$$

$$\delta W_{internal} = \delta W_{external} \longrightarrow \boxed{P_{shakedown} = 5.59\ M_p/L}$$

Figure 2.16 Upper Bound Method Example

To calculate the shakedown load, a virtual work approach is used. First, the elastic moment envelope is computed. This is shown in the top frame of Figure 2.16 and is identical to that shown in the top frame of Figure 2.15. The maximum positive and negative moments occur at points A and D, respectively. These points will be the locations of the plastic hinges in the shakedown mechanism, which is shown in the middle frame of the figure. Because this is a simple structure, the controlling mechanism for shakedown is obvious. For more complex

structures, several mechanisms may need to be considered to arrive at the correct shakedown load.

Once the moment envelope and mechanism are known, the internal and external virtual work are computed. These calculations are summarized in the bottom frame of Figure 2.16. The internal virtual work is the product of the plastic moment and the plastic hinge rotation at each hinge location. These values are added together to get the total internal virtual work ($\delta W_{internal}$). The external virtual work is the product of the moment from the elastic moment envelope and the plastic hinge rotation at each hinge location. These values are added together to get the total external virtual work ($\delta W_{external}$).

The shakedown load is calculated by equating the total internal and external virtual work. For the propped cantilever in this example, the shakedown load is equal to $5.59\ M_p/L$. For comparison, the load that causes first yield at the fixed end is $5.21\ M_p/L$ and the minimum static plastic collapse load is $5.83\ M_p/L$, occurring when the load is located a distance of $0.41\ L$ away from the pinned support (Fukumoto & Yoshida 1969).

2.6.2 Previous Research on Shakedown of Steel and Composite Beams

The majority of experimental testing completed in the area of shakedown has been conducted on steel-only beams, not on composite members. Small-scale tests were conducted by Klöppel (1936), Massonnet (1953), Gozum (1954), Sherbourne (1963), Fukumoto and Yoshida (1969), and Eyre and Galambos (1970), who all observed that the predicted shakedown loads were conservative, likely due to strain hardening of the steel, which was typically ignored in the predictions.

Larger-scale shakedown testing for bridge structures began in the 1970s and 1980s under the direction of the American Iron and Steel Institute (AISI) (Grubb & Carskaddan 1979, Carskaddan 1980, Grubb & Carskaddan 1981). Following some initial theoretical studies, the experimental research was focused primarily on the effects of slenderness and moment gradient on the inelastic moment-rotation behavior of composite I-girders. However, with the exception of one test consisting of an actual steel-concrete composite beam, the experiments were conducted on singly symmetric steel-only sections having larger top flanges than bottom flanges to represent a composite section in negative bending that engages the reinforcing bars in the deck. This research led to the development and publication of an AASHTO guide specification for “Alternate Load Factor Design” (ALFD), also known as autostress design, which detailed an iterative inelastic analysis procedure to incorporate yielding and moment redistribution into bridge design, but was restricted to steel sections with compact flanges and webs (AASHTO 1986).

Design using the ALFD guide specification was verified by tests on composite bridges and bridge models. Roeder and Eltvik (1985) conducted load tests on a new bridge designed using ALFD up to load levels that caused yielding and inelastic moment redistribution. Good behavior was observed throughout the test, and less permanent deformation and deck cracking was observed than predicted. Moore and Grubb (1990) tested a 40% scale model of a two-span, three-girder, composite bridge designed using ALFD provisions, although the girders had noncompact webs. This model bridge performed well under AASHTO specified design service loads, overloads, and maximum loads, deeming ALFD an appropriate design method for sections with noncompact webs. Similar good behavior under AASHTO-defined limit states was observed by Weber (1994) after testing of a 50% scale model of a three-span, fully composite, single bridge girder with a compact steel section designed according to the ALFD specifications.

However, a few other experimental studies indicated that composite girders may not actually achieve shakedown under repeated large loads. Bergson (1994) conducted shakedown testing on a 33% scale model of a three-span, four-girder bridge that was initially designed and constructed for the purposes of elastic testing. Results from this test indicate a loss in composite action at loads near the predicted shakedown load, although extensive cracking was observed in the under-designed deck at large loads. Flemming (1994) applied an actual moving load using a bogie that was rolled across a 50% scale model of a two-span, five-girder bridge to investigate the shakedown behavior of partially composite girders. One of the spans of the bridge was constructed as 80% composite, while the other span was only 50% composite. The deflections generally did not stabilize during shakedown testing, and degradation in the composite strength was observed with additional cycles at larger loads. Similar behavior was observed by Thirugnanasundralingam (1991) during testing conducted on two-span, fully composite girders under a moving load applied using a "rocker beam" which had a curved bottom flange so that as it rotated, the point of load application moved along the test specimen. The tests indicated that the experimental shakedown load was significantly lower than the theoretical value, as measured slips and deflections did not stabilize. It is useful to note here that these specimens showing poor shakedown behavior in these three studies were no more than ½-scale models and had deck thicknesses not exceeding 4 inches. It is possible that the unrealistic deck design may have contributed to the observed poor behavior.

2.7 AASHTO Moment Redistribution Provisions

The autostress design provisions that first appeared in the AASHTO ALFD guide specification document in the mid-1980s were introduced into the first edition of the AASHTO LRFD bridge design specifications nearly a decade later (AASHTO 1994). This supplemented the allowance of up to 10% moment redistribution from the interior piers for compact, well-braced girders. However, autostress design was never widely used by bridge engineers because it required an iterative inelastic analysis and was limited to only compact steel sections (Barth et al. 2004).

By the third edition of the LRFD specifications, the 10% moment redistribution provision was removed from the code and replaced by a simple, rational approach to estimate the redistribution moments based on shakedown behavior (AASHTO 2004). Details regarding the development of these provisions are provided by Hartnagel (1997). These optional provisions, which remain essentially unchanged through the specifications current at the time of this report, are located in Appendix B. The steps, illustrated in Figure 2.17 for a symmetric three-span continuous girder, are as follows:

- Ensure that the interior pier section and bridge geometry abide by the specified limits. In particular, the girders must be well-braced and have a compact compression flange. The web can be compact, noncompact, or slender to a certain extent, and bearing stiffeners are required. The bridge must not have horizontal curvature and the supports cannot exceed a 10° skew angle, nor can the cross frames be staggered.
- Conduct an elastic analysis of the bridge girder for the load combination of interest. Moment redistribution is allowed for Service II and all Strength load combinations. Obtain the elastic moment envelope (M_e).

- Compute the effective plastic moment capacity (M_{pe}) at each interior pier. This effective capacity accounts for the slenderness of the section and ensures that an adequate amount of plastic rotation can be attained for moment redistribution to occur.
- If the magnitude of the elastic moment at the interior pier exceeds the effective capacity, the difference between the two is the amount of moment that needs to be redistributed. This "redistribution moment" (M_{rd}) is limited to 20% of the elastic moment.
- Draw the redistribution moment diagram by connecting the computed residual moments at each pier with straight lines.
- Add the redistribution moment diagram to the elastic moment envelope, and check that the capacity is not exceeded at any other point along the bridge.

Elastic Moment Envelope

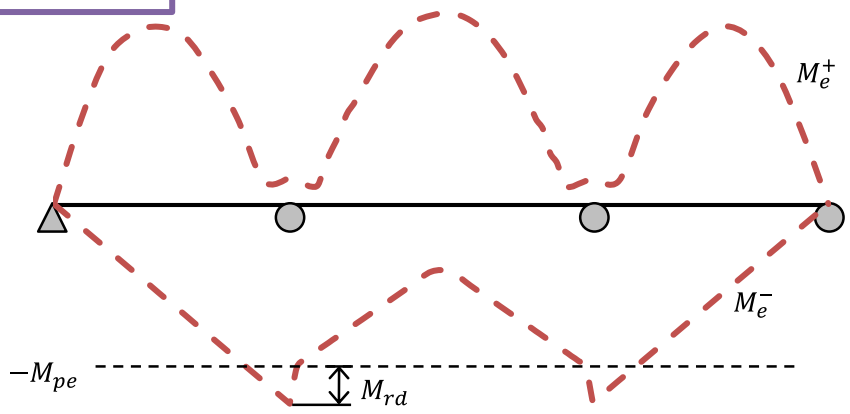

$$M_{pe} = \left(A - 2.3 \frac{b_{fc}}{t_{fc}} \sqrt{\frac{F_{yc}}{E}} - 0.35 \frac{D}{b_{fc}} + 0.39 \frac{b_{fc}}{t_{fc}} \sqrt{\frac{F_{yc}}{E} \frac{D}{b_{fc}}} \right) M_n \leq M_n$$

A = Constant between 2.63 and 2.90, depending on section properties and limit state
E = elastic modulus

b_{fc} = width of compression flange
t_{fc} = thickness of compression flange
D = web depth
F_{yc} = yield stress of compression flange

$$M_{rd} = |M_e| - M_{pe} \leq 0.2 M_e$$

Redistribution Moment Diagram

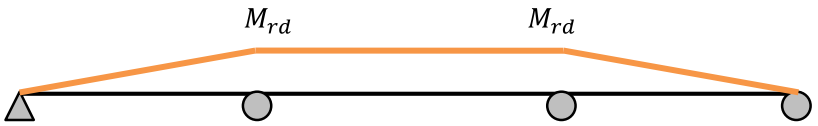

Resulting Moment Envelope

$$M_{total} = M_e + M_{rd}$$

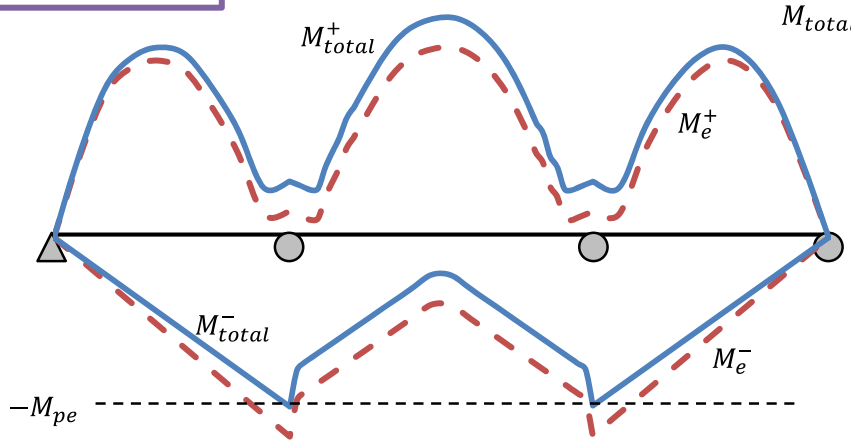

Figure 2.17 Simplified AASHTO Moment Redistribution Procedure

Chapter 3. Bridge Survey

3.1 Overview

To become familiar with the types of bridges that could be strengthened with post-installed shear connectors, a survey of non-composite steel I-girder bridges in Texas was conducted. Plans and inspection reports for a total of 25 bridges from eight TxDOT districts around the state were studied in detail during the course of this survey. Data was collected on general information, materials, bridge geometry, girder details, cross frame details, deck details, inspection information, traffic, and load rating. This chapter summarizes the findings from this survey.

3.2 General Information

The survey includes information from bridges in the Abilene, Beaumont, Dallas, El Paso, Houston, Laredo, San Antonio, and Yoakum districts. A map showing the bridge locations is given in Figure 3.1, and the bridge names and construction dates are shown in Table 3.1. All but three of the bridges were constructed between 1955 and 1965. Two were constructed in earlier years (1937 and 1947), while the third was constructed later (1973). These three bridges that fall outside the typical construction timeframe, which are shown in italics in Table 3.1, are the only two-girder bridges in the survey. Because they rely on a superstructure composed of both stringers and floor beams, these three bridges have very little in common with the other bridges surveyed. Thus, the following sections will ignore these two-girder bridges and will instead focus on the other 22 bridges. Section 3.9 briefly summarizes information about the two-girder bridges.

Eight of the bridges, including one of the two-girder bridges mentioned above, have had major modifications since construction, mostly to widen the structure. While all of the bridges were generally designed for non-composite behavior, ten of the bridges have some form of shear connectors at large spacing (2 feet or greater), sometimes only along the exterior girders or only in certain portions of a span. Many of the bridges make use of both steel and prestressed concrete girders, but only the steel spans were considered in this survey. While more than two-thirds of the bridges carry two lanes of traffic, a few three- and four-lane bridges are also present.

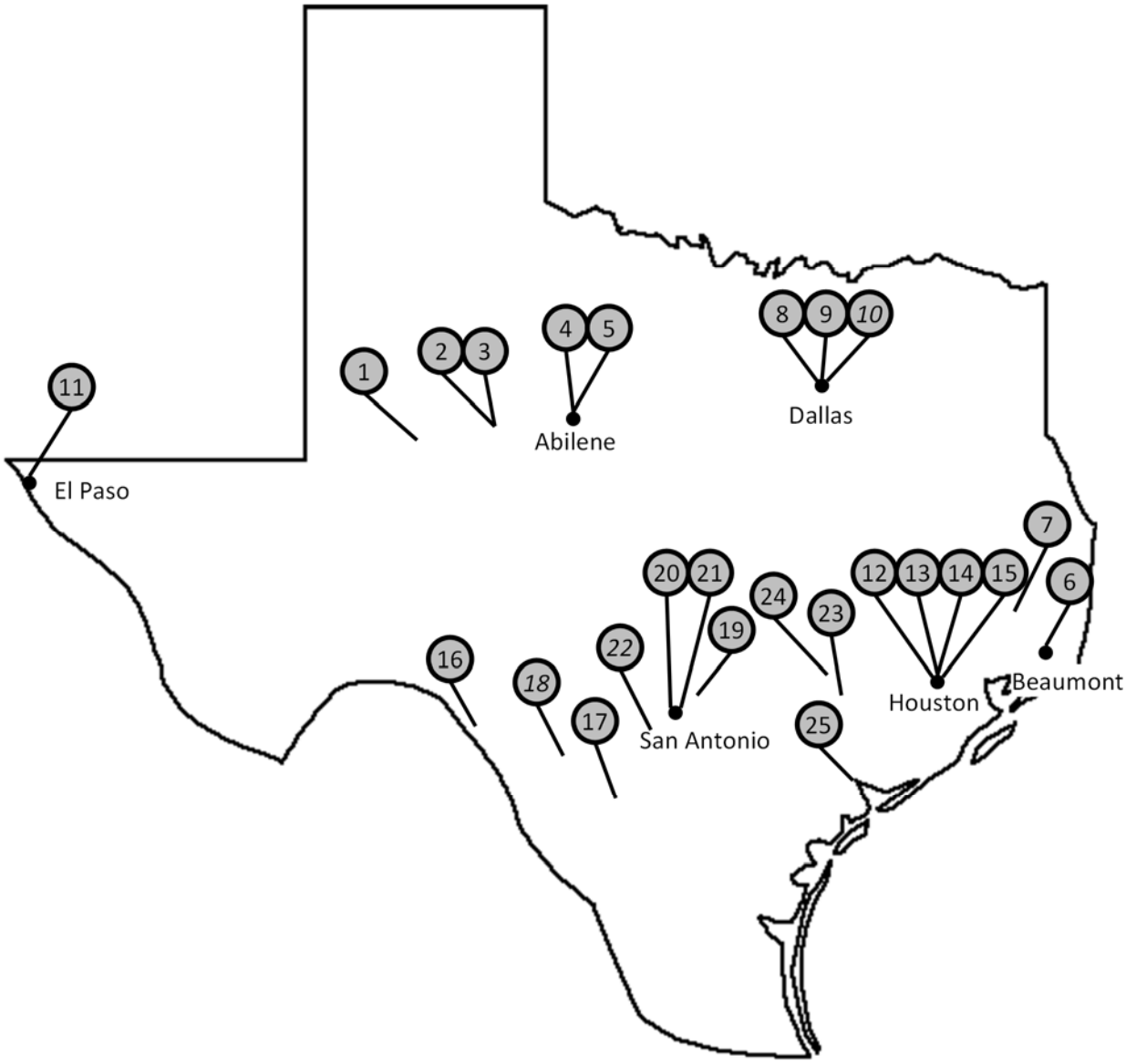

Figure 3.1 Locations of Surveyed Bridges

Table 3.1 Listing of Surveyed Bridges

Bridge Number	Bridge Name	Date Constructed
1	I-20 over T&P Railroad	1955
2	I-20/US-84 under Blackland Road	1958
3	I-20 under US-84	1958
4	US-83/US-277 over N 10th Street	1964
5	US-83/US-84/US-277 over S 7th Street	1964
6	I-10 under S Major Drive	1961
7	US-287/US-69 over Village Creek	1957
8	I-30/US-67 under St. Francis Avenue	1959
9	I-35E/US-77 over US-183	1959
10	*US-75 elevated portions in Dallas*	*1973*
11	FM-76 over Union Pacific Railroad	1965
12	I-45 frontage road ramp to Jefferson Street	1955
13	I-45 under W Dallas Street	1955
14	I-45 under N Main Street	1962
15	US-90 over Buffalo Bayou	1956
16	US-297 over T&NO Railroad and E Ogden Street	1955
17	I-35 over MoPac Railroad	1963
18	*US-83 over the Nueces River*	*1947*
19	FM-3009 over I-35	1965
20	I-410/US-16 over Ray Ellison Boulevard	1960
21	I-410/US-16 under Valley Hi Drive	1959
22	*I-35 over the Medina River*	*1937*
23	US-90 over the Colorado River	1956
24	FM-109 over Cummins Creek	1955
25	TX-35 over the Victoria Barge Canal	1960

3.3 Materials

The typical materials used in the construction of the surveyed bridges, including the structural steel, concrete, and deck reinforcement, are summarized in the following sections. In cases where the plans do not directly specify the material used, historical bridge specifications were consulted for typical materials used during the time period.

3.3.1 Structural Steel

From the early 1900s to 1954, structural steel used for bridges conformed to the ASTM A7 specification, which required a yield stress of at least 33 ksi. In 1954, the ASTM A373 specification was introduced as a structural steel for welding with a yield stress of 32 ksi, and either A7 or A373 could be used in bridge construction (USACE 2001). In 1960, the ASTM A36 specification was created through consolidation of A7 and A373, increasing the minimum yield stress to 36 ksi (ASTM 2008).

TxDOT bridge construction specifications in 1951 required the use of A7 steel for all structural steel applications in bridges (THD 1951). Similarly, AASHO bridge specifications through 1961 call for the use of A7 steel (AASHO 1961). In the 1961 TxDOT specifications, A373 steel or equivalent is required for main members such as girders, while secondary members including diaphragms and stiffeners could be constructed of A7, A373, or A36 steel. A36 steel was specified as the structural carbon steel for bridges for the first time in the AASHO specifications in 1965 (AASHO 1965). For unknown grades of steel, the AASHTO *Manual for Bridge Evaluation* recommends using a yield stress of 33 ksi for structures built between 1936 and 1963 and a yield stress of 36 ksi for structures constructed after 1963 (AASHTO 2011).

Only one set of plans inspected during the survey, which included two bridges constructed in 1964, specified the type of structural steel to be used for the girders. These plans called for either ASTM A36 or A373 steel. Because all other bridges in the survey were designed according to AASHO specifications prior to 1965, they are conservatively assumed to have used A7 steel and have a yield stress of 33 ksi.

3.3.2 Concrete

The deck concrete for all but one of the bridges investigated in the survey is specified as TxDOT Class A concrete. The final bridge was specified as Class X concrete, which is not present in any of the TxDOT specifications referenced in this report. This may refer instead to the AASHO specifications where Class X concrete is generally used for massive or lightly reinforced concrete (AASHO 1961). Table 3.2 summarizes the requirements for Class A concrete in 1961.

Table 3.2 Composition of Class A Concrete (THD 1961)

Minimum sacks of cement per cubic yard	5
Minimum 28-day compressive strength	3000 psi
Maximum water per sack of cement	6.5 gal
Range of slump	2–3 in.

3.3.3 Reinforcement

In the TxDOT specification from 1961 and the AASHO specifications through 1965, reinforcing bars were allowed to be fabricated as billet-steel bars (ASTM A15) or rail-steel bars (ASTM A16). Both of these standards specify a minimum yield stress of 33 ksi for structural grade material (ASTM 1963). Billet-steel bars were also available in intermediate or hard grade, with minimum yield stresses of 40 and 50 ksi, respectively. For unknown grades of steel, it is recommended to use 33 ksi and 40 ksi for the yield strength of reinforcing bars in bridges constructed before and after 1954, respectively (AASHTO 2011).

None of the surveyed bridge plans specified a particular type of steel to be used for the reinforcing bars. Nearly two-thirds of the bridge plans stated that a design allowable stress of 20,000 psi was used. Based on the construction dates of the surveyed bridges, it is assumed that the reinforcing bars in all bridges have a yield stress of 40 ksi.

3.4 Bridge Geometry

Just over half of the surveyed bridges are four-girder bridges, but the number of girders across the width of the bridge varies between three and ten within the survey. Girder spacing varies between 6 and 9 ft. Nearly half of the bridges are skewed to angles varying between 7° and 60°. Most of the bridges are straight, but five have horizontal curvatures up to 7.5°.

Among the 22 typical bridges in the survey, a total of 35 different steel units were studied. Six of these are simple spans, and were thus ignored. Of the remaining units, more than half are three-span. The rest are two-, four-, or five-span continuous units. The continuous span lengths vary from 40 to 270 feet, and the majority of the bridges have symmetric span layouts.

3.5 Girder Details

Most of the units in the surveyed bridges are rolled shapes, but there are four bridges with plate girder units as well. The following sections summarize the common girder shapes, splicing procedures, and cover plate details for units consisting of both rolled shapes and plate girders.

3.5.1 Rolled Shapes

The majority of the continuous units having steel beams composed of rolled shapes are 33- or 36-inch-deep wide flange sections, although depths as low as 27 inches are present. Only a few units have a section transition within the continuous unit. All webs and flanges are compact according to the current AASHTO specifications, assuming a yield stress of 33 ksi (AASHTO 2010). Splices are located near inflection points and spaced 30 to 70 feet apart.

Cover plates are welded symmetrically to the top and bottom flanges over most interior piers of the continuous units. Additionally, a few of the bridges have cover plates on the top and bottom flanges near midspan. The cover plates range from 5/16 to 1 inch thick and from 6 to 14 inches wide. The length of the cover plates vary from 8 to 48 feet, with the plates over 17 feet long located near midspan. Only one of the units with rolled shapes has bearing stiffeners (5 inches wide and 3/8 inches thick). No intermediate stiffeners are present.

3.5.2 Plate Girders

The four bridges with plate girder units either span over rivers or provide large highway connections with spans in excess of 100 feet long. The constant depth plate girders are 4 to 5 feet

deep, while the haunched girders vary between 6 and 10 feet deep along the length of the bridge. All of the flanges are compact, although a few are very close to the compact limit according to the current AASHTO specifications with a yield stress of 33 ksi (AASHTO 2010). Most of the webs are noncompact, and a few of the webs are slender.

Field splices are located near inflection points and are spaced 30 to 100 feet apart. Many shop flange and web splices are present along the length of the girders. Two of the four units have cover plates over the piers in addition to flange transitions. Bearing stiffeners vary in size from 6 to 12 inches wide and 1/2 to 3/4 inches thick. Intermediate stiffeners are 5 to 8 inches wide, around 3/8 inches thick, and spaced at 2.5 to 6 feet, often on alternating sides of the girder.

3.6 Cross Frame Details

While the member sizes vary slightly depending on the girder spacing and skew angle, the cross frames for all bridges in the survey are of the three general types shown in Figure 3.2 below. Typical member sizes are also shown in the figure. All connections are welded. Cross frame spacing varies between 16 and 21 feet along the bridges, and there is not always a cross frame located at interior piers.

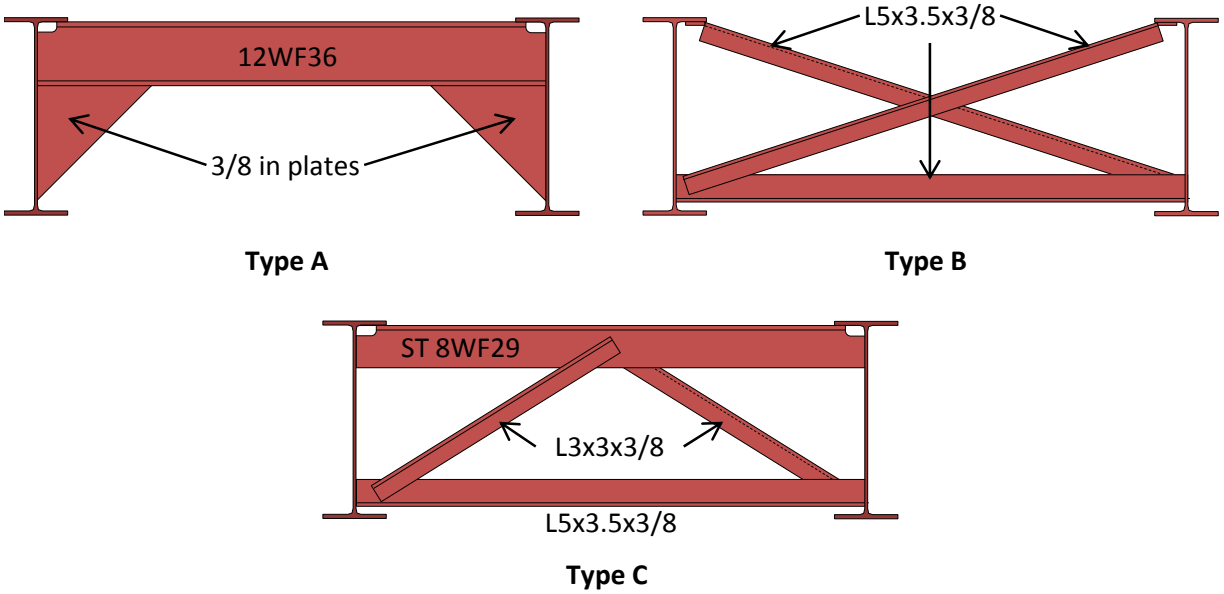

Figure 3.2 Typical Cross Frame Types and Member Sizes

Type A cross frames consist of a typically 12-inch-deep wide flange section connecting the top flanges of the girders, usually with triangular 3/8-inch thick plates extending nearly to the bottom flange below. In a few cases, these plates are trapezoidal, rectangular, or not present at all. These cross frames are usually placed at the ends of units, including at abutments. In skewed bridges, Type A cross frames are always skewed.

Type B cross frames are X-shaped frames constructed of single angle members, almost exclusively L5x3.5x3/8 sections. The connection details vary among the bridges. In most cases, the angles are welded directly to the girder, but in a few bridges the angles are welded to a stiffener. Type B cross frames are located in the interior of units except for at construction joints.

Type C cross frames are K-shaped frames in which an 8-inch deep T-section attaches the top flanges, the diagonals are typically L3x3x3/8 angles, and another slightly larger angle section is welded horizontally near the bottom flanges. Again, the connection details vary depending on whether or not stiffeners are used. Type C cross frames are located in the interior of units at construction joints.

3.7 Deck Details

In most of the bridges surveyed, the deck is 6.5 inches thick. However, the thickness generally varies from 6 to 7.25 inches. Cover to the center of the deck reinforcement is usually 1.5 inches, but a few bridges have a 2-inch top cover. Typically #5 reinforcing bars are used throughout the deck, but some bridges use #4 bars in the bottom mat of the transverse reinforcement or for longitudinal reinforcement.

All bridges have bent transverse bars that follow the moment diagram of the cross section of the bridge (see Figure 3.3). These bars are located near the top of the deck over the girders and near the bottom of the deck between the girders. These bent bars are alternated with straight transverse bars in the top and bottom mat. Spacing between the bent and straight transverse bars is 5 to 7 inches.

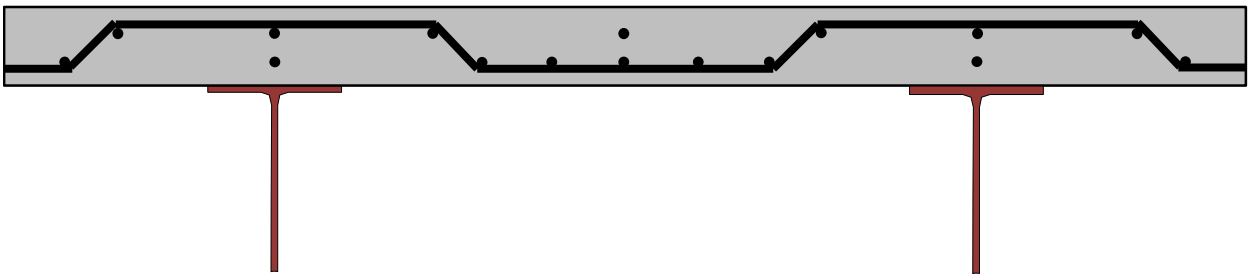

Figure 3.3 Typical Details of Deck Cross-Section Showing Bent Transverse Bars

All longitudinal bars are straight and do not have a typical spacing within the cross section, as illustrated in Figure 3.3. Longitudinal bars are placed at each inside corner of the bent bars, and distributed as needed in between. The figure shows the typical number of longitudinal bars placed around the bent transverse bars, although some bridges had more or less bars than depicted above.

The decks were typically poured in a specific sequence, with construction joints spaced 20 to 45 feet apart. Reinforcing bars span the length of each segment between construction joints with no splices. Most bridges have 30-inch long #5 dowels spaced 2 feet apart as the only reinforcement crossing the joints. A few bridges have no reinforcement crossing the construction joints.

3.8 Bridge Condition and Usage

In addition to the bridge geometry and structural details, current information about bridge condition and usage were also gathered in the survey. This includes inspection reports and photos, traffic information, and load ratings.

3.8.1 Inspection Reports

The most recent inspection report was collected for each bridge in the survey to gather an understanding of the typical condition of these bridges. The report rates different components of the bridge on a scale from 0 to 9, with 0 being a failed condition and 9 an excellent condition. Generally, superstructure and substructure ratings ranged from 5 to 7, or fair to good. Deck ratings varied from 4 to 8, or from poor to very good. A few of the bridges have had significant repairs, most often to the deck.

One very common problem noted on the inspection reports regarding the superstructure is rust. Most bridges have minor rust on all steel elements, with more severe rust often occurring on the cross frames under construction joints. Additionally, the bearings tend to have moderate rust and are often rotated to the maximum capacity. A few bridges have cracked welds on the cross frames or at the beam-bearing connections. Finally, a few of the bridges have minor to moderate impact damage.

The concrete substructure and deck have minor to moderate cracking, spalling, and delaminations in almost all cases. Some bridges have exposed rebar in the piers or in the soffit of the deck. A few bridges have expansion joints that have been either paved over, closed, or filled with debris, while others have open, leaking joints. A few of the piers have minor impact damage or evidence of poor consolidation.

3.8.2 Bridge Usage

The average annual daily traffic (AADT) varies widely from 2,000 to 265,000 vehicles per day over the bridges surveyed. This variation is largely due to location, as some of the bridges are located on main highways in large cities while others are river crossings far away from any town. The percentage of the AADT composed of trucks also varies greatly from 3% to 80% for similar reasons.

Of all of the bridges surveyed, only six have been explicitly load rated using detailed calculations. The others have been given a load rating based on the design load and the current condition of the bridge. Inventory ratings, which reflect the load a bridge can carry on an everyday basis, vary between HS 12 and HS 20. Operating ratings, which indicate the maximum overload a bridge can carry, range from HS 20 and HS 27. These ratings correspond to design loads in the AASHTO *Standard Specifications for Highway Bridges* using either Allowable Stress or Load Factor methods (AASHTO 2002). For comparison, a new bridge designed according to this specification would have an inventory load rating at or exceeding HS 20.

3.9 Two-Girder Bridges

As mentioned previously, 3 of the 25 bridges in the survey are two-girder bridges with a deck system consisting of floor beams and stringers. These bridges were ignored in the discussion above because they have very little in common with the other 22 bridges surveyed. This is partially because they were constructed significantly earlier (1937 and 1947) or later (1973), and partially because of the different floor system. This section will briefly describe each of these bridges, noting the similarities and differences as compared to the bridges discussed above.

3.9.1 I-35 over the Medina River

During the course of this research, this bridge was demolished and replaced by a new structure. However, its features are worth noting as other similar bridges may still be in existence. Originally built in 1937, this bridge had with two lanes and a 26-foot girder spacing. The bridge was not skewed or curved. It was widened and re-decked in 1974, but the widened portion was constructed compositely and was not structurally attached to the original bridge. The three-span bridge was 270 feet long and constructed of 5- to 8-foot deep haunched plate girders. The girders were built from plates and angles riveted together, and additional flange plates were added to increase the flange thickness where needed. The deck was 8 inches thick, and the bent bars spanned in the longitudinal direction, following the moment diagram created by the floor beam supports.

3.9.2 US-83 over the Nueces River

Constructed in 1947, this bridge has two lanes, an 18-foot girder spacing, and no skew or curvature. The bridge has many 50-foot long approach spans composed of rolled sections, similar to the bridges described in the previous sections of this chapter. However, there are two haunched plate girder units that span over the river. The first is a two-span 400-foot long unit, while the second is a three-span, 600-foot long unit. The girders vary from 8 to 10 feet in depth and are constructed from welded plates. The deck is 8.25 inches thick and again, the bent bars run longitudinally over the floor beams.

3.9.3 US-75 Elevated Portions in Dallas

This elevated highway was built in 1973 and spans over the Dallas metropolitan area. Although many units comprise the several miles of this elevated highway, this survey only looked at two of the units. The first is a three-span, 205-foot long unit with a 46-foot girder spacing. The second is a 500-foot long unit with girder spacing varying between 42 and 60 feet along the length. The two girders in this unit are supported separately, with one having seven piers and the other having six piers. Both units are curved approximately 5° in plan. The majority of the girder sections are a constant 6 feet deep, although a haunch up to 10 feet deep exists in a few locations. The post-tensioned deck is 10.5 inches thick.

3.10 Summary

A survey of 25 non-composite bridges from 8 districts around the state of Texas was conducted to determine the typical characteristics of bridges that could potentially be strengthened using post-installed shear connectors. Data collected in the survey includes general information, material properties, bridge geometry, girder details, cross frames, and deck details. Excluding the three atypical two-girder bridges with floor beams, the remaining bridges have several commonalities as well as some variation among these categories. This survey served as a basis for the analysis and laboratory testing discussed in the remainder of the report.

Chapter 4. Concept Studies

4.1 Overview

Following the bridge survey, initial concept studies were carried out to evaluate the feasibility of the proposed strengthening methods. These studies were conducted on a total of 13 continuous bridge units, or all of the three-span units amongst the surveyed bridges. First, all of the bridge units were load rated to characterize the existing strength. Then, strengthening criteria were set, and the bridges were strengthened to achieve the targeted load rating. This chapter discusses the procedures and results of these initial studies.

4.2 Bridges Investigated

All 13 of the three-span continuous units from the bridge survey were included in the concept studies, incorporating span lengths between 45 and 100 feet and girder spacing of between 7 and 8.5 feet. Rolled steel sections comprise all of the units, which are generally 33 to 36 inches deep. The lightest section is a W27x94 and the heaviest is a W36x194. Most of the units have cover plates at the interior piers, and approximately half of the units also have cover plates near the middle of the spans.

Almost all of the bridges considered in these studies carry two lanes of traffic, but a few are striped for three or four lanes. While the majority of the bridges are not skewed or curved, a few have skews up to 55° and horizontal curvatures up to 7.5°. Any effects of skew and curvature were not considered in these evaluations. Deck thicknesses varied between 6.5 and 7 inches.

Material properties were assumed based on common construction practices at the time, as they were usually not specified in the plans. It is likely that A7 steel was used for the girders of all of these bridges, so a yield stress of 33 ksi was chosen. A compressive strength of 3000 psi was assumed for the deck.

4.3 Strengthening Method

As part of the concept studies, two approaches to strengthening existing steel girder bridges were evaluated for feasibility and efficiency:

1. Strengthen all regions of the bridge by post-installing shear connectors to create composite action. In the negative moment regions, engage the deck reinforcement in composite action with the steel beams.
2. Strengthen only the positive moment regions using post-installed shear connectors. Allow yielding to occur in the steel beams in the negative moment regions over the interior piers, and let the moments redistribute to the surrounding strengthened positive moment regions as necessary.

Figure 4.1 and Figure 4.2 illustrate the increase in flexural capacity and stiffness, respectively, of the girders comprising a typical bridge from the survey as a function of the composite ratio (η). These figures demonstrate the efficiency of partial composite action in the positive moment regions. For example, by adding 30% of the shear connectors that would be required for full composite action ($\eta = 0.3$), increases of nearly 40% in strength and 80% in stiffness are achieved for this particular girder. The figures also demonstrate the limitations of

composite behavior in the negative moment regions. For a fully composite section in the negative moment region ($\eta = 1$), an increase in both the flexural capacity and stiffness of only 10% can be achieved.

The minimal benefits of developing composite action in negative moment regions present a potential problem with the first strengthening approach. Additionally, some of the bridges in the survey have deck construction joints located at the pier sections with either no or minimal continuous deck reinforcement passing through the joint. If there is no reinforcement through the joint or if the reinforcement is not adequately developed, no flexural capacity in negative bending can be gained through composite action. Due to the limited ability for composite action to provide a significant amount of strength to the negative moment regions and the lack of continuous deck reinforcement at interior piers of some of the surveyed bridges, this first method was discarded and the focus of the research was placed on the second strengthening method.

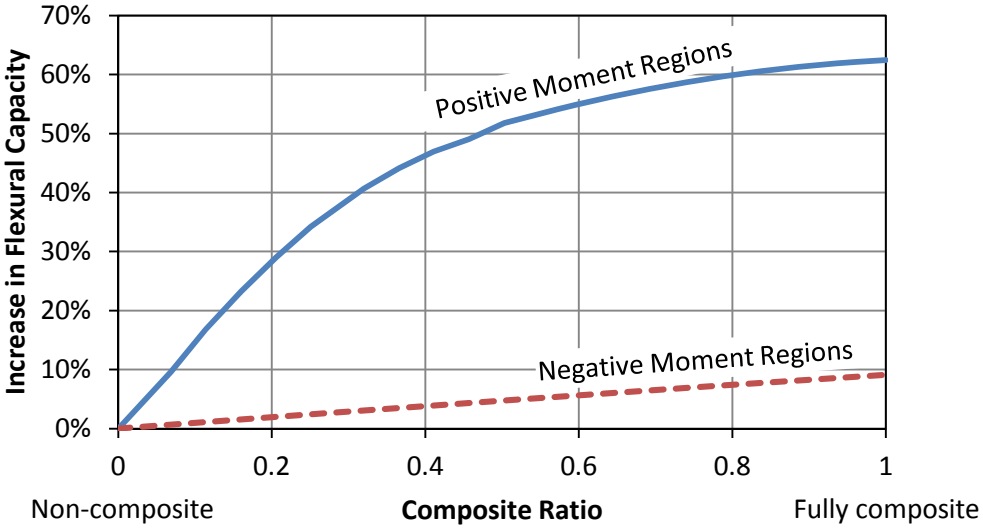

Figure 4.1 Flexural Capacity of Partially Composite Girders

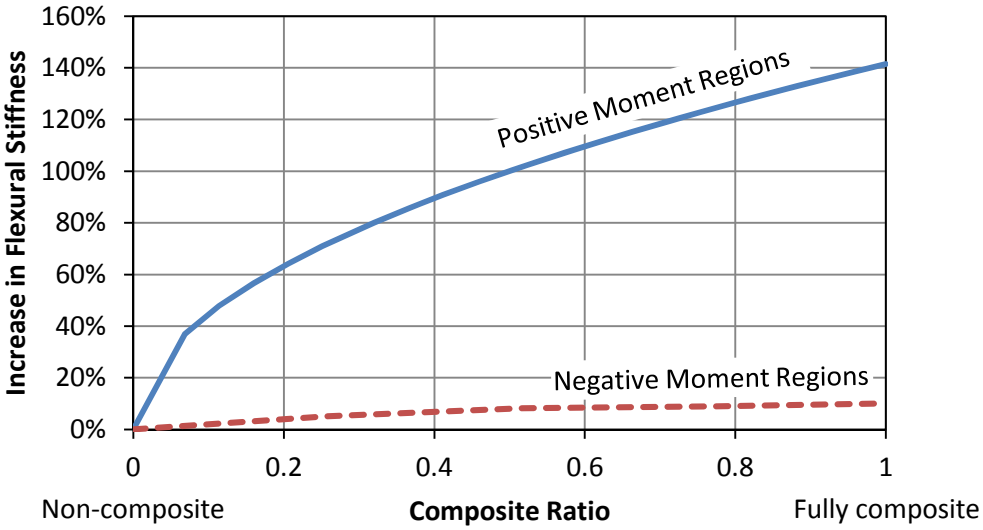

Figure 4.2 Flexural Stiffness of Partially Composite Girders

4.4 Overview of Load Rating

Load rating provides a comparison of the load-carrying capacity of an existing bridge to the loads that are used in current design practices. This is a way to evaluate the safety of an existing bridge that was designed for different, usually smaller, loads.

4.4.1 Types of Load Rating and Limit States

The AASHTO *Manual for Bridge Evaluation* specifies procedures for conducting a load rating of an existing bridge using three methods: allowable stress rating, load factor rating, and load and resistance factor rating (AASHTO 2011). Load factor rating, based on the load factor design provisions from the most recent version of the AASHTO *Standard Specifications for Highway Bridges*, was chosen for the purposes of these studies to be consistent with typical TxDOT practices (AASHTO 2002).

A complete and thorough load rating would check flexure, shear, and axial forces at all locations in every member as well as the connections and any other details. The final reported load rating of a bridge would be the smallest rating calculated anywhere along the bridge. However, for a particular type of bridge, the controlling sections and limit states can often be easily identified beforehand to simplify the process. For the continuous steel I-girder bridges considered in this study, the flexural capacity of the girders will usually control, especially if the girders are composed of rolled sections. For built-up sections with stiffeners and very thin webs, a load rating for shear should also be considered. Connections, such as girder splices, are not normally considered in the rating process but can be if necessary or desired. Since the bridges considered here are composed of rolled sections and the welded girder splices carry low levels of load, only the flexural behavior was considered in the load rating.

Load ratings for strength can be computed at both inventory and operating rating levels. The inventory rating is associated with load magnitudes used in the design of a new bridge and makes use of the same load factors. Live loads equivalent to the inventory rating should be able to be resisted indefinitely throughout the life of the bridge, barring any fatigue or durability-related failures. The operating rating represents the maximum load the bridge can sustain. Repeated application of this large level of load to the bridge is not recommended (AASHTO 2011).

The limit states considered in these load ratings were Overload and Maximum Load as defined by the AASHTO standard specifications (AASHTO 2002). The Overload limit state restricts permanent inelastic deformations from heavy permit vehicles that may be occasionally allowed on the bridge (Hansell and Viest 1971). It corresponds to the Service II limit state in the LRFD specifications, and restricts the maximum stresses in the steel girder to 80% and 95% of the yield stress for non-composite and composite sections, respectively. Because the AASHTO specifications do not allow for partially composite design, it is unclear what limiting stress should be used for partially composite sections, but a 95% limit has been chosen for these studies. When moment redistribution is considered from the interior supports, the stress limit at the Overload limit state is ignored in those regions. The Maximum Load limit state is associated with the ultimate capacity of the bridge and corresponds to the Strength I limit state in the LRFD specifications when primarily considering gravity loads. Limit states involving serviceability, lateral loads, or other types of loads are generally not considered in load rating. The fatigue limit state can be investigated using provisions in the *Manual for Bridge Evaluation* if desired (AASHTO 2011).

4.4.2 Load Rating Procedures

The first step in load rating is to conduct a structural analysis of the existing bridge using the live load corresponding to the chosen rating method. For the load factor rating conducted here, this was an HS 20 live load as defined in the AASHTO standard specifications and summarized in Figure 4.3.

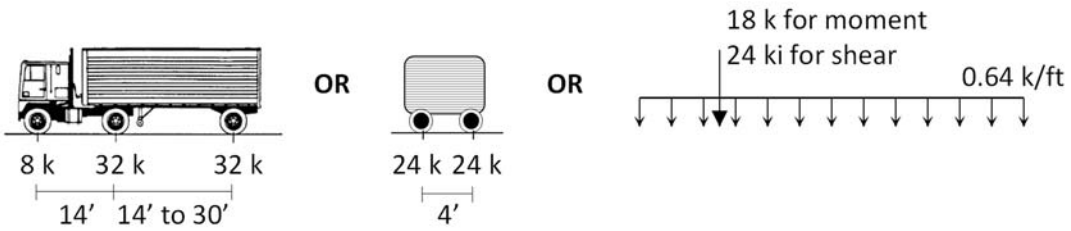

Figure 4.3 HS 20 Live Load (AASHTO 2002)

Next, the flexural capacities of the critical sections of the bridge are calculated. For load factor rating, the capacity is calculated using the design provisions in the AASHTO standard specifications. For a compact, laterally braced section in flexure, the capacity is taken as the plastic moment (M_p) for the Strength I limit state. For the Service II limit state, the capacity refers to the limits on maximum stress in the steel beam. Actual or estimated in situ material properties should be used in the load rating calculations. Because this information was not readily available for these studies, the recommended material properties from the *Manual for Bridge Evaluation* were used (AASHTO 2011).

The next step is to compute the rating factor, which represents the fraction of the live load that the bridge can safely carry. The bridge can adequately resist the full live load if the rating factor is greater than or equal to unity. A rating factor is calculated for every critical section for both the inventory and operating rating levels. Generally, the rating factor (RF) is defined as the ratio of the capacity available to resist live loads to the factored live load:

$$RF = \frac{C - A_1 D}{A_2 (L + I)} \qquad \textit{Equation 4.1}$$

where C is the capacity of the section, D is the dead load force effect, $(L + I)$ is the live load force effect including the impact factor or dynamic allowance, and A_1 and A_2 are load factors that depend on the type and level of the load rating. For load factor rating, A_1 is taken as 1.3 for both the inventory and operating levels, and A_2 is taken as 2.17 for the inventory rating and 1.3 for the operating rating. Because the only difference between the inventory and operating load rating calculations is the load factor on the live load (A_2), the two ratings will differ by a constant factor for all bridges. The operating rating will always be 1.67 times greater than the inventory rating.

The final step in the rating procedure is to express the rating factor in terms of the live load. This is simply done by multiplying the rating factor by the magnitude of the HS load used in the structural analysis. For example, for the HS 20 load used here, the rating factor is multiplied by 20. The lowest inventory and operating load ratings from every section along the bridge are then chosen as the final load ratings for the bridge.

The load rating calculations were carried out through the BAR7 computer program (PennDOT 2010). This software, developed by the Pennsylvania Department of Transportation,

analyzes a single girder line of a bridge using the provisions outlined in the *Manual for Bridge Evaluation.*

4.5 Load Rating Results

The 13 three-span bridges from the survey included in the concept studies were load rated before and after strengthening to evaluate the proposed strengthening method. Figure 4.4 shows a bar graph summarizing the results for existing and strengthened bridges. No moment redistribution was considered for the existing non-composite bridge girders. All girders were strengthened to a composite ratio of 30%, and the figure illustrates the variation in load rating for the strengthened girders both with and without consideration of moment redistribution.

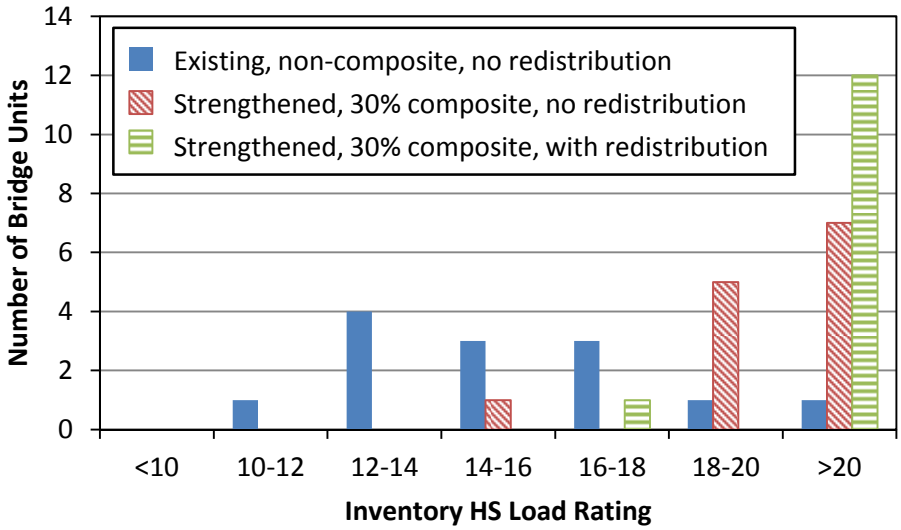

Figure 4.4 Load Rating Results

The existing bridges have inventory load ratings varying from HS 10.5 to HS 21.6, with 12 of the 13 bridges falling below the HS 20 target. The controlling load rating for all 13 of the existing bridges was the Overload limit state in one of the positive moment regions along the girders. This indicates that these bridges are good candidates for the proposed strengthening method, which is most effective in regions of the bridge dominated by positive bending. The Overload limit state is expected to control over the Maximum Load limit state for compact well-braced steel sections that can develop the full plastic moment capacity (Mertz 2004).

Without considering any moment redistribution, the strengthened bridges have inventory load ratings ranging from HS 15.0 to HS 23.9 with just over half of the strengthened bridges exceeding the HS 20 target. The controlling load rating for all of these girders is the Overload limit state in the negative moment regions, indicating that composite behavior has provided a significant strength gain in the positive moment regions. It also indicates that considering moment redistribution can further increase the load rating.

All but one of the 13 bridges have an inventory load rating exceeding HS 20 after strengthening to a composite ratio of 30% and considering moment redistribution. For most of the girders, the controlling load rating for this case is the Maximum Load limit state in negative moment regions, although a few bridges are controlled by the Overload limit state in positive

bending. It is important to note here that the greatest contributor to the increase in the load rating by considering moment redistribution is from the removal of the stress limits at the interior supports so that the girder is allowed to reach the effective plastic moment at these locations under the Overload limit state. This leads to a large increase in the defined capacity at the Overload limit state, which often results in a significant increase in the load rating without actually requiring any moments to be redistributed. For all bridges in this study, the flexural capacity at an interior pier for the Overload limit state increases by 35% to 45% as the stress limit is removed and the effective plastic moment is allowed.

The only bridge that required moments to be redistributed in addition to this increase in capacity is the single bridge that remained below the HS 20 rating target. To reach an HS 20 inventory rating, this bridge must be strengthened to nearly fully composite in the positive moment regions with 13% of the elastic moment at the interior supports redistributed to the adjacent span regions.

4.6 Summary

Thirteen three-span bridge units from the survey were investigated to evaluate the feasibility of the proposed strengthening method involving post-installed shear connectors and inelastic moment redistribution. The existing non-composite bridges were nearly all load rated below an HS 20 inventory level, which was chosen as the strengthening target for these studies. By adding post-installed shear connectors for a composite ratio of 30% and considering moment redistribution, all but one of the bridge units can be strengthened to an inventory load rating exceeding HS 20. The results of these initial concept studies are promising for strengthening existing non-composite bridges in this manner.

Chapter 5. Fatigue Testing

5.1 Overview

Because the fatigue limit state often controls the design of conventional welded stud shear connectors in a bridge, it is necessary to consider the fatigue strength in developing post-installed shear connectors. The main goals of this phase of research were to obtain additional data on the fatigue resistance of the adhesive anchor connector in order to more confidently recommend design equations, and to investigate the effect of stress reversal on the fatigue behavior. This chapter describes the laboratory test setup and results for the small-scale direct-shear fatigue testing on individual connectors.

5.2 Test Setup

The tests investigating stress reversal were modeled after the fatigue testing completed in TxDOT project 0-4124 (Kwon et al. 2007). A direct-shear test setup was adopted, in which a single shear connector attaches a steel plate to a concrete slab, as shown in Figure 5.1. By applying a cyclic load to the end of the plate with a 100-kip capacity hydraulic ram, the connector is loaded in nearly pure shear. The 1-inch thick steel plate, measuring 12 inches wide and 60 inches long, represents the top flange of the girder in a composite bridge beam. The 7.5-inch thick concrete slab, with details shown in Figure 5.2, represents the deck. While the slab is slightly thicker than the bridges in the survey, the reinforcement layout is representative of the surveyed bridges. The slab was bolted to the strong floor to resist any movement, and the load was measured using a load cell with a capacity of 100 kips. The connectors were installed following the procedure described in Section 8.4 using 7/8-inch diameter threaded rods and Hilti HIT-HY 150-MAX structural adhesive. An embedment depth of 4.5 inches was used for all connectors.

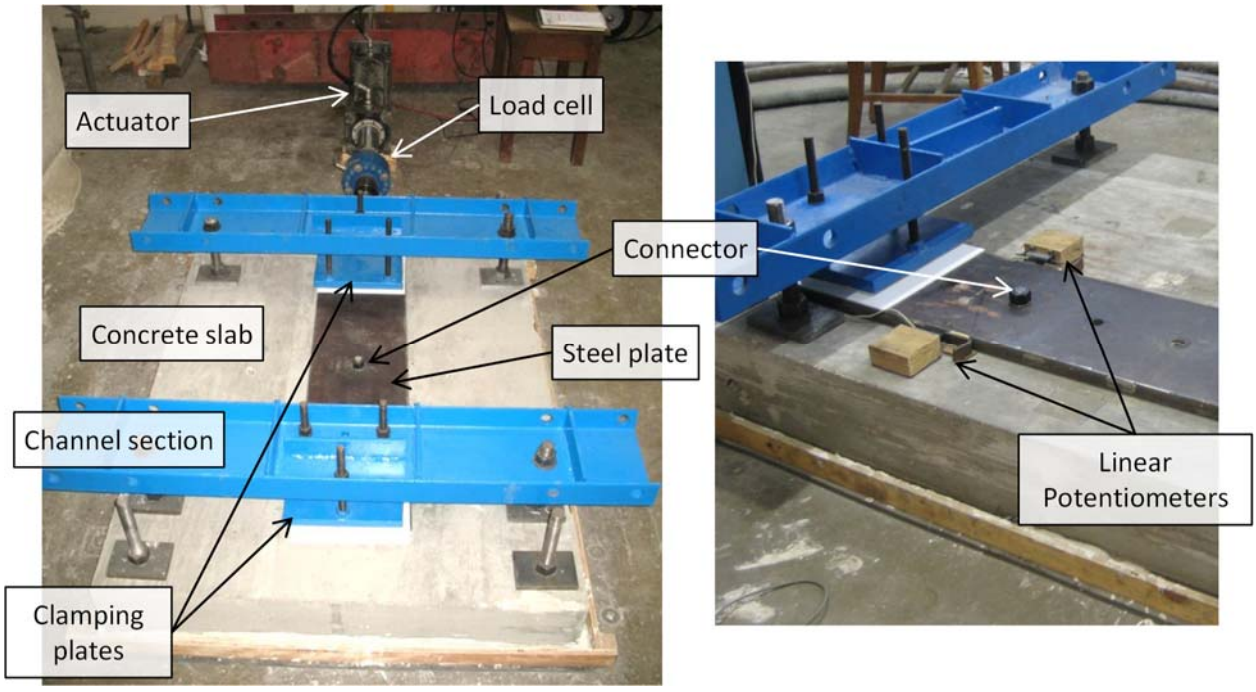

Figure 5.1 Direct-Shear Test Setup

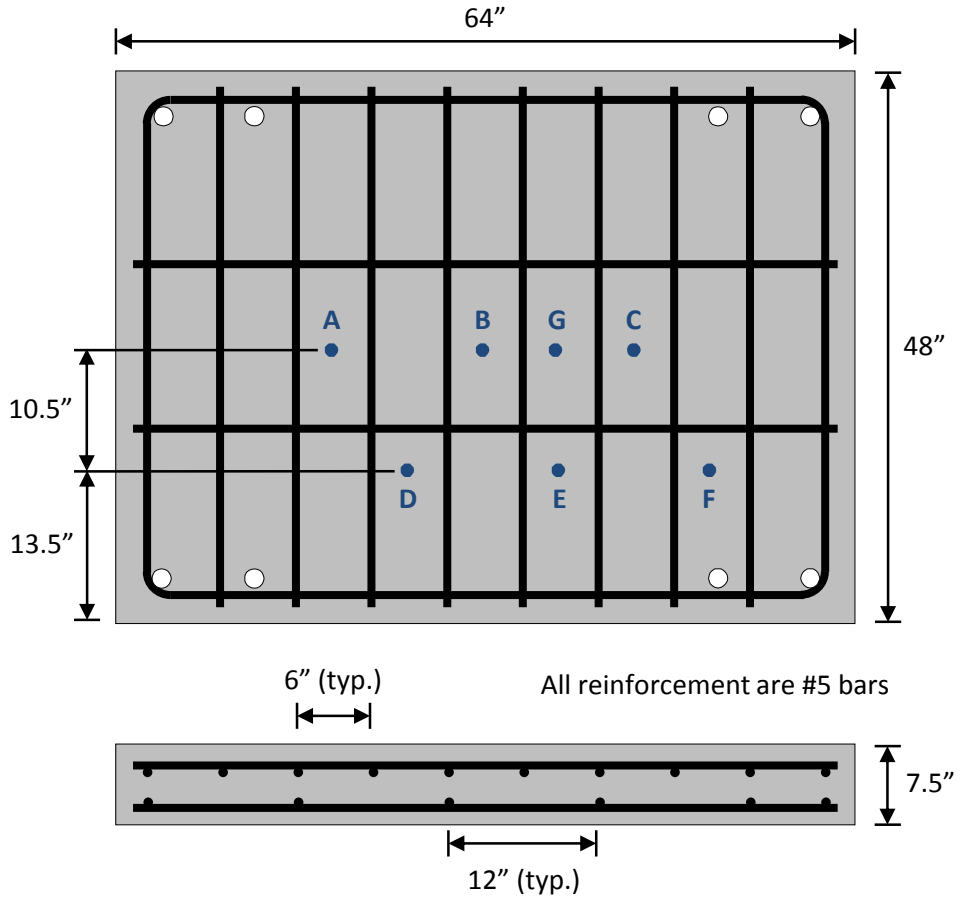

Figure 5.2 Slab Details including Connector Locations

As shown in Figure 5.1, two channels spanning across the slab were attached to smaller plates that help to resist uplift of the loading plate. Polytetrafluoroethylene (PTFE) sheets placed between the clamping plates and the loading plate minimized the friction. Except for the first test, all specimens were instrumented with two linear potentiometers located on either side of the plate at the location of the connector, as shown in Figure 5.1. These linear potentiometers measured the slip, or relative motion of the steel plate across the concrete slab, indicating the amount of deformation the connector undergoes. During one test, the plate was also instrumented with several strain gages to confirm that the load was being transferred between the plate and the slab primarily through the connector and not by friction.

Using this setup, the load can be applied to the shear connector in either one or both directions. Unidirectional tests were conducted by only pulling and releasing the plate, while reversal tests consisted of both pulling and pushing the plate across the slab. During unidirectional tests, a minimum load of 1 kip (or approximately 2 ksi) was maintained at all times to ensure that no accidental load reversal occurred. Reversal tests were conducted symmetrically with equivalent peak loads in the positive and negative directions. For a 20 ksi load range, a unidirectional test would range from 2 to 22 ksi, while a reversal test would range from -10 to +10 ksi. The stress range is determined by dividing the load by the effective shear area, or 80% of the gross area for adhesive anchor connectors which have threads in the shear plane. The effective shear area for the 7/8-inch diameter adhesive anchors that were tested here is 0.48 square inches.

The small-scale fatigue tests were conducted using a closed loop control system as described in detail in Patel (2013). The unidirectional and reversal tests were conducted under sinusoidal loading with a frequency of 4 Hz and 1 Hz, respectively. A few cycles of data were collected at regular intervals to track the trends in slip as the tests progressed. A sampling rate of 500 Hz was used, and the time interval between data collection varied depending on the stress range and expected fatigue life of each particular connector.

The test matrix is shown in Table 5.1, with all 26 specimens listed in the order in which the tests were conducted. Of these tests, 17 were performed under unidirectional loads, while the remaining 9 were performed under reversed load. Generally, three tests at each stress range were conducted at a variety of locations on eight different concrete slabs. Figure 5.2 depicts the positions on the slab where connectors were located for testing. Three unidirectional tests, marked with an “a” after the test number in Table 5.1, did not fail after at least 2 million cycles of loading. For these three tests, the stress range was increased and the test was continued, as indicated by a “b” after the test number. All of the reversal tests failed in fatigue at the initial stress range.

Table 5.1 Test Matrix for Direct-Shear Fatigue Tests

Unidirectional Tests						Reversal Tests		
Test #	**Stress Range (ksi)**	**Slab #, Position**	**Test #**	**Stress Range (ksi)**	**Slab #, Position**	**Test #**	**Stress Range (ksi)**	**Slab #, Position**
1	45	1B	10	30	5A	1	25	3B
2	25	2B	11	30	6C	2	35	5B
3	45	4A	12	20	6A	3	35	6E
4a	25	4F	13	20	6F	4	30	7B
4b	45	4F	14a	15	6D	5	25	7E
5	45	4E	14b	35	6D	6	30	7G
6	25	4D	15	35	7A	7	35	8B
7	25	5F	16a	20	7C	8	25	8G
8	35	5E	16b	35	7C	9	30	8E
9	35	5D	17	30	7F			

5.3 Test Results: Stress Range Approach

The results from all tests are plotted along with those from TxDOT project 0-4124 in Figure 5.3. The tests that did not fail are plotted with an arrow below the data point. Results from the tests at higher stress ranges following these “run-out” tests are not included in the graph. The design S-N curve from the current AASHTO LRFD specifications is included for comparison.

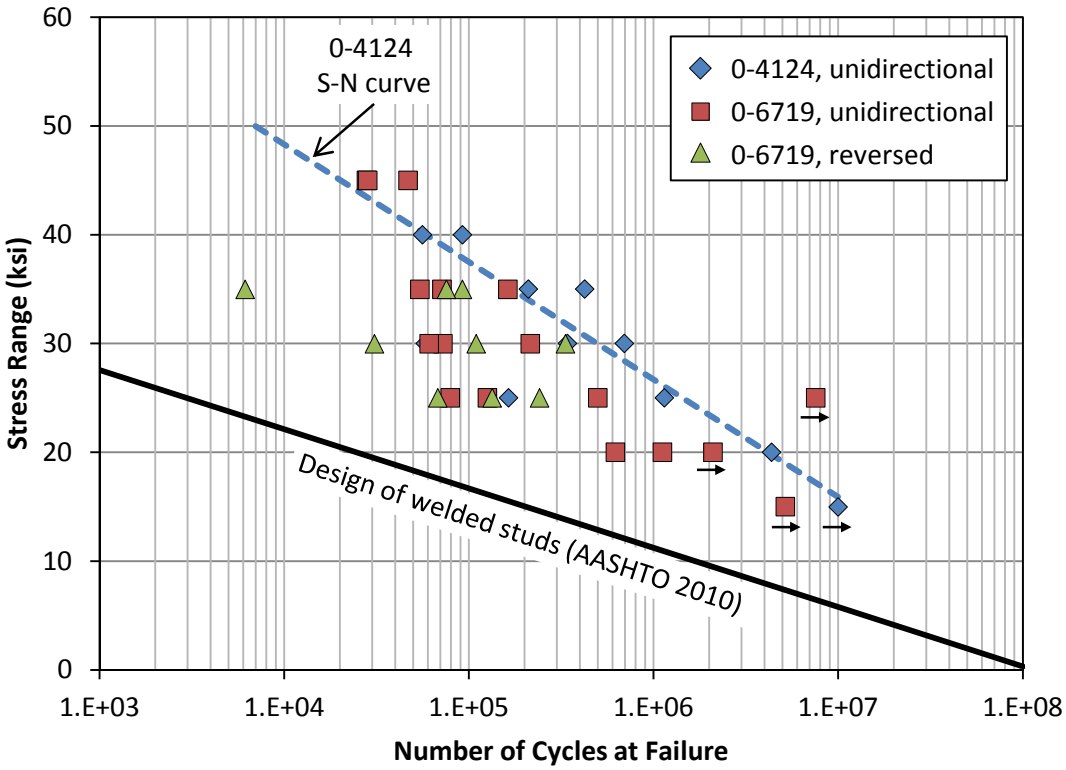

Figure 5.3 Direct-Shear Fatigue Testing Results for the Adhesive Anchor

Though the results are scattered, it seems that the adhesive anchors tested under unidirectional loading in this project exhibit slightly poorer fatigue performance than those tested in 0-4124. This could be a result of many different factors, including variation in the properties of the concrete slabs, different overall dimensions of the test specimens and test setup, slight and unintended differences in installation of the connectors, and the use of a different type of Hilti adhesive, as the particular adhesive used in the previous research was no longer available. Variations along these lines are to be expected, especially if these connectors are used to strengthen bridges in the field in the future. Additionally, connectors tested under reversed loading conditions seem to perform similarly to those tested under unidirectional loads. Although the results are scattered, one major conclusion that can be drawn from these results is that the design S-N curve recommended by previous researchers may be unconservative.

5.4 Test Results: Slip Range Approach

An alternate way to view the results is in terms of the slip range that the connector was subjected to throughout the testing, rather than the applied stress range. Figure 5.4 shows a representative load-slip behavior of a connector for a single cycle in a unidirectional test. As illustrated in the figure, the slip range was calculated as the difference between the maximum and minimum values of slip measured during one cycle. As each test progressed, these maximum and minimum values of slip tended to increase, but the slip range remained fairly constant after about the first 100 cycles. One possible reason for this observed increase in the maximum and minimum slip is that permanent compressive deformations occur in the adhesive and accumulate

with increasing number of cycles. The connector stiffness, calculated by dividing the applied load by the slip range, varied between 500 and 1600 kips per inch for all unidirectional tests.

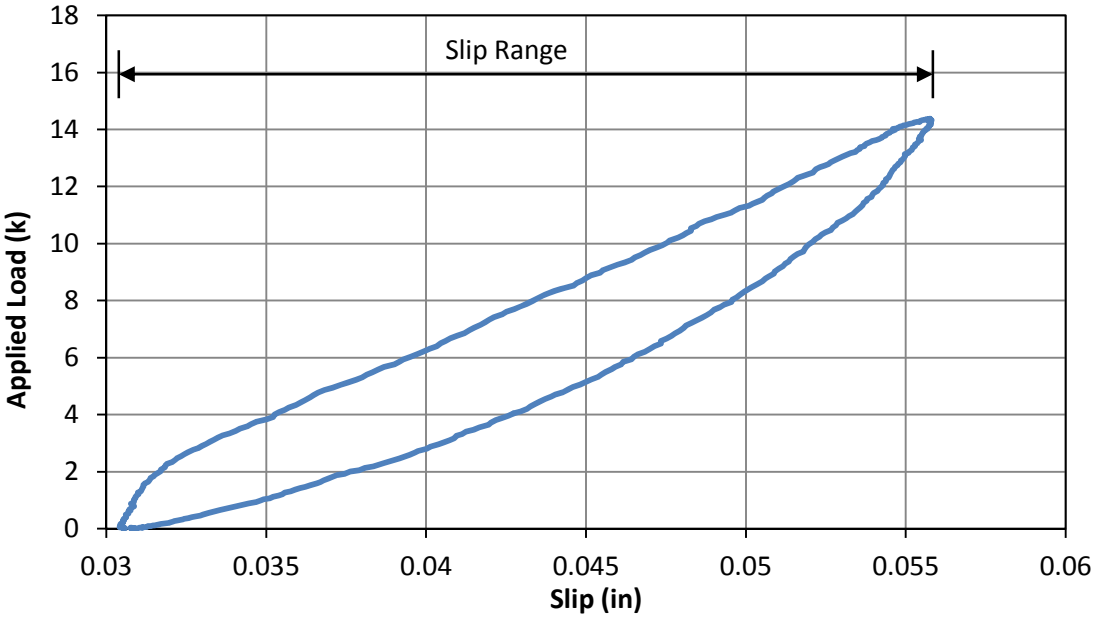

Figure 5.4 Representative Load-Slip Curve for One Cycle of Unidirectional Loading

A representative load-slip curve for a reversal test is shown in Figure 5.5. Unlike the unidirectional load-slip curve, which follows an oblong-shaped path, the reversal curve has a more complex shape. This is primarily due to deterioration of the adhesive surrounding the connector that was observed in several of the reversal tests as the number of cycles increased. This deterioration caused the formation of a region in which the connector slips, essentially free of stress, as the load is reversing direction, as indicated in the figure in the area labeled "gap region." A method to calculate the "effective slip range," or the slip range outside of this gap region, was developed and is described in Patel (2013). This effective slip range is a more useful parameter than the total slip range in describing the fatigue behavior of a connector, because it corresponds to the slip that causes stress in the connector. Although the total slip tended to increase, often to a large extent, over the course of a test, the effective slip typically remained fairly constant after the first few cycles.

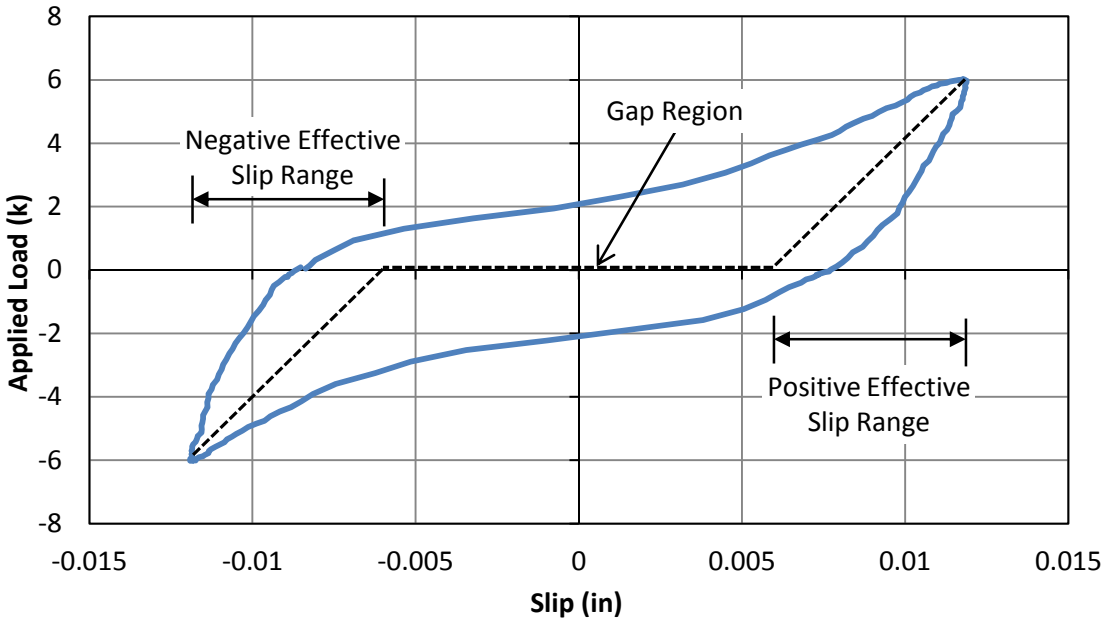

Figure 5.5 Representative Load-Slip Curve for One Cycle of Reversed Loading

It is important to note here that the observed adhesive degradation took place primarily around the portion of the connector embedded in the steel plate. The hole drilled in the plate was 1/8 inches larger in diameter than the threaded rod of the connector, placing an upper bound on the size of this gap region. During cycling with significantly degraded adhesive, the slip through the gap region was easy to observe visually. The number of cycles before the adhesive that filled the hole in the steel plate was fully degraded depended on the magnitude of the stress range.

The results from both the unidirectional and reversal direct-shear fatigue tests are plotted in Figure 5.6 in terms of slip range. Slip was not recorded regularly during the fatigue tests conducted in project 0-4124, so no comparison can be made to the previous testing. This figure illustrates that the effective slip range for the reversal tests exhibits much more scatter than the slip range for the unidirectional tests. This scatter in the data from the reversal tests may be due, at least in part, to the approximate method to estimate the effective slip.

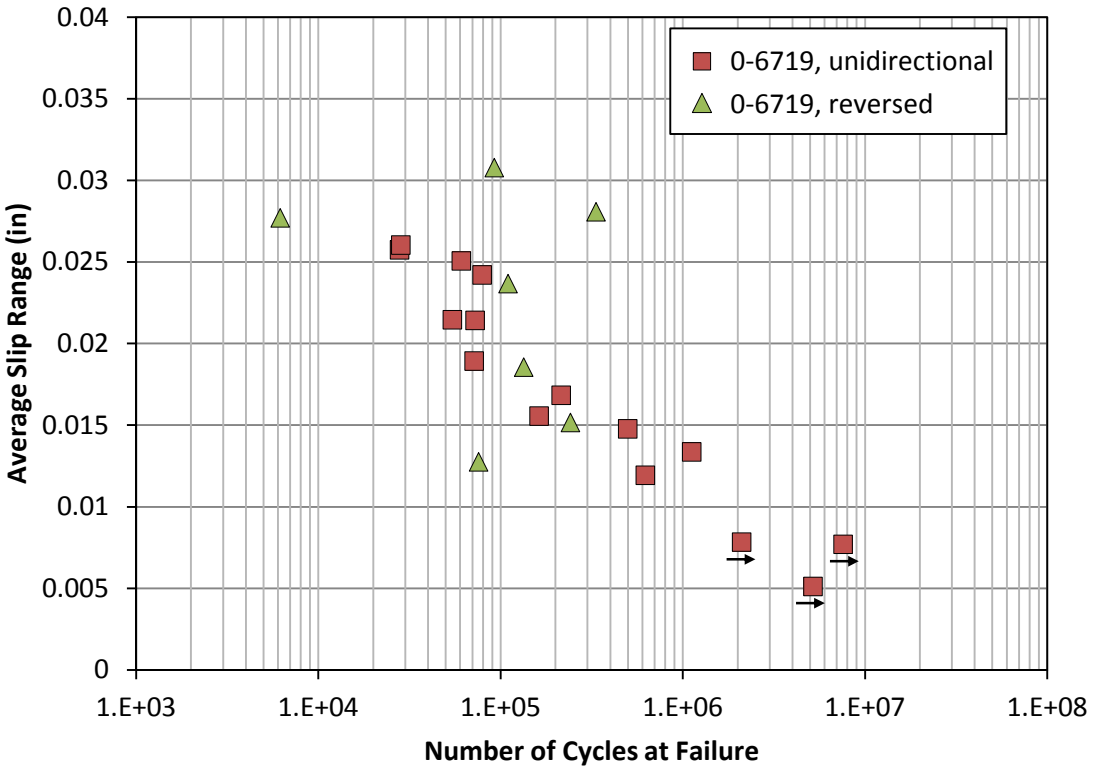

Figure 5.6 Direct-Shear Fatigue Testing Results for the Adhesive Anchor

Because the slip range depends both on the properties of the connector and on the properties of the adhesive and concrete surrounding the connector, viewing the results in terms of slip range instead of stress range removes the variable conditions of the concrete and adhesive around the connector as well as any human error during the installation process. The effect of this can be seen in Figure 5.7, which compares the results based on the stress range to those based on the average slip range for the unidirectional tests. The reduced scatter of the unidirectional tests when presented in terms of slip range, rather than stress range, can be seen in the figure. The R-squared value for the best-fit line for the unidirectional tests is 0.66 in terms of stress range and 0.86 in terms of average slip range. Slightly fewer data points are plotted for average slip range than for stress range due to lack of adequate slip data for two of the tests. Based on this data, Patel (2013) suggested endurance limits for stress range at 15 ksi and slip range at 0.008 inches.

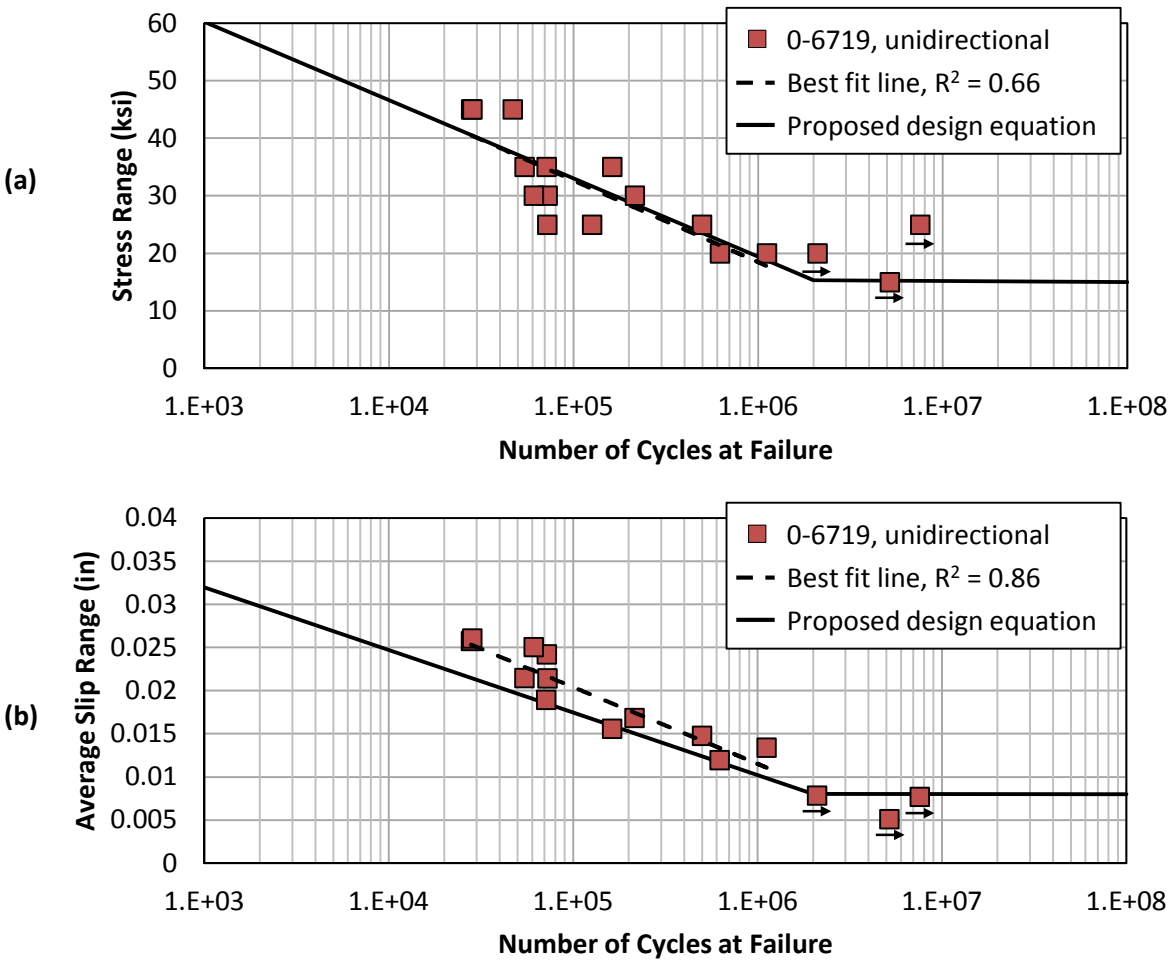

Figure 5.7 Comparison of Unidirectional Direct-Shear Results based on (a) Stress Range and (b) Average Slip Range

Fig 5.7 also shows the proposed design equations for both stress range (S_r) and slip range (s_r) as a function of the number of cycles of fatigue life (N), which are as follows:

$$S_r = 101 - 13.6\,log(N) \geq 15\ ksi \qquad \textit{Equation 5.1}$$

$$s_r = 0.0537 - 0.00725\,log(N) \geq 0.008\ in \qquad \textit{Equation 5.2}$$

While the stress range design equation closely matches the best fit line to the data, the slip range design equation tends towards the conservative side of the data. The reason for this discrepancy in the slip range equation is to maintain consistency in the design approach from both a stress and slip standpoint. As discussed in Chapter 8, the proposed fatigue design method requires an analysis that explicitly considers the slip at the steel-concrete interface of a partially composite girder and models the connectors as springs to connect the two materials. For fatigue loading, these connectors can be modeled simply as linear elastic springs, in which the stiffness directly relates the slip to the force in the connector. Based on the data from these small-scale fatigue tests, a stiffness of 900 kips per inch is recommended for a single connector. This value of stiffness corresponds to the stiffness relating the endurance limits of 15 ksi and 0.008 inches,

using the effective area to convert from stress to force. The design equations were developed to maintain an approximate stiffness of 900 kips per inch at all values of N.

5.5 Summary

A total of 26 direct-shear fatigue tests were conducted on the adhesive anchor under both unidirectional and reversed loading conditions. Though the results are scattered, they suggest that the unidirectional specimens described here performed slightly poorer than those in previous research when viewed in terms of stress range. This indicates that the design S-N curve recommended by project 0-4124 may be unconservative. Additionally, stress reversal during testing did not seem to adversely affect the fatigue performance at stress ranges of up to 35 ksi, even though significant degradation of the adhesive was observed in several of the reversal tests. Organizing the data in terms of slip range, rather than stress range, decreases the scatter significantly, indicating that deformation tends to correlate better to fatigue life than does the applied load.

Chapter 6. Large-Scale Testing

6.1 Overview

Following the initial concept studies and the small-scale fatigue testing, a large-scale experimental program was developed and executed to investigate the structural performance of continuous bridge girders strengthened with post-installed shear connectors. To represent the many different types of load a bridge girder may be subjected to over its lifetime, the girder was tested under elastic loads, fatigue loads, and large repeated loads requiring moment redistribution before monotonic testing to failure. This chapter provides details of the test specimen, the test program, and the resulting behavior under all types of loading considered.

6.2 Specimen Design

A single girder line of a two-span bridge with symmetric 42-foot long spans was chosen for testing. This span length is near full-scale, as 50-foot long exterior spans are common amongst the existing Texas bridges that were surveyed. Testing a single girder line conservatively eliminates interaction and load-sharing between adjacent girders and helps to simplify the interpretation of the results.

The specimen was designed to represent a typical bridge girder from the survey, and experience and knowledge gained from previous research influenced the shear connector layout. However, it was difficult to replicate material properties from the mid-1900s due to lack of availability of older materials. Thus, instead of ASTM A7 steel, which has a specified minimum yield stress of 33 ksi, ASTM A992 steel was used for the steel beam. The design compressive strength for the concrete deck was 3 ksi, which is typical for existing bridges, although reinforcing bars with a nominal yield stress of 60 ksi were used in lieu of bars with a 40 ksi yield stress that are likely present in the existing bridges.

As shown in Figure 6.1, the specimen consisted of a W30x90 rolled wide flange section with a 6.5-inch thick, 6.5-foot wide concrete deck. This steel beam is lighter and more slender than any found in the bridge survey and thus represents a conservative case for rolled steel members that could be found in bridge applications while preserving a realistic member depth. The deck dimensions are also representative of the decks of the surveyed bridges, although the width is slightly smaller than the typical girder spacing (7 to 8 feet). The smaller deck width, which was constrained by the geometry of the test setup, is not expected to have significantly affected the test results, because the strength of the girder is ultimately controlled by the strength of the shear connection, rather than that of the deck. The deck reinforcement was designed based on the findings from the bridge survey, and the reinforcement layout is shown in Figure 6.1. Pairs of adhesive anchors were used for shear connectors.

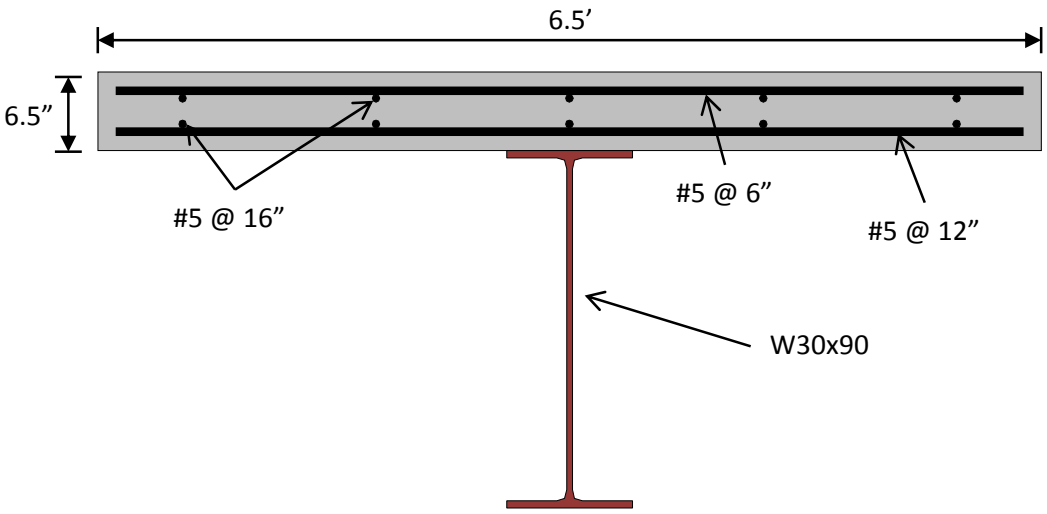

Figure 6.1 Cross Section View of Large-Scale Test Specimens

The symmetric two-span beam, shown in Figure 6.2, has two 42-foot long spans with a 12-inch overhang of the steel beam and a 6-inch overhang of the concrete deck on each end. Full-depth stiffeners were welded to each side of the web at the three support points to assist in bracing the beam during casting and to prevent localized failures at points of concentrated loads. A bolted splice in the steel beam was located 7 feet from the interior support in the south span. The splice was designed for 75% of the shear and moment capacity of the member, according to the AASHTO LRFD specifications (AASHTO 2010). Loads were applied to the beam in the four locations labeled A through D in the figure.

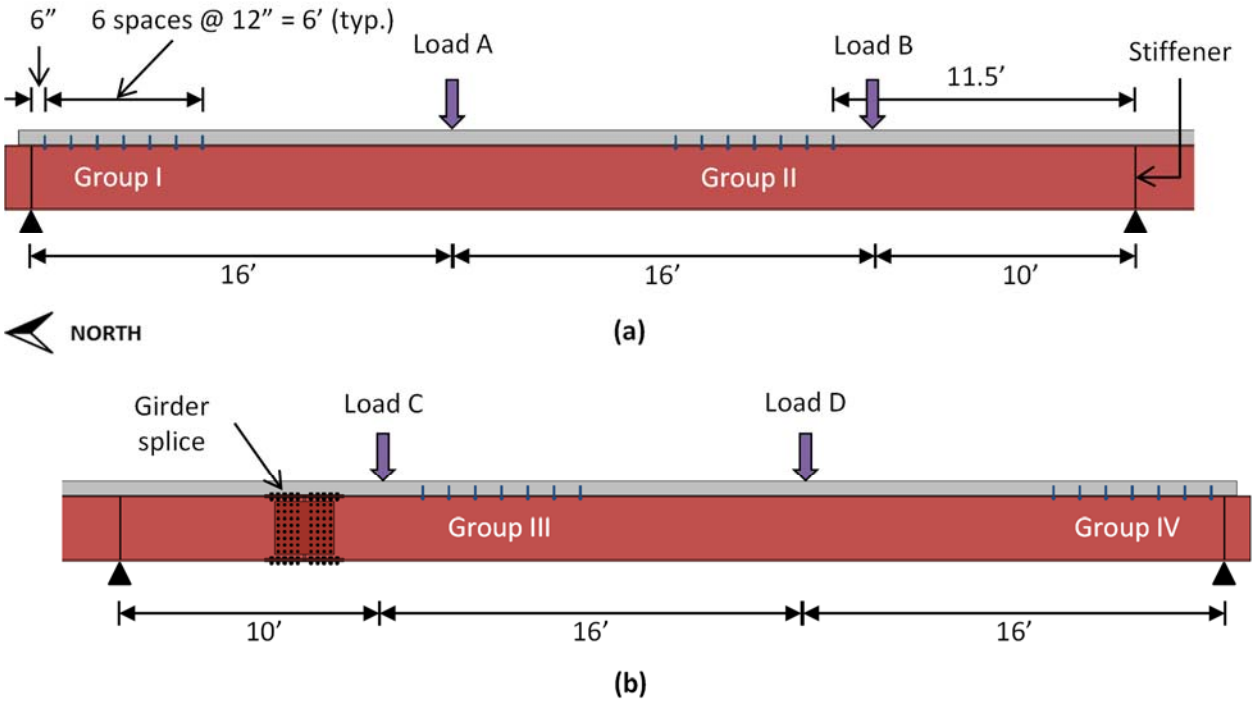

Figure 6.2 Elevation View of Test Specimen – (a) North span and (b) South span

The girder was designed as 30% composite with adhesive anchor shear connectors concentrated in four groups near points of zero moment and spaced at 12 inches longitudinally, as denoted in Figure 6.2. Groups I and II are in the north span, while groups III and IV are placed at symmetric locations in the south span. Transversely, the connectors were spaced approximately 6 inches apart on either side of the web. Each group consisted of seven pairs of connectors to reach the desired composite ratio.

6.3 Specimen Construction

The specimen was constructed in several steps, as depicted in Figure 6.3. First, the steel beams were erected (a) and spliced together (b). Next, the deck formwork, which was constructed previously, was put in place (c). After laying and tying the mats of reinforcement (d), the deck was cast (e). The formwork was removed after one week of curing.

Figure 6.3 Specimen Construction – (a) Steel erection, (b) Splice plates, (c) Deck formwork, (d) Deck reinforcement, and (e) Deck casting

6.3.1 Connector Installation

The 7/8-inch diameter shear connectors were installed approximately two months after the deck was cast, using the process described in Section 8.4 and summarized here. First, a 1-inch diameter hole was drilled through the top flange of the steel beam using a magnetic drill. Next, a 15/16-inch diameter hole was drilled into the concrete deck, through the hole in the steel beam, using a hammer drill. To maintain a 2-inch top cover for the connectors, as required by the AASHTO LRFD specifications for conventional welded shear studs, this hole was 4.5 inches deep (AASHTO 2010). The hole was then cleaned with compressed air and a brush. Finally, the adhesive was injected into the hole and the connector rod was inserted. A newer version of the same Hilti adhesive used in the small-scale fatigue testing was used for this large-scale testing (HIT-HY 200-R). The adhesive was viscous enough to not run downwards out of the hole and to keep the threaded rod in place immediately after insertion. The rod did not need to be held for any time while the adhesive cured. The threads below the underside of the top flange were wrapped with duct tape to prevent any adhesive from reaching that area. Excess adhesive was wiped off immediately with a rag. After allowing at least one hour for the adhesive to cure, a washer and nut were placed on the threaded rod of the connector and tightened to a torque of 125 ft-lb, as specified by the adhesive installation instructions.

6.3.2 Material Testing

To characterize the material strengths of the components of the specimen, several material tests were conducted on the steel beam, concrete deck, reinforcing bars, and threaded rod comprising the connectors. The results from these tests are summarized in Table 6.1.

Table 6.1 Material Properties of Girder Specimen

Material	Span	Yield Stress	Ultimate Stress
Steel beam	North	Flange: 52.4 ksi Web: 54.7 ksi	Flange: 71.7 ksi Web: 72.3 ksi
	South	Flange: 56.0 ksi Web: 54.8 ksi	Flange: 77.4 ksi Web: 78.3 ksi
Concrete deck	Both	N/A	4.7 ksi
Rebar	Both	61.7 ksi	99.0 ksi
Connectors	Both	N/A	Tension: 134 ksi Shear: 87.7 ksi

The steel beams on either side of the splice were manufactured in different heats, so the material properties differ slightly between the north and south spans. The properties were obtained by uniaxial tension testing of 8-inch long coupons that were produced from both the flange and web of each steel beam. The static yield stress is reported in the table, as it is the most comparable to the slow load rates used in laboratory testing. All strength calculations were completed using the average yield stress from the two flange coupons taken from each beam.

The concrete material properties were determined by 28-day compression testing of 4-inch-diameter, 8-inch-tall cylinders that were cast along with the deck. To account for the two trucks of ready-mix concrete that were required to complete the total volume of the deck, the

cylinders were made from a mixture of concrete from both trucks. Tension testing of the deck reinforcement was also conducted.

Shear and tension tests were conducted on the threaded rod used for the adhesive anchor shear connectors, and are discussed in more detail in Patel (2013).

6.4 Laboratory Test Setup

The test setup, pictured in Figure 6.4, consisted of three support structures and three load frames. While the interior support (b) was designed to allow for essentially free rotation and longitudinal translation through means of a circular bar, the two end supports (c) allowed for minimal motion in both directions due to the flexibility of the slender W30x90 sections that served as the supports. Global rotation about the longitudinal axis was prevented by the V-shaped frames under the deck at the end supports (c). The bottom flange of the steel beam was braced laterally at 10- to 16-foot intervals using steel plates attached to short wide flange columns at each load frame (d, e). Sheets of polytetrafluoroethylene (PTFE) were used to reduce friction at all bracing locations. Hydraulic rams with 400- or 500-kip capacities were mounted on the load frames and used to apply load to the top of the deck of the specimen. Load cells with 100- or 500-kip capacities were placed at all load and support locations. The load frames, shown in the figure for testing in the north span, were reconfigured as needed to accommodate testing in the south span.

Figure 6.4 Test Setup – (a) Overall view, (b) Interior support, (c) End support, (d) Load frame, and (e) Lateral bracing

6.5 Instrumentation

In addition to load, vertical deflections, interface slip, and longitudinal strain were measured at several points along the specimen, as shown in Figure 6.5 and Figure 6.6 for shakedown testing and fatigue testing, respectively. The figures depict the instrumentation layout for testing in the north span, but mirrored layouts were used for testing in the south span. Deflections were measured with either linear potentiometers with a 4-inch stroke or string potentiometers with a 10-inch stroke. Slips were measured with linear potentiometers with a 2-inch stroke. These potentiometers were attached to the underside of the deck and measured displacement relative to a small steel angle fixed to the underside of the top flange. More than 250 strain gages with a 6-mm length were glued to the steel beam and deck reinforcement to monitor longitudinal strain in many locations. These gages were used to monitor the neutral axis depth, which indicates the amount of composite action, and to estimate the force carried by a pair of connectors.

To obtain an approximate measurement of the connector force and stress, sets of strain gages were placed through the depth of the steel beam 6 inches to either side of a connector pair. From the measured strains, the curvature was approximated, and the axial force in the steel beam was computed. The force carried by a connector pair was then estimated by taking the difference between the axial force in the steel beam on either side of the connectors. It was assumed that the two connectors in each pair shared the load equally. The shear stress in an individual connector was then calculated by dividing the connector force by the effective shear area.

Figure 6.7 shows the locations of the strain gages in a cross section for different types of testing, and Figure 6.8 contains photographs of the various types of instrumentation.

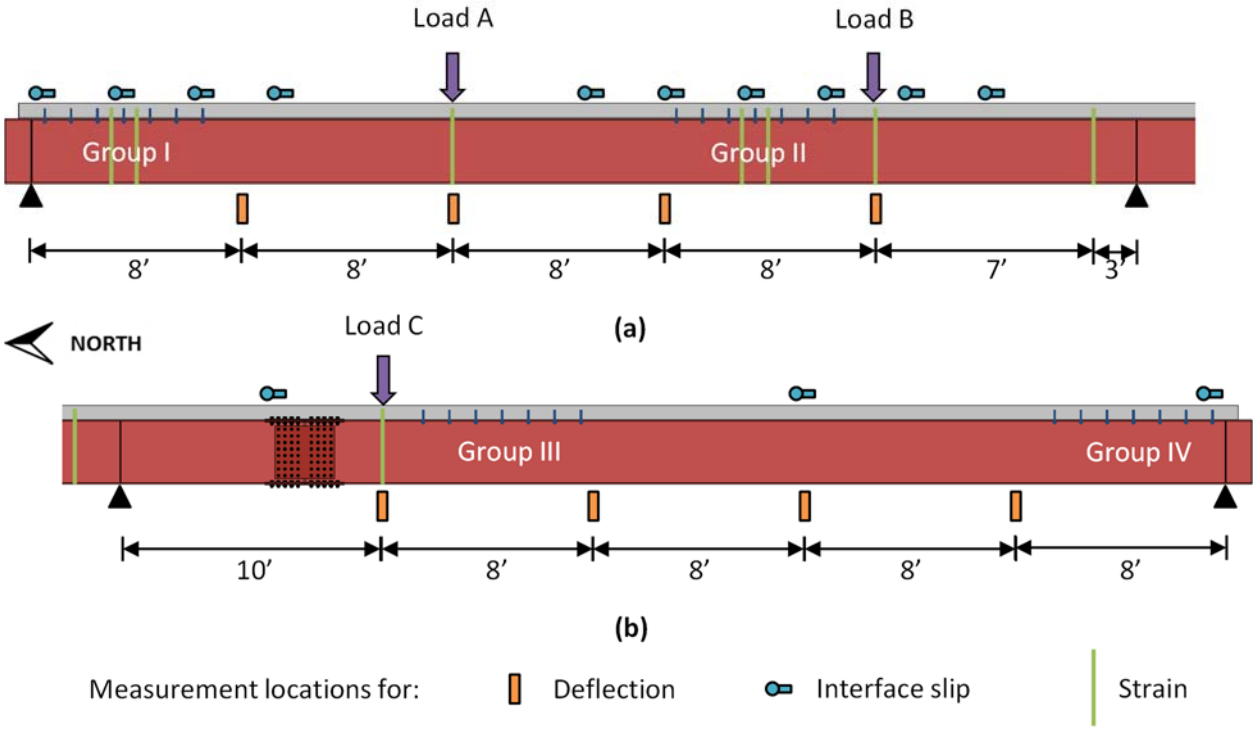

Figure 6.5 Instrumentation for North Span Shakedown and Ultimate Strength Tests – (a) North Span and (b) South Span

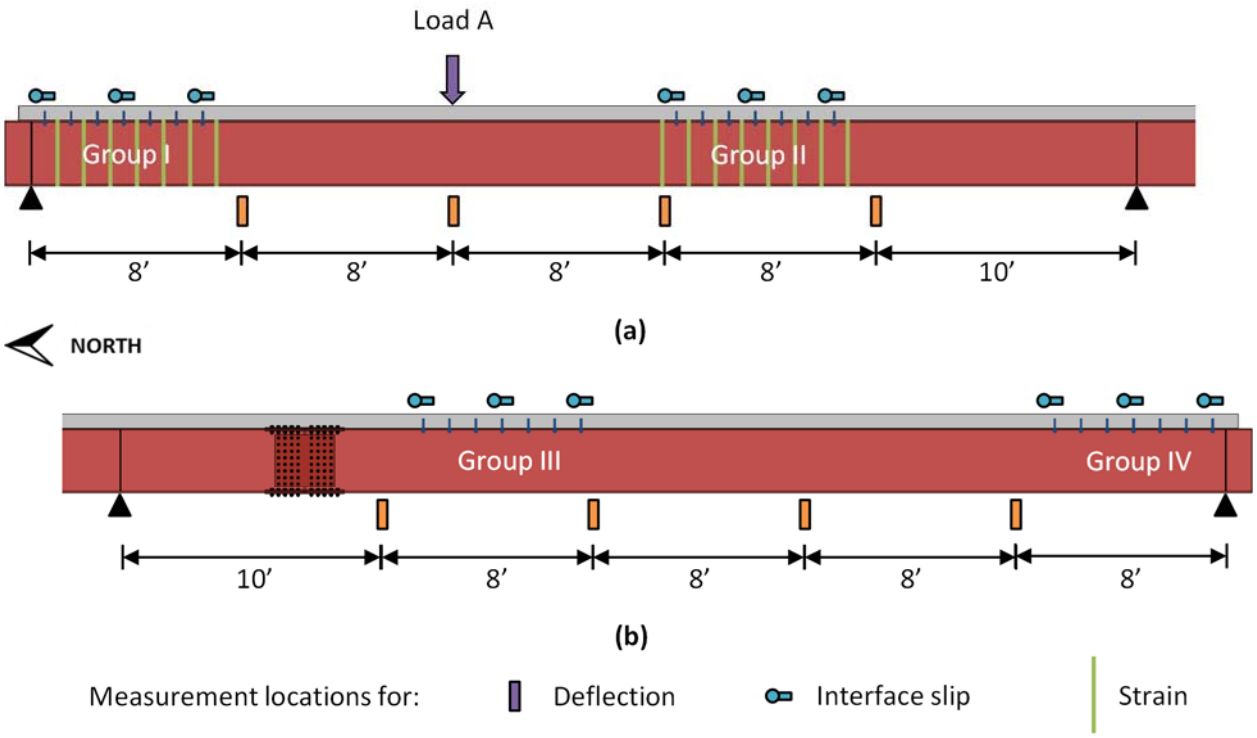

Figure 6.6 Instrumentation for North Span Fatigue Test – (a) North Span and (b) South Span

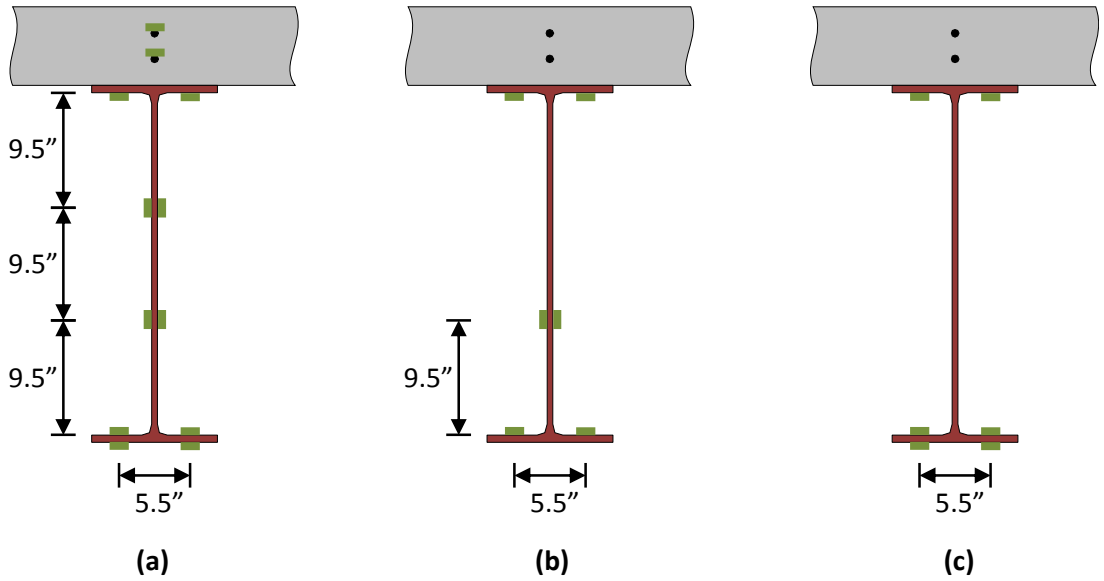

Figure 6.7 Cross Section Strain Gage Locations for (a) Shakedown and Ultimate Strength Tests, (b) North Span Fatigue Test, and (c) South Span Fatigue Test

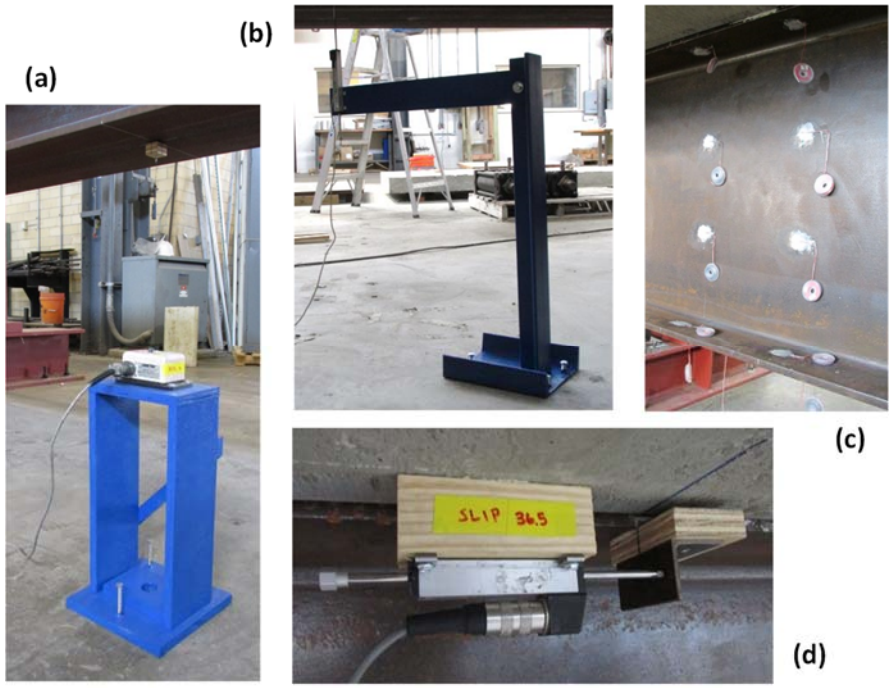

Figure 6.8 Instrumentation – (a) String Potentiometer, (b) Linear Potentiometer for Deflection Measurements, (c) Strain Gages, and (d) Linear Potentiometer for Slip Measurements

An optical motion tracking system (Optotrak Certus™) was used to monitor the localized inelastic deformations in the steel beam during strength testing at the three critical locations, namely at the location of Loads A and D and at the interior support. This system is composed of "markers," which are attached to the specimen and emit rapid pulses of infrared light, and "position sensors," which track the location of each marker in 3D space to an accuracy of 0.01 mm. Post-processing of the data consisted primarily of computing longitudinal strains, curvatures, and estimating the spread of the inelastic behavior along the length of the girder. The layout of the markers for each region is shown in Figure 6.9.

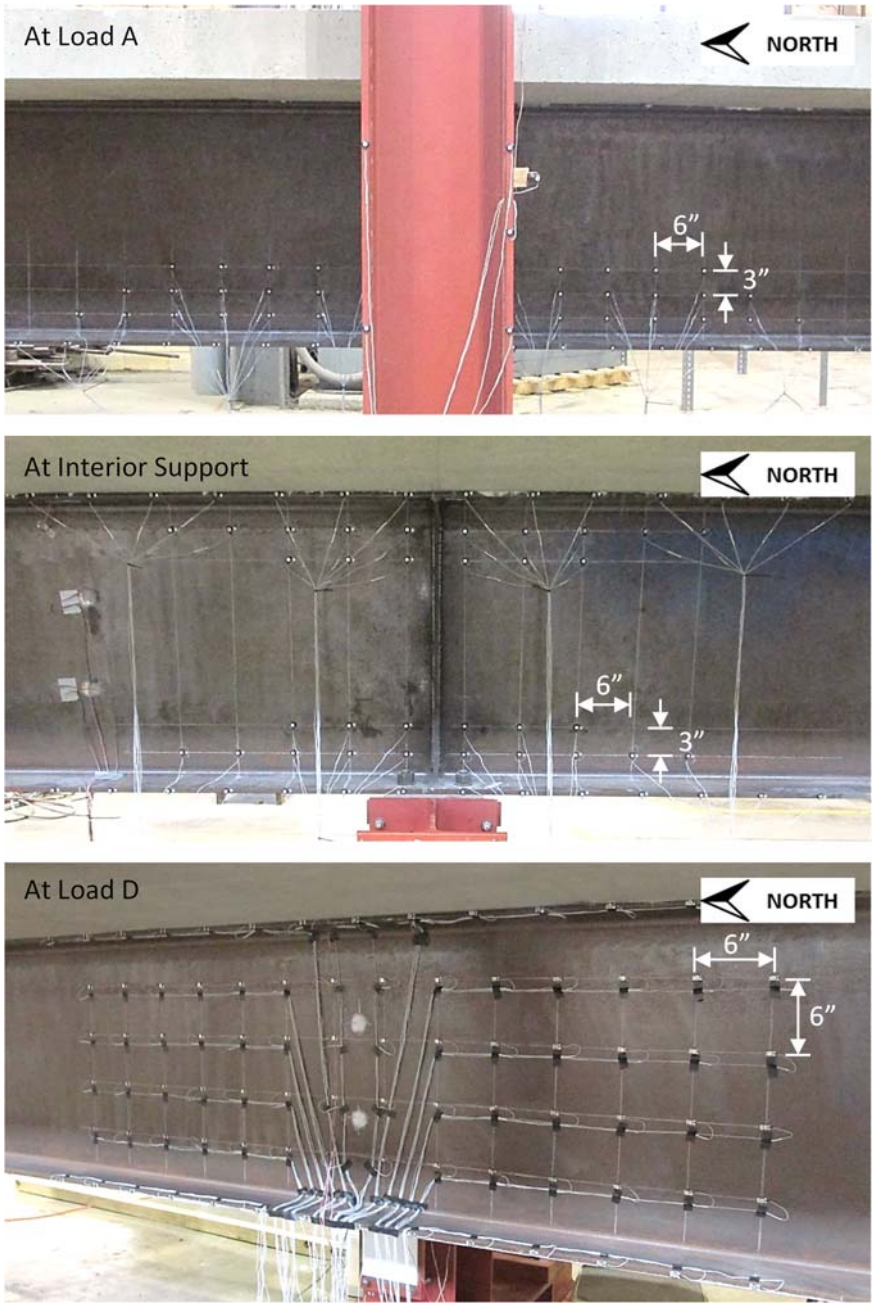

Figure 6.9 Layout of Optical System Markers

6.6 Test Program

The girder was subjected to several different types of loading over the course of approximately 6 months to simulate the various loads a bridge may be exposed to throughout its lifetime. Because of the difficulty of applying realistic bridge traffic loads in the laboratory, the effects of moving loads were simulated using cycles of strategically placed point loads at the four locations indicated in Figure 6.2. Generally, the two spans were treated separately, since applying load in one span puts very little demand on the shear connectors in the opposite span. The main exception to this is the shakedown testing, in which the yielding that occurred at the

interior support affected the behavior of both spans. The following summarizes the eight phases of testing, listed chronologically:

1. Elastic testing of the non-composite girder in the north span
2. Elastic testing of the composite girder in the north span
3. Shakedown testing in the north span
4. Fatigue testing in the south span
5. Fatigue testing in the north span
6. Shakedown testing in the south span
7. Ultimate strength testing in the south span
8. Ultimate strength testing in the north span

6.6.1 Elastic Testing

Before installing the connectors, non-composite testing under small loads in the elastic range was conducted. This was done only in the north span, and consisted of a few cycles of Load A up to 40 kips. The purpose of this initial testing was two-fold. Firstly, it was necessary to break the natural bond at the interface between the bottom of the deck and the top flange of the girder to simulate the likely condition of most existing non-composite bridges. Secondly, it provided a baseline for the stiffness and general behavior of the non-composite girder.

After installing the connectors, the same elastic testing was conducted on the partially composite beam to compare the stiffness of the two girders. During the elastic testing phase, the maximum stress in the steel did not exceed 35% of the yield stress.

6.6.2 Fatigue Testing

Fatigue testing was conducted under the repeated application of Load A in the north span and Load D in the south span. These loads cause the largest deflections of the girder and thus place a significant slip demand on the shear connectors in both groups in the loaded span. Based on analysis of four existing bridges from the survey, a load range of 50 kips was chosen for the first fatigue test, which was conducted in the south span during the fourth phase of testing. This load range induced slip ranges in the laboratory specimen approximately equivalent to the maximum slip range expected under AASHTO fatigue loading of four typical existing bridges that were analyzed while planning for the fatigue testing. After very good fatigue performance under a load range of 50 kips, it was decided to conduct the second fatigue test in the north span under a larger load range of 75 kips.

These fatigue tests were conducted using a closed loop control system similar to that used in the small-scale fatigue tests. Each load cycle was applied using a sine wave with varying frequency depending on the load magnitude and induced deflections. A minimum load of 2 kips was maintained throughout testing so that the piston of the hydraulic ram always remained in contact with the specimen. While the fatigue tests were run 24 hours a day, the tests were stopped generally at least once per day to collect data during one or two cycles in which the load was controlled manually and applied much more slowly.

6.6.3 Shakedown Testing

The phenomenon of shakedown was investigated using load cycles of increasing magnitude, alternating between loads that cause large positive moments and loads that cause large negative moments. The loads were cycled back and forth at the same magnitude until the deflection from one cycle to the next did not change significantly, indicating that the girder had shaken down. In other words, a residual moment distribution had been achieved such that no additional yielding would occur in future cycles of the same or lesser loads, leading to purely elastic behavior. A change in maximum deflection of less than 0.01 inches was chosen prior to testing as a reasonable criterion for shakedown behavior. Following shakedown at a particular load level, the loads were increased and the process continued.

The loading scheme illustrated in Figure 6.10 for the north span was developed for the shakedown testing. It consisted of first applying Load A to cause a large positive moment in the north span, engaging the connectors in groups I and II to create composite action. Then, Load A was removed, and Loads B and C were applied simultaneously to cause a large negative moment at the interior support. As shown in the figure, these three loading points allow for the approximation of an AASHTO live load moment envelope for one span by achieving the peak or near-peak values in both positive and negative moment. A similar but mirrored configuration was used to conduct shakedown testing in the south span, using Load D instead of Load A, which engages the connectors in groups III and IV in composite behavior.

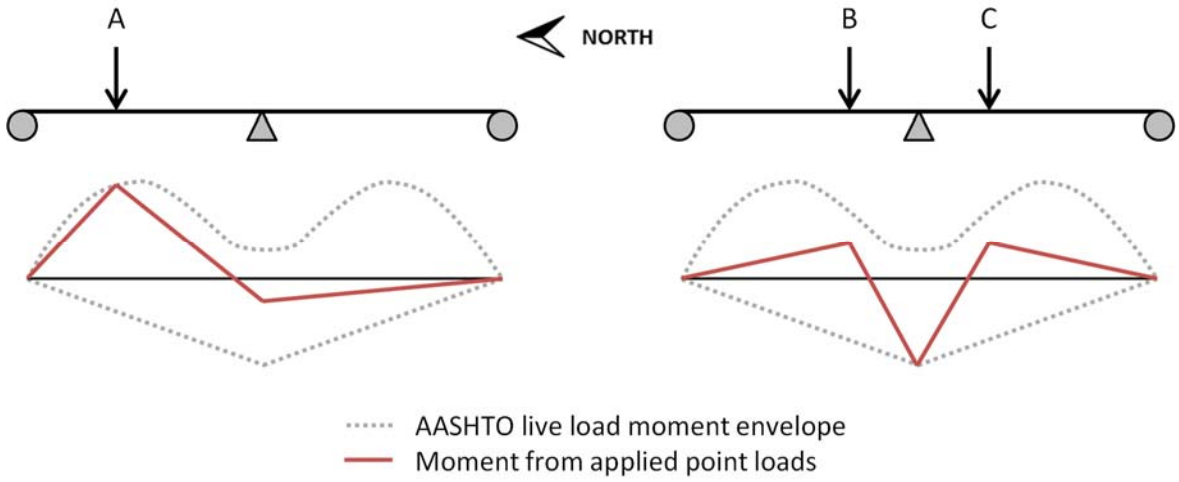

Figure 6.10 Loading Scheme for Shakedown Testing

The relative magnitude of Loads A to Loads B and C controls the relative moment demand on the positive and negative moment regions, and thus controls the amount of moment redistribution that must occur as the beam shakes down. The magnitudes of the loads were chosen to achieve the 20% maximum amount of moment redistribution allowed by the AASHTO LRFD specifications, meaning that the elastic moment at the interior support exceeds the capacity by 20% (AASHTO 2010). This corresponds to a ratio of the magnitude of Load A to the magnitude of each of Loads B and C of 0.87. This ratio was approximately maintained throughout the entirety of the shakedown testing, especially in the inelastic range.

6.6.4 Ultimate Strength Testing

The final phases of testing consisted of monotonic loading to failure to observe the ultimate strength of the girder as well as the post-peak load behavior. Ultimate strength testing was conducted under Load A in the north span and Load D in the south span. In the elastic range, data was recorded at 5 to 10 kip load increments. Beyond the elastic range, data was recorded at deflection increments of 0.25 inches.

6.7 Test Results

6.7.1 Elastic Testing

Figure 6.11 shows the load-deflection behavior of the girder under elastic loading for the non-composite and partially composite cases. The deflections were reduced by a factor of approximately two after installation of the connectors, indicating an increase in stiffness of nearly 100%. The dotted and dashed lines represent the predicted deflected shape from a 3D finite element model of the non-composite and partially composite girder, respectively. The experimental deflections are slightly smaller than the predicted deflections in both cases. This is likely a result of friction, which was not included in the model.

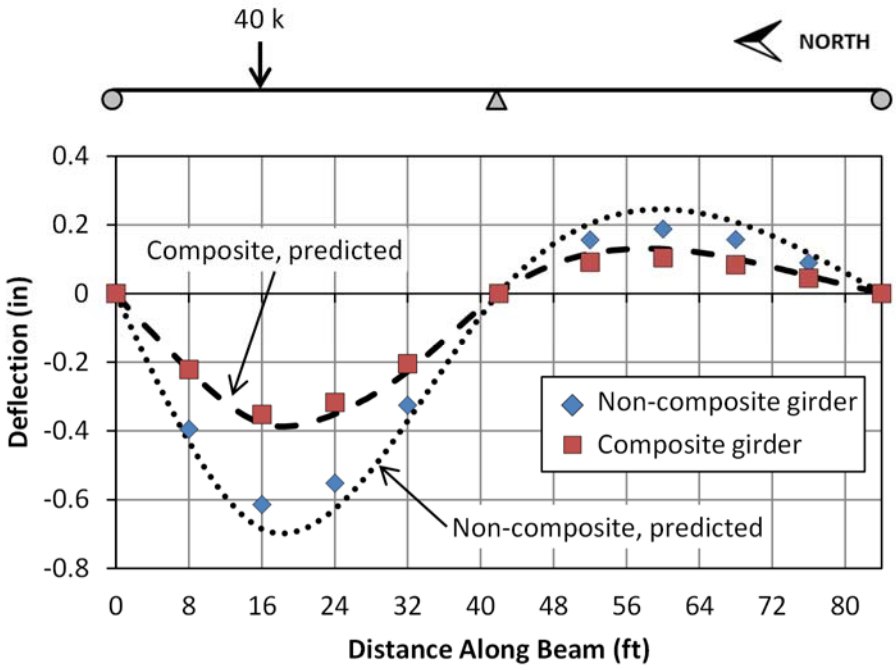

Figure 6.11 Elastic Testing Results

6.7.2 Fatigue Testing

Fatigue testing was conducted in both spans during different phases of testing. In the south span, fatigue testing was carried out before shakedown testing, while the reverse was true for the north span.

South Span Testing

South span fatigue testing consisted of repeated application of Load D at a load range of 50 kips and a frequency of 0.85 Hz. Figure 6.12 shows the predicted and observed slip range profiles along the beam for the first cycle of load. The predicted slip range profile was determined using the method described in Appendix A with a connector stiffness of 1600 kips per inch. This value is at the upper end of the range of connector stiffness that was observed in the small-scale fatigue testing. As it can be seen in the figure, there is a reasonable agreement between predicted and observed behavior using this value of stiffness. At the start of the test, the shear connectors in the south span were required to withstand slip values between 0.005 and 0.015 inches, which are representative of slip values that shear connectors are expected to undergo in a typical bridge under HS 20 fatigue truck loading.

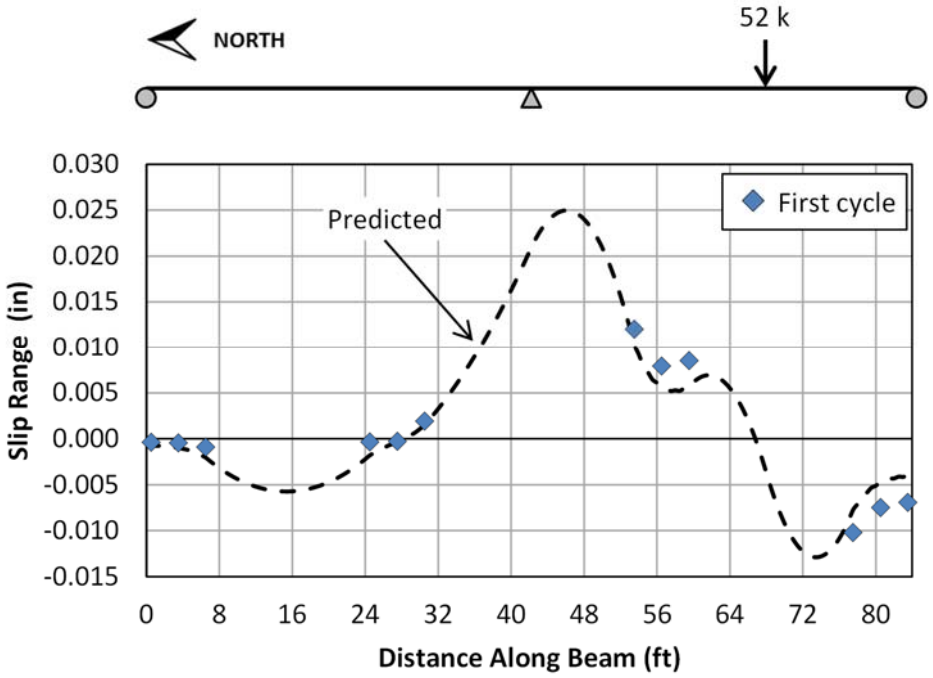

Figure 6.12 Slip Profile for the First Cycle

However, as the fatigue test progressed, a significant reduction in the slip range was observed. After 2 million cycles and no connector failures, a 50% reduction in the slip range had occurred for almost all of the connectors. This phenomenon is illustrated in Figure 6.13 for three connectors in each of groups III and IV in the south span. These results indicate a significant difference from the small-scale fatigue tests where the slip range remained essentially constant during the entire fatigue life for tests in which the connector was loaded in only one direction. These small-scale tests also designated a fatigue slip range endurance limit of 0.008 inches, suggesting that connectors subjected to slip ranges lower than this limit have effectively infinite fatigue life. Because of the significant reduction in slip range with cycles in the large-scale tests, it is difficult to evaluate this proposed endurance limit.

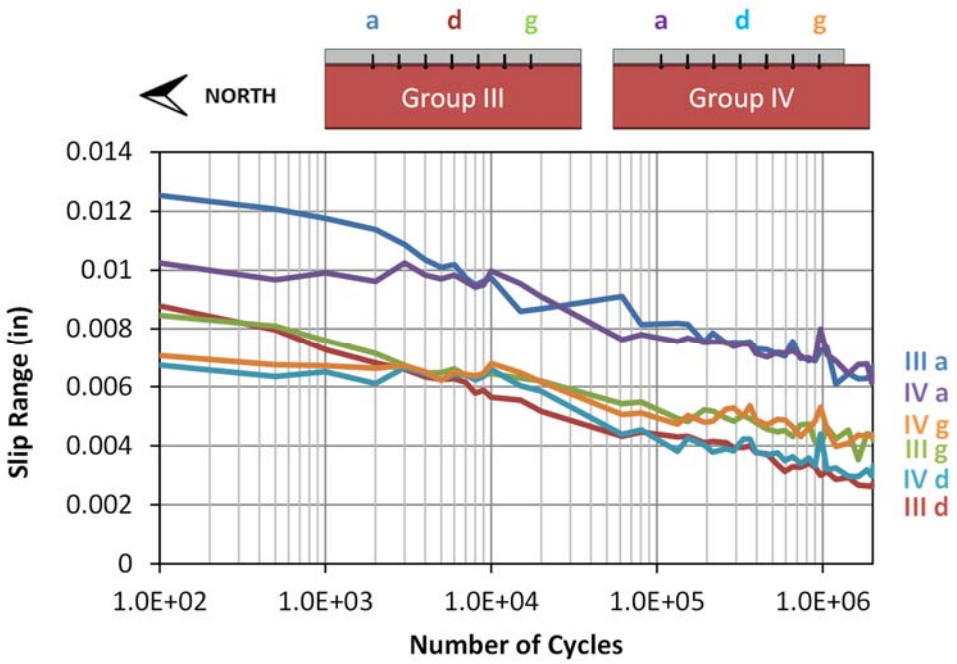

Figure 6.13 Slip Range Variation during South Span Fatigue Test

Figure 6.14 shows the variation in the estimated stress range with number of cycles of load for connectors at all locations in group III. Contrary to the slip range, however, the stress range remained fairly constant throughout the test for all of the connectors. Coupled with the observed decrease in slip range, this indicates that the connector stiffness is effectively increasing as the test progressed. The connectors in this test exhibited very good fatigue behavior as no failures were observed after 2 million cycles at estimated stress ranges from 10 ksi to more than 25 ksi. For comparison, the fatigue life of connectors in the small-scale tests at a stress range of 25 ksi varied from 70,000 to 500,000 cycles. At a stress range of 20 ksi, the connectors in the small-scale tests exhibited fatigue lives of 600,000 to more than 2 million cycles.

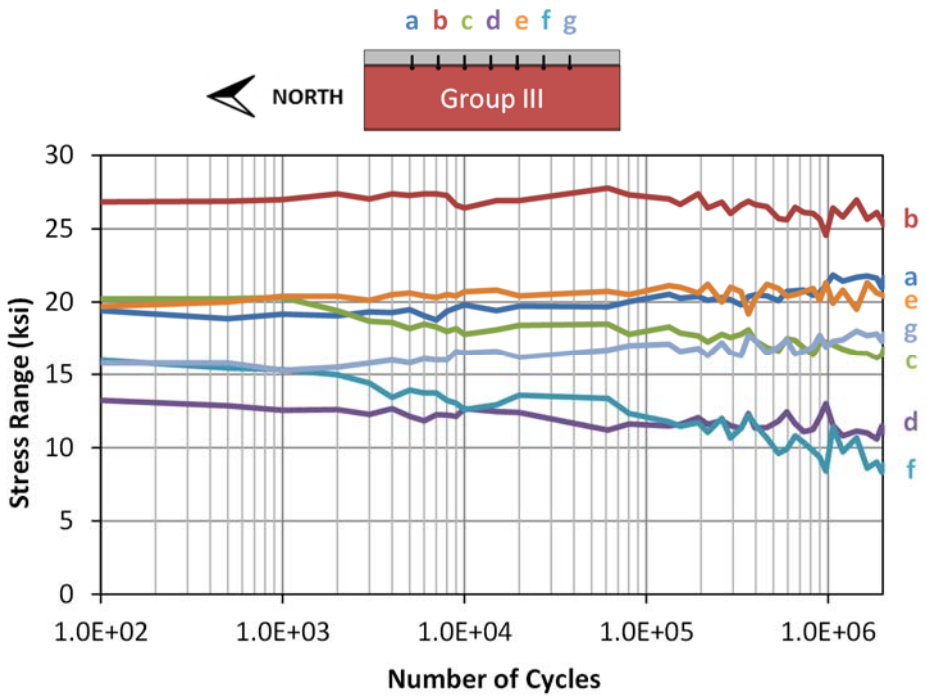

Figure 6.14 Stress Range Variation during South Span Fatigue Test

Figure 6.15 shows the force-slip behavior of a single connector at several points during the fatigue test. This data is from the northernmost connector in group III, which was subjected to the largest slip range during the test. The decreasing slip range and approximately constant connector force with increasing number of cycles are both evident in the figure. However, the figure also indicates an increase in the residual slip, or the slip measured when the connector is unloaded, as the test progresses up to more than 0.01 inches. One possible explanation for this behavior is that the adhesive that fills the space around the threaded rod in the deck and in the top flange of the steel beam undergoes slight permanent deformations with each cycle. If this compressive deformation leads to a stiffer connector response, it could also explain the reduction in slip range with cycles.

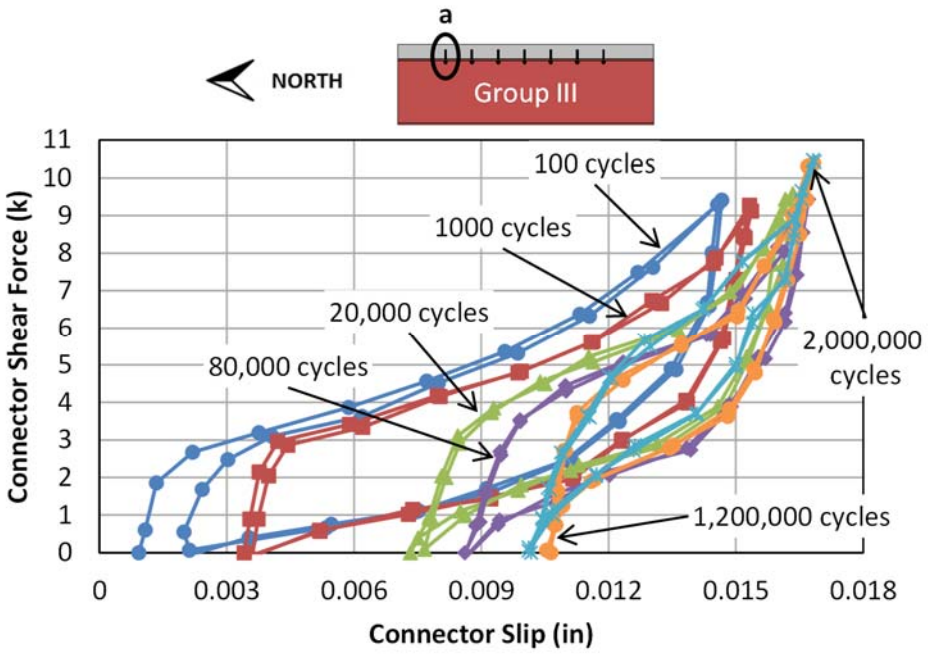

Figure 6.15 Connector Shear Force-Slip Behavior during South Span Fatigue Test

North Span Testing

Once the fatigue testing in the south span was complete, fatigue testing in the north span was started. Unlike in the south span, shakedown testing had been conducted in the north span prior to the fatigue testing. While residual slips of up to 0.06 inches were accumulated in the north span connectors, no connector failures or otherwise poor behavior were observed during the shakedown testing (see Section 6.7.3). Because of the very good fatigue performance of the south span connectors under a 50-kip load range, it was decided to increase the load range to 75 kips for fatigue testing in the north span, which was conducted using Load A. A lower frequency of 0.45 Hz was required for this test due to the larger load and deflection. This 75-kip load range put slip and force demands on the shear connectors well beyond what would be expected from AASHTO HS 20 fatigue loading.

Figure 6.16 and Figure 6.17 show the slip range and stress range variation with the number of cycles of load for fatigue testing in the north span. Note that very different trends were observed in this test than in the south span test. Instead of decreasing, the slip range increased with the number of cycles to very large values. Also, rather than remaining constant, the connector forces varied greatly with a general downward trend as the number of cycles increased.

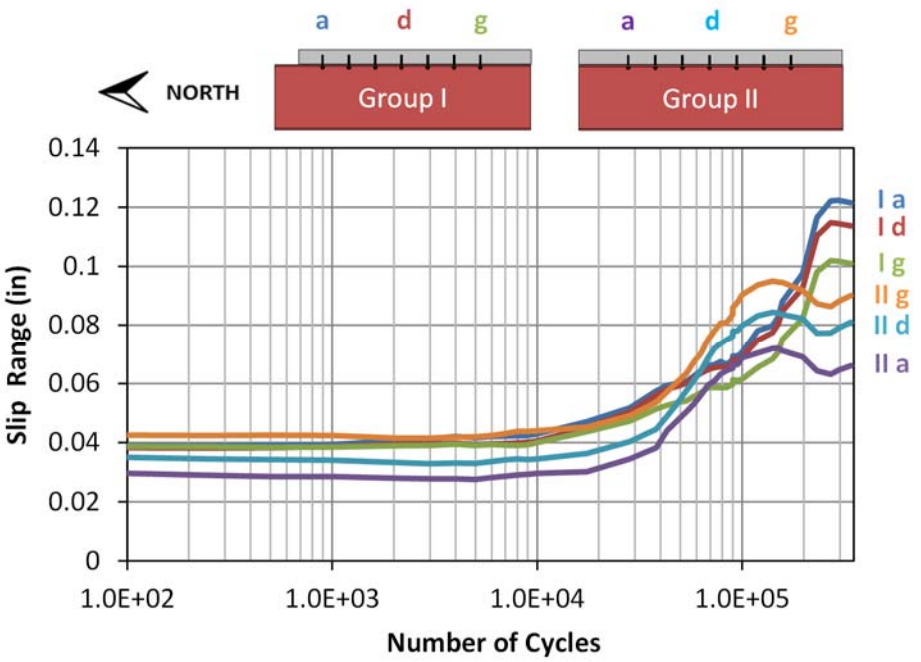

Figure 6.16 Slip Range Variation during North Span Fatigue Test

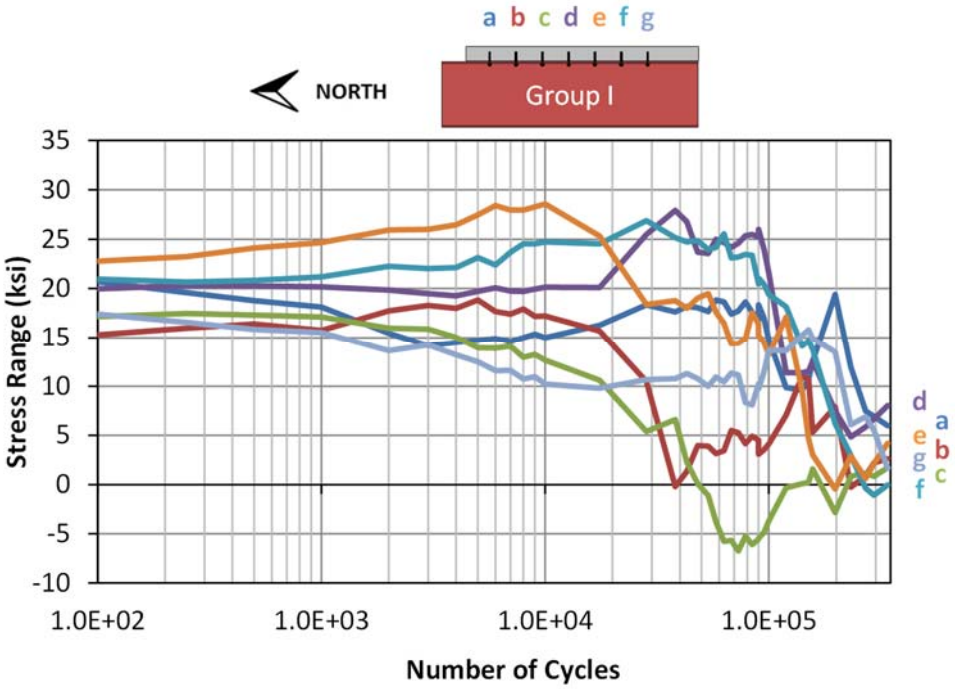

Figure 6.17 Stress Range Variation during North Span Fatigue Test

This vastly different behavior as compared to the south span test can be explained by degradation of the adhesive around the threaded rod in the top flange of the steel beam, similar to that observed in the small-scale fatigue testing under reversed loading. As the north span test

progressed, the adhesive slowly disintegrated into a powder and accumulated on the bottom flange of the steel beam, as shown in Figure 6.18(a). As in the small-scale tests, the loss of the adhesive led to the formation of a "gap" region, through which the threaded rod of the connector could slip without transmitting any load. Figure 6.18(b) shows the gap region of a north span connector in a photograph taken after all testing was complete. The maximum size of this gap region due to adhesive degradation is 1/8 inches, which is the difference between the 7/8-inch diameter of the threaded rod and the 1-inch diameter of the hole. The maximum slip range observed by the end of the north span fatigue test had nearly reached this value. Because the degradation took place more quickly in some connectors than in others, the load distribution between connectors changed constantly during the test, as illustrated in the erratic stress range variation in Figure 6.17.

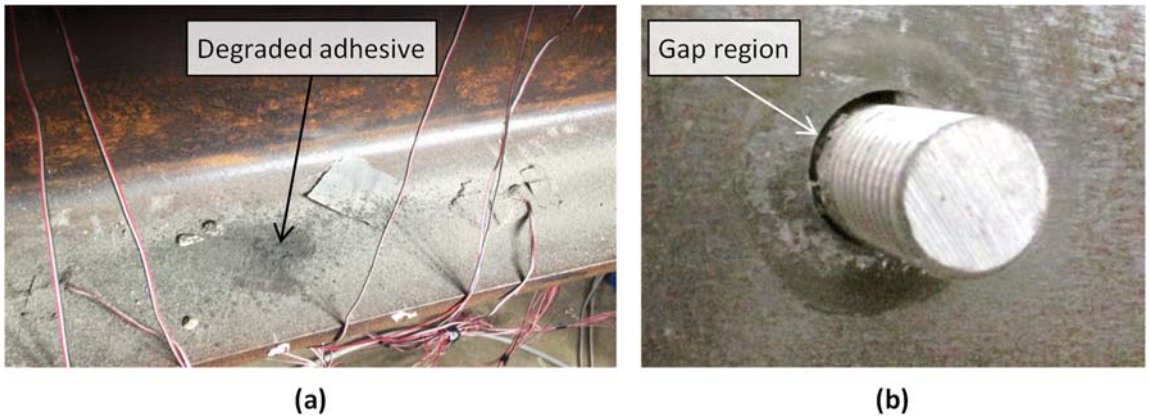

Figure 6.18 Visual Observations of Adhesive Degradation – (a) Powdered adhesive and (b) Gap around connector

As the adhesive degraded and the connectors were able to slip without transmitting any force, the behavior of the girder trended towards that which would be expected for a non-composite girder. This is illustrated in Figure 6.19, which compares the measured deflections near the beginning and end of the fatigue test to the predicted 30% composite and non-composite cases. A connector stiffness of 500 kips per inch, which is on the low end of the stiffness range observed in the small-scale tests, was used for the initial 30% composite prediction. This stiffness value was chosen because the connectors in the north span had previously been exposed to large loads during the shakedown testing, and thus exhibited a less stiff response than those in the previously untested south span. The north span fatigue test was stopped after approximately 330,000 cycles because the connectors were taking very little force, and the girder was exhibiting nearly full non-composite behavior.

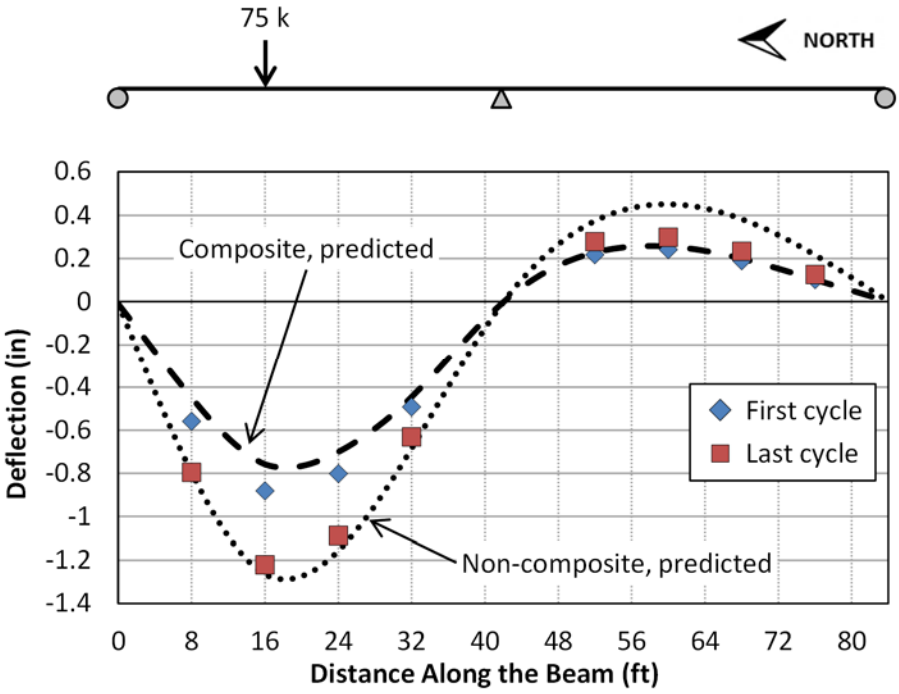

Figure 6.19 Deflection Change during North Span Fatigue Test

Summary of Fatigue Testing Results

Generally, the adhesive anchor shear connectors behaved well in fatigue, with no fatigue failures occurring in the testing of either span. In the south span test, which was conducted under a load range that placed similar force and slip demand on the connectors as would be expected in a typical strengthened bridge, very consistent behavior was observed throughout 2 million cycles of load, despite a gradual increase in residual slip and a gradual decrease in slip range. During the north span test, which was conducted at a load range 50% greater than that of the south span test and after shakedown testing of the north span, degradation of the adhesive between the threaded rod and the top flange of the steel beam was observed in all connectors. This degradation led to the formation of a gap region allowing the connectors that were over-stressed to slip without transmitting force. With increasing cycles of load, the girder trended towards non-composite behavior.

Because a bridge does not require its full strength to resist service-level loads, this adhesive degradation is not necessarily detrimental to the performance. In fact, this "self-correcting" behavior of the connectors may actually prevent fracture of the threaded rods under fatigue loads. Rather than repeatedly stressing the threaded rods until fatigue-induced fracture occurs, the adhesive degradation softens the shear connection and effectively reduces the stress range applied to the connectors. As shown in the ultimate strength testing results in Section 6.7.4, the connectors can slip through the gap region and re-engage at large loads so that the composite strength can be developed if necessary.

6.7.3 Shakedown Testing

Both spans were subjected to shakedown loading during two different phases of testing. The north span shakedown test was conducted prior to any fatigue testing, while the south span shakedown test was conducted after all fatigue testing was complete. While this may have contributed to differences in the observed behavior between the two spans, a more likely source of any discrepancies is the order in which the testing was conducted, because the load step involving Loads B and C is identical in both testing phases. During the north span testing, a significant amount of yielding was observed at the interior support under Loads B and C, as discussed later in this section. However, during south span testing, yielding under Loads B and C began much later, because large magnitudes of these loads had already been applied to the specimen. The effects of this are prevalent in all of the results presented in this section.

Table 6.2 summarizes the loading protocol for both shakedown tests, denoting the predicted elastic and shakedown limit loads. The predicted shakedown behavior was based on a simple plastic hinge analysis assuming that 20% moment redistribution occurs from the interior support. Testing in the north span was stopped at a load level approximately 5% beyond the predicted shakedown limit to preserve the specimen for future testing. The south span shakedown test was continued until significant local buckling of the web and bottom flange began to occur at the interior support, nearly 15% beyond the predicted shakedown limit load.

Table 6.2 Summary of Loading for Shakedown Testing

	Load Magnitude (k)		Cycles to Shakedown		Net Residual Deflection (in)	
	A or D	B & C	North	South	North	South
	46	55	2	2	0.00	0.00
	70	85	2	2	0.01	0.00
	91	110	2	2	0.03	0.00
	108	130	2	3	0.06	0.00
	120	145	2	2	0.10	0.01
	131	158	2	2	0.14	0.05
Elastic Limit	140	160	3	3	0.17	0.06
	144	165	3	2	0.22	0.07
	148	170	4	3	0.25	0.09
	152	175	4	3	0.29	0.09
	157	180	5	3	0.35	0.11
	161	185	5	3	0.46	0.15
	165	190	6	3	0.54	0.18
	170	195	5	3	0.54	0.22
	174	200	7	4	0.65	0.25
	178	205	7	4	0.76	0.30
Shakedown Limit	183	210	8	7	0.91	0.39
	187	215	9	8	1.07	0.52
	191	220	11	10	1.22	0.67
	200	230	--	14	--	1.14
	209	240	--	(1)*	--	1.44
	Total Cycles:		89	84		

*Testing stopped after one cycle due to local buckling at interior support region

Shakedown was observed at all load levels prior to the occurrence of local buckling, as the change in girder deflection was reduced below the 0.01-inch criteria after multiple cycles of loading. This deflection was measured at either Load A or Load D for north and south span testing, respectively. Generally, with increased load magnitudes, more cycles were required for the girder to shake down. Fewer cycles were required to achieve shakedown during testing of the south span than during testing of the north span, especially at load levels between the predicted elastic and shakedown limits. The south span also accumulated smaller amounts of residual deflection than did the north span. Both of these observations result from the order in which the testing was conducted, since yielding was occurring primarily in positive bending during south span testing, rather than in both positive and negative moment regions as in the north span testing. Inelastic behavior in only one region facilitates a more rapid stabilization of the residual moments, and thus of the residual deflections as well.

The overall load-deflection behavior of the girder during both shakedown tests is summarized in Figure 6.20. The graphs depict only the behavior under the application and removal of Load A for the north span test and of Load D for the south span test. The square data points indicate the peak load and deflection for each cycle, while the solid lines show the load-deflection behavior of the last cycle for several load levels. The dotted and dashed lines represent the predicted peak load-deflection behavior of a non-composite and composite girder, respectively, based on simple plastic hinge analyses. The predicted shakedown load of the composite girder is nearly 50% greater than that of the non-composite girder, indicating a significant strength gain at the shakedown limit state as a result of post-installing shear connectors.

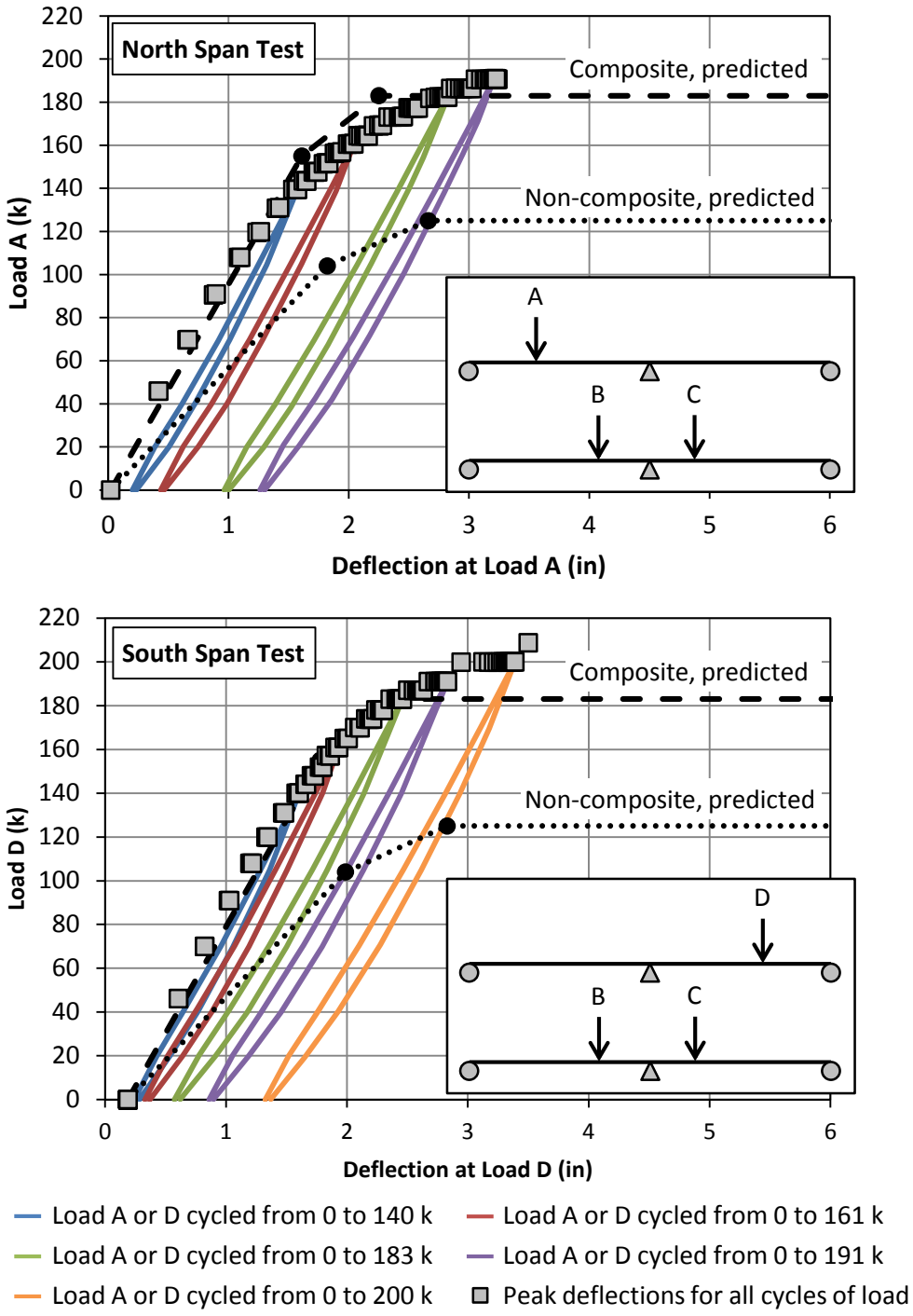

Figure 6.20 Load-Deflection Behavior during Shakedown Testing

While the peak load-deflection behavior for both spans closely resembles the shape of a typical monotonic test of a composite girder, each individual cycle was nearly elastic. Small permanent inelastic deflections accumulated from one cycle to the next at a decreasing rate during cycles at a particular load magnitude. This is indicated in Figure 6.21, which shows the change in peak deflection from one cycle to the next for several magnitudes of load during north span testing.

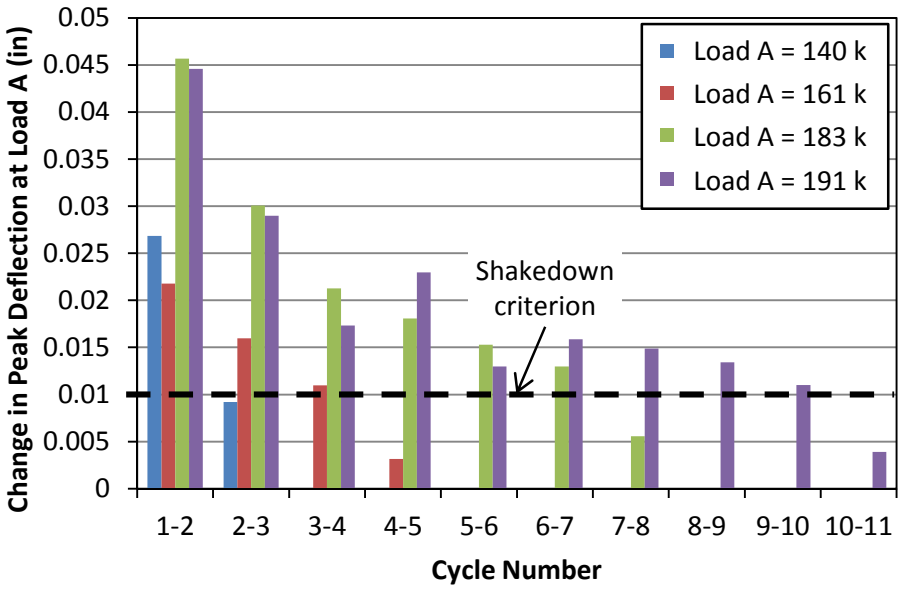

Figure 6.21 Incremental Deflections during North Span Shakedown Testing

To monitor the level of composite behavior during testing, the depth of the neutral axis in the steel beam was tracked using both strain gages and the optical system. As shown in Figure 6.22(a), in partially composite regions dominated by positive bending, the neutral axis remained significantly above the theoretical non-composite neutral axis, which is located at mid-depth of the steel beam, indicating composite behavior. Because of interface slip, plane sections do not remain plane, and it is difficult to predict the theoretical neutral axis location for a partially composite section at any given time. However, using simple plastic theory, the location of the fully plastic neutral axis can be determined, and is also shown in the figure. As the load increases, the neutral axis initially moves downward in the section, possibly due to a reduction in stiffness of the connectors or a change in the interface friction, but seems to trend back upwards towards the theoretical plastic neutral axis at higher loads. Non-composite behavior was generally observed for the interior support region dominated by negative bending, as indicated by the neutral axis location very near to the mid-depth of the steel beam in Figure 6.22(b).

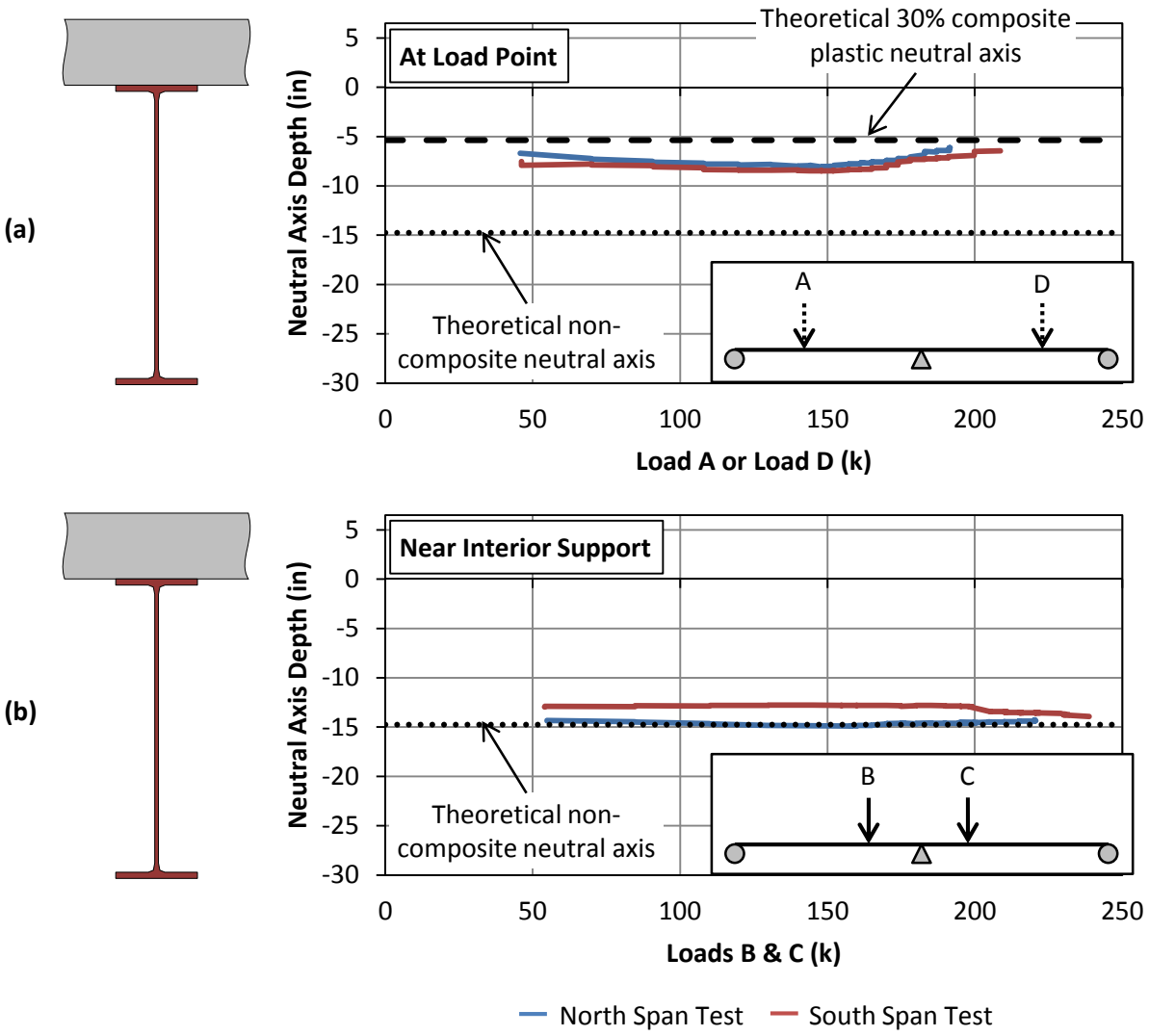

Figure 6.22 Depth of Neutral Axis during Shakedown Testing

The data from the optical system, along with visual observations of the whitewashed regions during testing, allowed for determination of the spread of plasticity over the yielded zone in both positive and negative bending. The yielding in positive moment regions was spread over a large area of the bottom flange at least three feet on either side of the load point and penetrated into the bottom portion of the web more than one-third of the depth of the section by the end of the shakedown testing. This large spread of yielding, illustrated by the bottom flange strains from the north span test in Figure 6.23(a), is expected for a composite section that reaches first yield at around 75% of the predicted plastic capacity. On the contrary, the yielding at the interior support was concentrated in a small region less than one foot on either side of the support point, as illustrated in Figure 6.23(b). The non-composite section has a yield moment of approximately 85% of the plastic moment capacity, allowing for a much smaller spread of plasticity between first yield and maximum capacity. The steep moment gradient at the interior support during the application of Loads B and C also contributes to the concentrated yielding seen in this region.

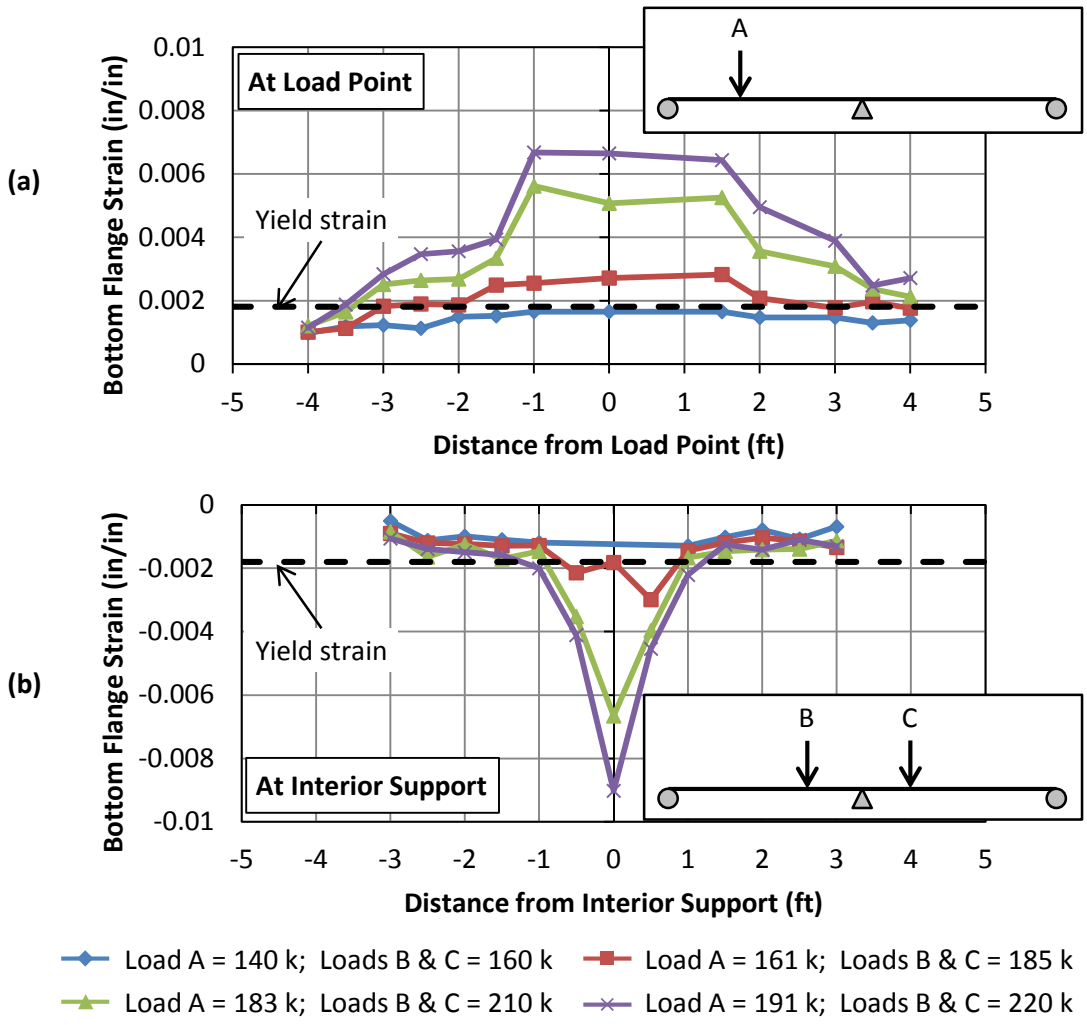

Figure 6.23 Spread of Yielding during North Span Shakedown Testing

The connector force-slip behavior at various load levels throughout the shakedown testing is shown in Figure 6.24 for the instrumented connectors in all four groups. The solid lines represent the behavior during the north span test while the dashed lines reflect the behavior during the south span test. For reference, the recommended design strength of a 7/8-inch diameter adhesive anchor is 30.1 kips, as calculated by Equation 8.1. As the tests progressed and the load levels increased, large connector forces and slips were observed. Residual connector forces up to 4 kips were estimated in some cases, indicating residual moments and stresses in the partially composite girder, although it is difficult to discern between error or drift in the strain gage readings and significant measured residual values. Although the data from the north and south span tests are not very comparable, especially for the connectors in groups I and IV, it is important to note that only one connector pair was instrumented out of seven in the group. Small differences in adhesive quality or degradation can change the connector stiffness and impact the distribution of load between the connectors in a single group. This is a possible source of the discrepancy in connector force between the north and south span tests in Figure 6.24(a). Additionally, while the range of slip in one cycle of load was similar between the two tests, the

south span connectors accumulated less residual slip as the test progressed. This is likely a result of the order of testing, as less residual deflection was also observed during the south span testing.

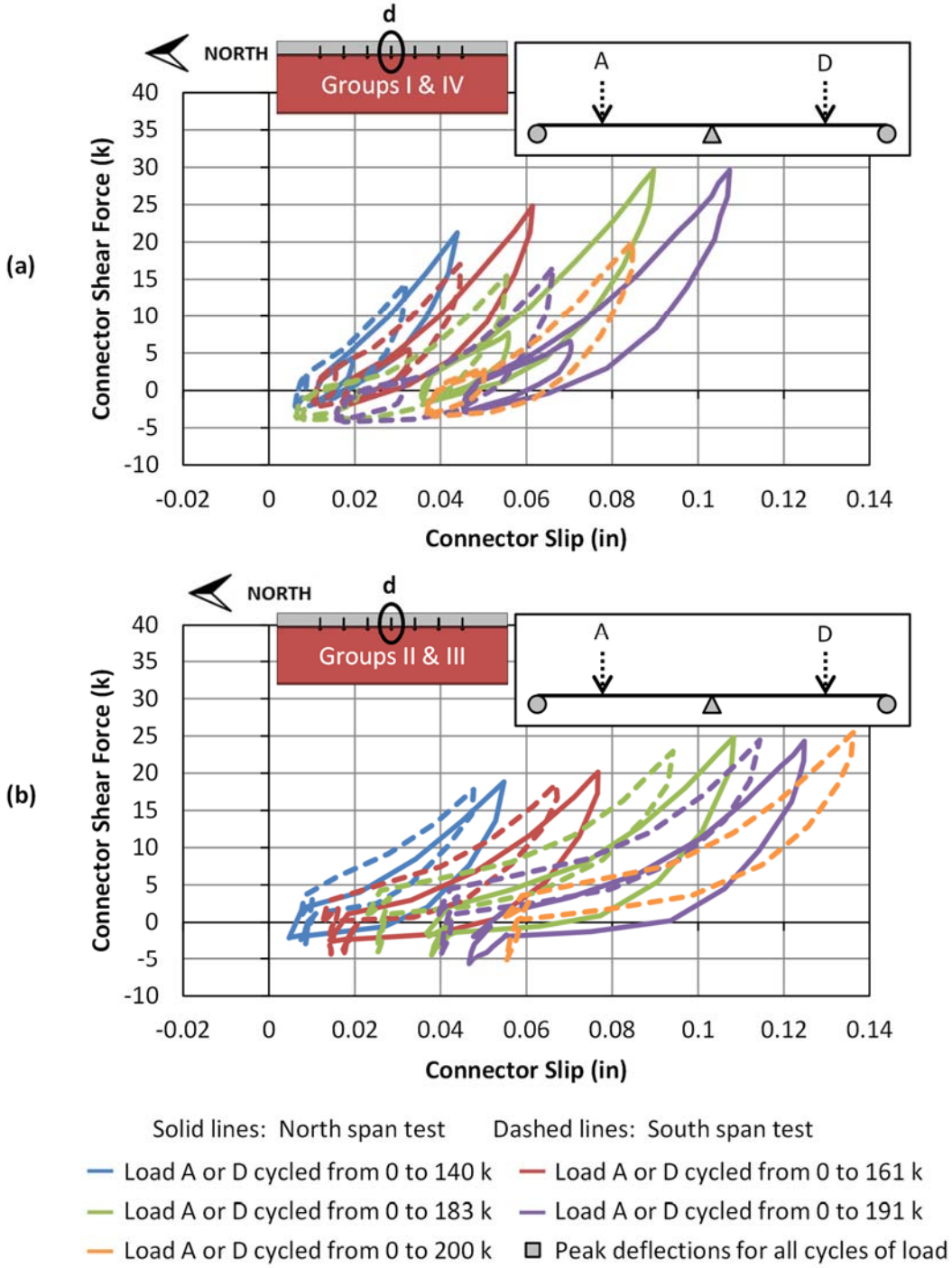

Figure 6.24 Connector Shear Force-Slip Behavior during Shakedown Testing

Generally, very good behavior was observed during the shakedown tests in each span, both before and after fatigue testing was conducted. Shakedown occurred at loads up to 10% greater than the predicted shakedown limit load, and the girder behaved elastically at loads of equal or lesser magnitude after shaking down. The majority of the differences in the behavior between the two spans likely comes from the order in which the testing was conducted, as significant yielding occurred in both positive and negative moment regions during the north span test, and only primarily in the positive moment regions during the south span test. While the north span test was stopped at loads just beyond the estimated shakedown limit to preserve the specimen for future testing, the south span test was continued until local buckling occurred in the bottom flange and web at the interior support.

6.7.4 Ultimate Strength Testing

Following all fatigue and shakedown testing, each span of the specimen was loaded monotonically to failure by Load A in the north span and Load D in the south span. Prior to this phase of testing, no shear connector failures had occurred. However, significant degradation of the adhesive of nearly all of the connectors in the north span had been observed during fatigue testing. Despite all of the previous loading, the girder behaved very well under ultimate strength testing, exceeding the predicted strength by approximately 10% in both spans. This is illustrated in the load-deflection plot in Figure 6.25, in which the experimental results, shown as solid lines, are compared to the predicted composite and non-composite behaviors, represented as dashed and dotted lines, respectively. The experimental data presented is based on the total deflection of the girder, indicating that some residual deflection was present before ultimate strength testing began. The predicted behavior was determined by simple plastic hinge analysis and does not consider any initial residual deflections.

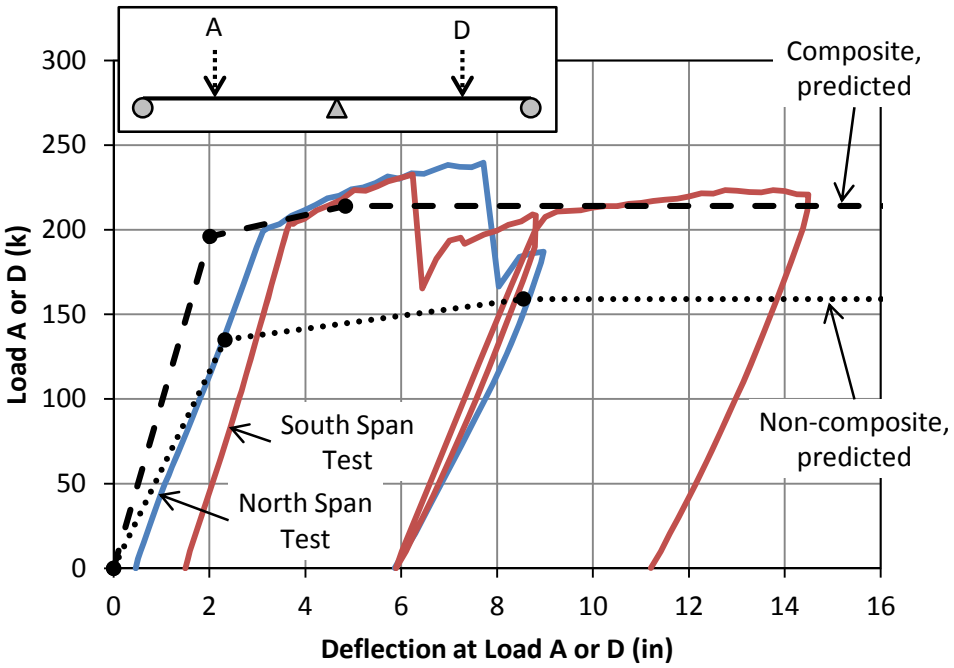

Figure 6.25 Load-Deflection Behavior during Ultimate Strength Testing

In both spans, elastic behavior was observed up to a load of approximately 200 kips, which was near the maximum load that had been previously applied during the shakedown testing. This reinforces the concept of shakedown behavior, as the girder will behave elastically for any load less than or equal to the previously applied shakedown load. The north span, however, exhibited a significantly lower stiffness in the elastic range than did the south span. This is a result of the degradation of the adhesive during fatigue testing in the north span. With no adhesive present, gap regions were formed between the threaded rod of the connectors and the holes in the top flange of the steel beam, allowing the connectors to slip through that region without transmitting any force. This effectively resulted in non-composite behavior of the girder and a significant stiffness reduction. Once a connector reached the end of the gap region, it came in to bearing with the steel flange and began transmitting shear force again, as would be expected in a composite girder.

Connector failure occurred at a total deflection of between 6 and 8 inches for both spans. The larger deflection at connector failure in the north span test is likely due to the degraded adhesive, which required larger slips and deflections before the all of the connectors re-engaged in composite action. In each test, all or nearly all connectors in one group fractured simultaneously. The connectors in group I failed in the north span test while the connectors in group III failed in the south span test, causing a 30–35% drop in load in both tests.

After failure of the connectors, the girder picked up load quickly, well beyond the predicted non-composite capacity. This indicates that some composite behavior was still occurring, possibly from friction allowing the transfer of shear force between the steel and concrete at the interface. The maximum stroke of the hydraulic ram was reached in both tests around a total deflection of 9 inches, upon which the girder was unloaded to a residual deflection of just below 6 inches. The south span was reloaded, after stacking several thick steel plates on top of the deck at the load location, to a total deflection beyond 14 inches before the maximum stroke of the ram was again reached, the girder was unloaded, and the testing was stopped.

The photographs in Figure 6.26 show the final state of the specimen after ultimate strength testing was complete. Three photos (a, b, and e) illustrate the yielding patterns in the whitewashed portions of the steel beam at the locations of Load A, Load D, and the interior support. As can be seen in the photo, some local buckling in the compression flange and web are present at all three locations. The remaining photos (c, d, and f) depict the cracking on the underside of the deck at the location of Load A, the crushing of the deck at the location of Load D, and the cracking on the top side of the deck over the interior support. The crack patterns have been traced over for emphasis, with dotted lines representing cracks that formed when the formwork was removed and dashed and solid lines indicating cracks that occurred during shakedown testing and ultimate strength testing, respectively. Cracks were generally spaced on the order of 6 inches apart, which corresponds to the transverse rebar spacing.

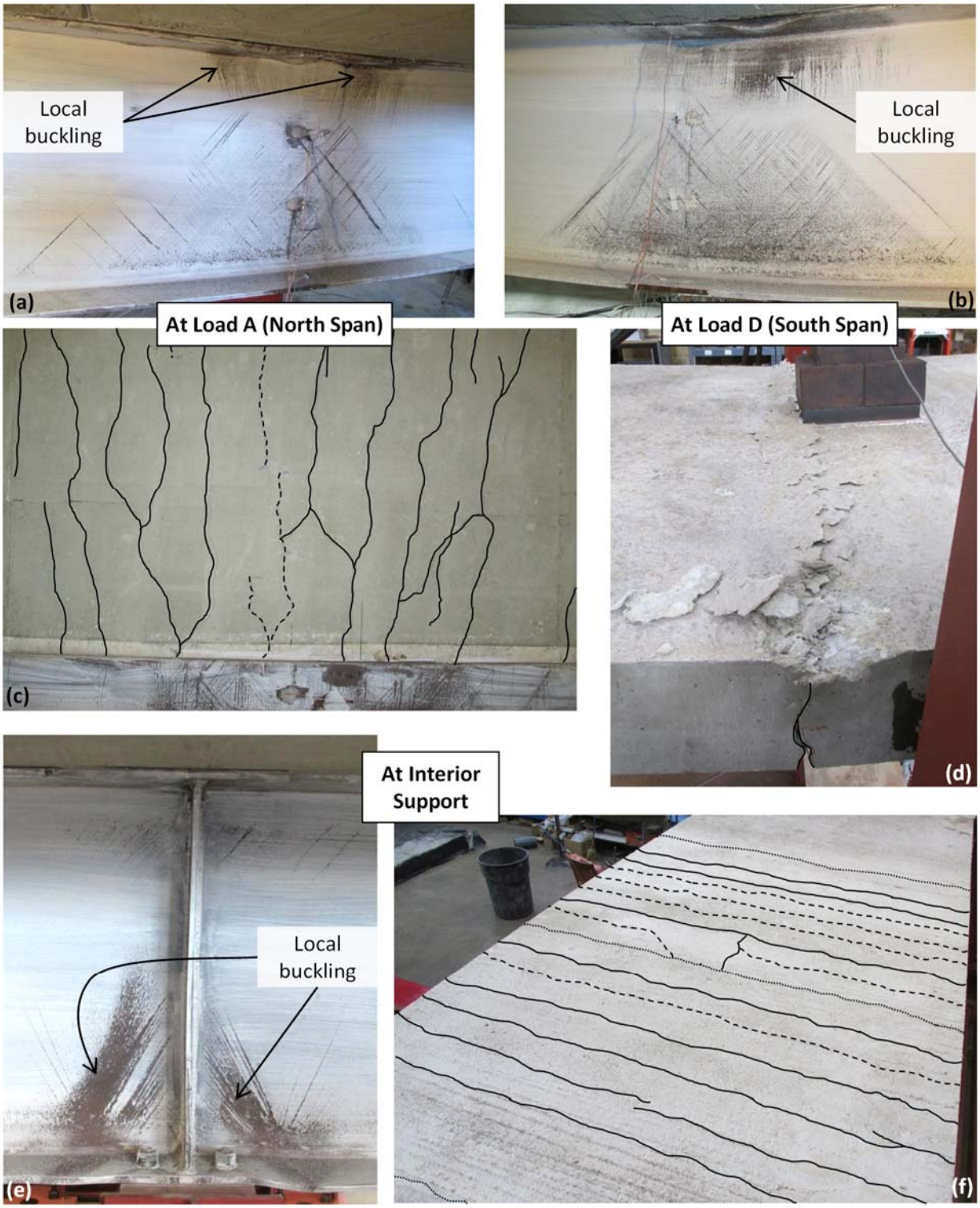

Figure 6.26 Photographs of Final State of Specimen

The connector force-slip behavior during ultimate strength testing was measured for the same four pairs of connectors as for the shakedown testing. Two pairs of instrumented connectors were located in the north span, at the middle of groups I and II. The remaining two

pairs of instrumented connectors were at symmetric locations in the south span at the middle of groups III and IV. Figure 6.27 illustrates the connector behavior during ultimate strength testing, including the point of connector failure in both spans. Significantly different behavior was observed with all four of these pairs of connectors in terms of stiffness, strength, and ductility. This is likely because only one pair of connectors was instrumented out of each seven-pair group, and the load-sharing properties within a group are complex, especially after all of the previously conducted fatigue and shakedown testing. However, the effects of the adhesive degradation are very evident in the force-slip behavior of the connector pair near the inflection point in the north span (in Group II). This pair of connectors underwent a slip of nearly 0.2 inches before picking up any significant force. The pair of north span connectors near the beam ends (in Group I) seems to have re-engaged in composite action much sooner and exhibited significant ductility, holding a force of approximately 20 kips through more than 0.15 inches of slip.

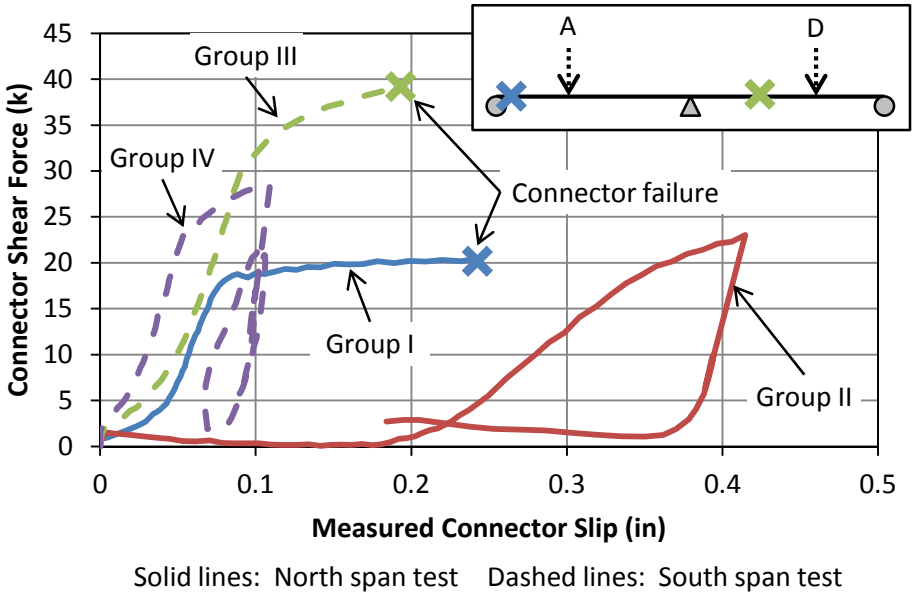

Figure 6.27 Load-Slip Behavior of Connectors during Ultimate Strength Testing

Of the 28 connectors that failed during ultimate strength testing, all but three fractured at the steel-concrete interface. The remaining three, all located in Group I near the end of the girder in the north span, fractured at a depth of approximately 1 inch into the concrete deck. Local crushing of the concrete was observed around these connectors when the deck was removed. The photograph in Figure 6.28 shows a typical failed connector along with the three connectors that fractured in the deck.

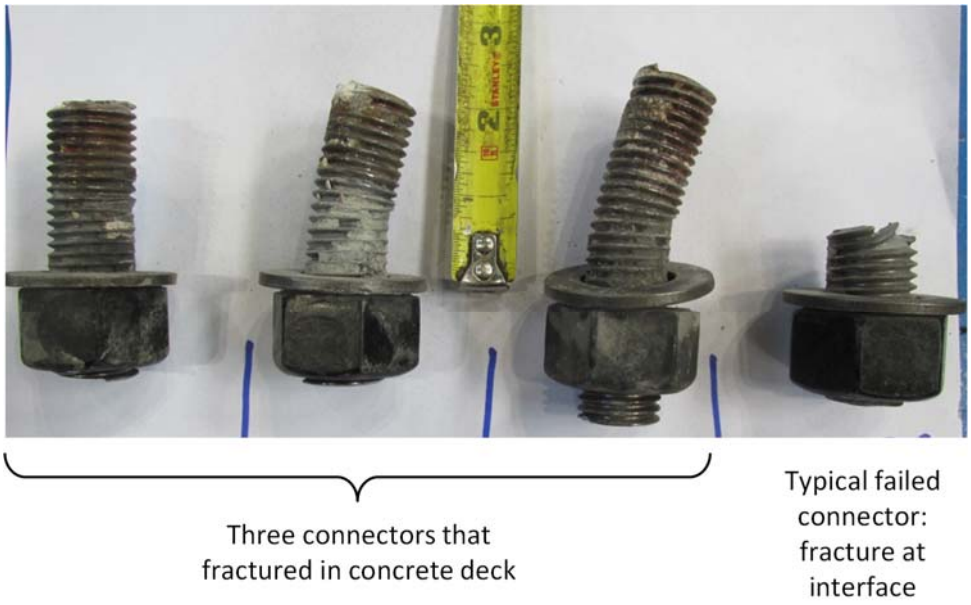

Figure 6.28 Fractured Connectors

Both spans of the girder exhibited very good behavior under ultimate strength testing, despite the demanding program of prior fatigue and shakedown loading the specimen was subjected to. The predicted strength was exceeded by approximately 10% in both spans, and the connectors that had significant adhesive degradation from previous fatigue testing re-engaged in bearing with the top flange of the steel girder to create composite action under large loads.

6.8 Summary

A large-scale testing program to investigate the behavior of partially composite bridge girders strengthened with post-installed shear connectors under a variety of loading scenarios was conducted. The single girder specimen performed very well throughout fatigue, shakedown and monotonic loading, exhibiting resilient and ductile behavior while exceeding the predicted capacity at all limit states. The results of the 6-month test program indicate that strengthening existing bridges in this manner should provide good long-term performance.

Chapter 7. Parametric Studies

7.1 Overview

Previous research indicated that the ductility at peak strength of a bridge strengthened with post-installed shear connectors is improved if the connectors are concentrated near points of low moment, rather than distributed uniformly along the entire length of the girder (Kwon 2008). For fatigue design, however, the elastic response of the girder should also be considered. Thus, parametric studies were conducted to investigate the effects of the shear connector layout on the performance of a bridge under elastic-level loads, with a focus on the demand placed on the connectors at the fatigue limit state. This chapter describes the program and results of these studies.

7.2 Program for Parametric Studies

Five key parameters that likely affect the elastic behavior of shear connectors in continuous partially composite girders were chosen as the variables in the parametric study. These parameters are:

- Span length and exterior-to-interior span length ratio
- Connector stiffness
- Location of the connector groups within each span
- Spacing of the connectors within each group
- Number of connectors in each group (composite ratio)

For simplicity, the parametric studies were limited to three-span continuous bridge units, which were very common in the bridge survey. To cover the range of typical span lengths from the survey, the three bridge girder geometries shown in Figure 7.1 were chosen for analysis. These geometries come directly from bridges in the survey and are representative of a wide range of the surveyed bridges. The span lengths in these bridges vary from 50 feet to 100 feet and the ratio of exterior span length to interior span length varies from 0.6 to 1.0. A concrete compressive strength of 3 ksi was assumed throughout the analysis, corresponding to a Young's modulus of 3120 ksi for the deck material. The steel was assumed to have a Young's modulus of 29000 ksi.

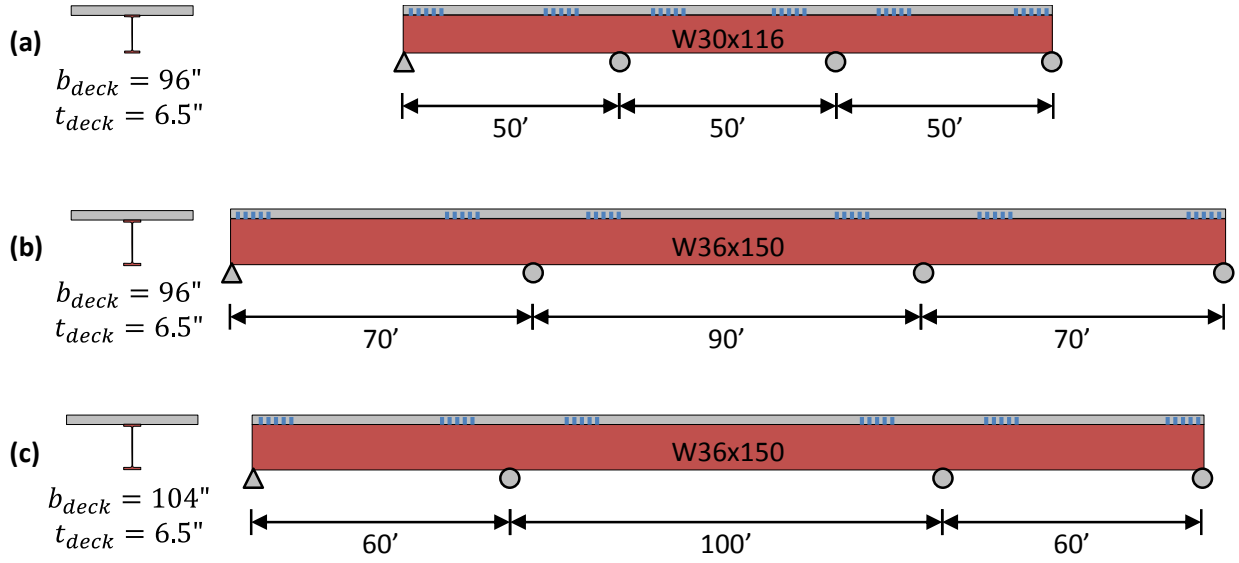

Figure 7.1 Bridge Girders Considered in the Parametric Studies

The stiffness of the individual connectors was varied over the course of the parametric studies. In all of the analyses, the connectors were treated as linear elastic springs so that the slip of the connector and the force carried by the connector were proportionally related by a constant stiffness (K). A wide range of stiffness values were observed in the small-scale fatigue testing described in Chapter 5, from 500 kips per inch to 1600 kips per inch. For the purposes of the parametric study, stiffness values of 500 kips per inch, 800 kips per inch, and 1200 kips per inch were chosen for analysis.

The placement of the groups of connectors within each span was also varied in these studies, with the exception of the groups at each end of the girder. These end groups were always located very near the beam ends, with the end connector pair placed at a distance of half of the connector spacing from the exterior support. The location of the remaining interior connector groups was defined by the variable α, which indicates the position of the connector pair closest to the interior pier as a fraction of the span length, as shown in Figure 7.2. Low values of α represent connector groups close to the interior support, while high values of α indicate that the connectors are located near the middle of the span. The values considered for α were 0.1, 0.15, 0.2, 0.25, 0.3, 0.35, and 0.4.

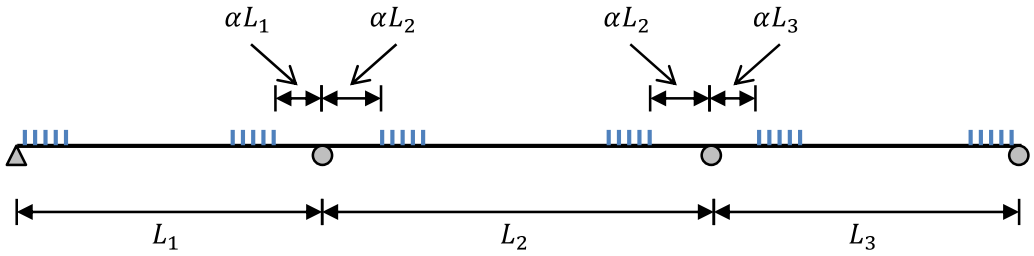

Figure 7.2 Location of Interior Connector Groups

Three different values for the spacing of the connectors within a single group were considered: 12 inches, 18 inches, and 24 inches. With the span lengths and number of connectors used in this study, a connector spacing beyond 24 inches tends to approach the condition of uniformly spaced connectors, rather than connectors in concentrated groups. The connector spacing is referred to by the variable S in this chapter.

The effects of varying the composite ratio were investigated by changing the number of connectors placed in each group, denoted by the variable N. Values of N considered in the parametric studies were 10, 16, and 22 connectors. Since the connectors are installed in pairs, these values will be referred to as 5, 8, and 11 pairs of connectors. Figure 7.1 shows girders that have been strengthened with five pairs of connectors in each group. Because the composite ratio depends not only on the number of connectors provided, but also on the geometry and material properties of the steel beam and concrete deck, the corresponding composite ratios are different for the three bridges shown in Figure 7.1. For girder (a), 5, 8, and 11 pairs of connectors correspond to composite ratios of 26%, 41%, and 56%, respectively. For girders (b) and (c), the corresponding composite ratios are 20%, 32%, and 43%, respectively.

All possible combinations of these five parameters would result in a total of 567 analyses. However, some combinations with shorter span lengths, larger numbers of connectors, larger connector spacing, and longer distances away from the interior supports were not compatible with the geometry of the bridge, as the connectors in different groups would overlap. Thus, 79 possible combinations were excluded, leaving 488 possible combinations that were analyzed in the parametric studies.

Each moving load analysis was conducted using a program developed using Visual Basic in Microsoft Excel. Because the focus of these parametric studies was on locating the connectors for optimized fatigue performance, an HS 20 fatigue truck, shown in Figure 7.3, was used as the moving load for all analyses. The provisions of the AASHTO LRFD specifications were followed for the fatigue limit state, which uses a fixed 30-foot rear axle spacing (AASHTO 2010). The analyses were conducted on single girder lines, and the truck axle loads were multiplied by the load factor and the impact factor for the Fatigue II limit state, along with the appropriate distribution factor, prior to analysis. These factors are summarized in Table 7.1. The axle loads were generally reduced to 35% to 40% of those shown in the figure, depending on the geometry of the bridge.

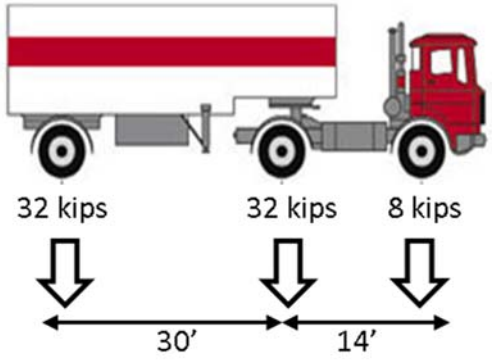

Figure 7.3 AASHTO HS 20 Fatigue Truck

Table 7.1 Load Factors Applied to Fatigue Truck Axle Forces

Load Factor	AASHTO Provision
Fatigue II Limit State Load Factor: $LL = 0.75$	Table 3.4.1-1
Impact Factor for Fatigue Limit State: $I = 1.15$	Table 3.6.2.1-1
Distribution Factor for Interior Girders: $DF = \frac{1}{MF} \cdot \left[0.06 + \left(\frac{S}{14}\right)^{0.4} \left(\frac{S}{L}\right)^{0.3} \left(\frac{K_g}{12.0Lt_s{}^3}\right)^{0.1}\right]$	Table 4.6.2.2.2b-1

The spreadsheet-based analysis was conducted using the procedure described in Appendix A, which is based on elastic beam theory in which the steel beam and concrete deck are represented as independent components attached to each other by discretely located pairs of shear connectors. The truck was moved across the girder in increments of 4 feet in both directions, and the force and slip in each shear connector was computed at each increment. When each analysis was complete, a slip range envelope was constructed by taking the difference between the maximum and minimum slip at every location along the beam. A force range envelope for each connector was developed in the same manner. Note that the force range and slip range are directly related through the connector stiffness.

Of particular interest in the results of each analysis was the maximum slip and force ranges for any connector along the girder. To optimize the fatigue behavior of the strengthened girder, the lowest possible slip and force ranges are desirable. The distribution of slip and force ranges within each connector group was also of interest. A more even distribution within a group is likely to be more efficient because a single connector pair is not required to resist significantly more force than the others. The slip envelopes for the entire girder, including the locations between connectors, was also extracted from the analyses to assess the level of composite behavior along the length of the girder.

7.3 Results of Parametric Studies

7.3.1 Variation of Span Length

Generally, the same trends were observed in the analysis of the three different bridge geometries shown in Figure 7.1. Because larger girder deflections result in more interface slip, higher slip and force demands on the connectors were generated for longer spans under the same value of load. Despite the difference in span lengths and exterior-to-interior span length ratios between the three bridges, the critical connector that was subjected to the maximum slip and force range of all the connectors along the girders was in the interior span for all analyses. In general, the resulting behavior of the connectors in all three bridge girders was similar. For simplicity, the results and plots presented in the remainder of this chapter are all from girder (b) in Figure 7.1.

7.3.2 Variation of Connector Stiffness

Of all of the parameters in this study, variations in the connector stiffness provided results that were the most difficult to interpret. Generally, increasing the connector stiffness leads to lower connector slip values and higher connector forces under the same loading conditions,

with the percentage change in slip usually exceeding the percentage change in force. However, this relationship is not linear because the horizontal motion of slip is induced in the girder from the vertical deflection caused by bending, and the two motions must be compatible with each other.

In groups with a small number of connectors closely spaced, increasing the connector stiffness tends to greatly reduce the slip but only slightly increase the force. This is illustrated in Figure 7.4(a) by comparing the steep slope of the slip range data to the shallower slope of the force range curve. This means that for these conditions, the force range in the connectors is not significantly affected by the connector stiffness. However, for larger number and spacing of connectors, the force range and the slip range tend to both be affected significantly by changes in connector stiffness, as can be seen in the similar magnitudes of slope for the force range and slip range data in Figure 7.4(b) and (c). In this figure, the connectors are located using a value of α of 0.15. Because these trends are unclear and nonlinear, it is recommended to choose a connector stiffness near the middle of the range observed experimentally and be consistent throughout analysis and design procedures. The results presented in the remainder of this chapter were obtained using a connector stiffness of 800 kips per inch.

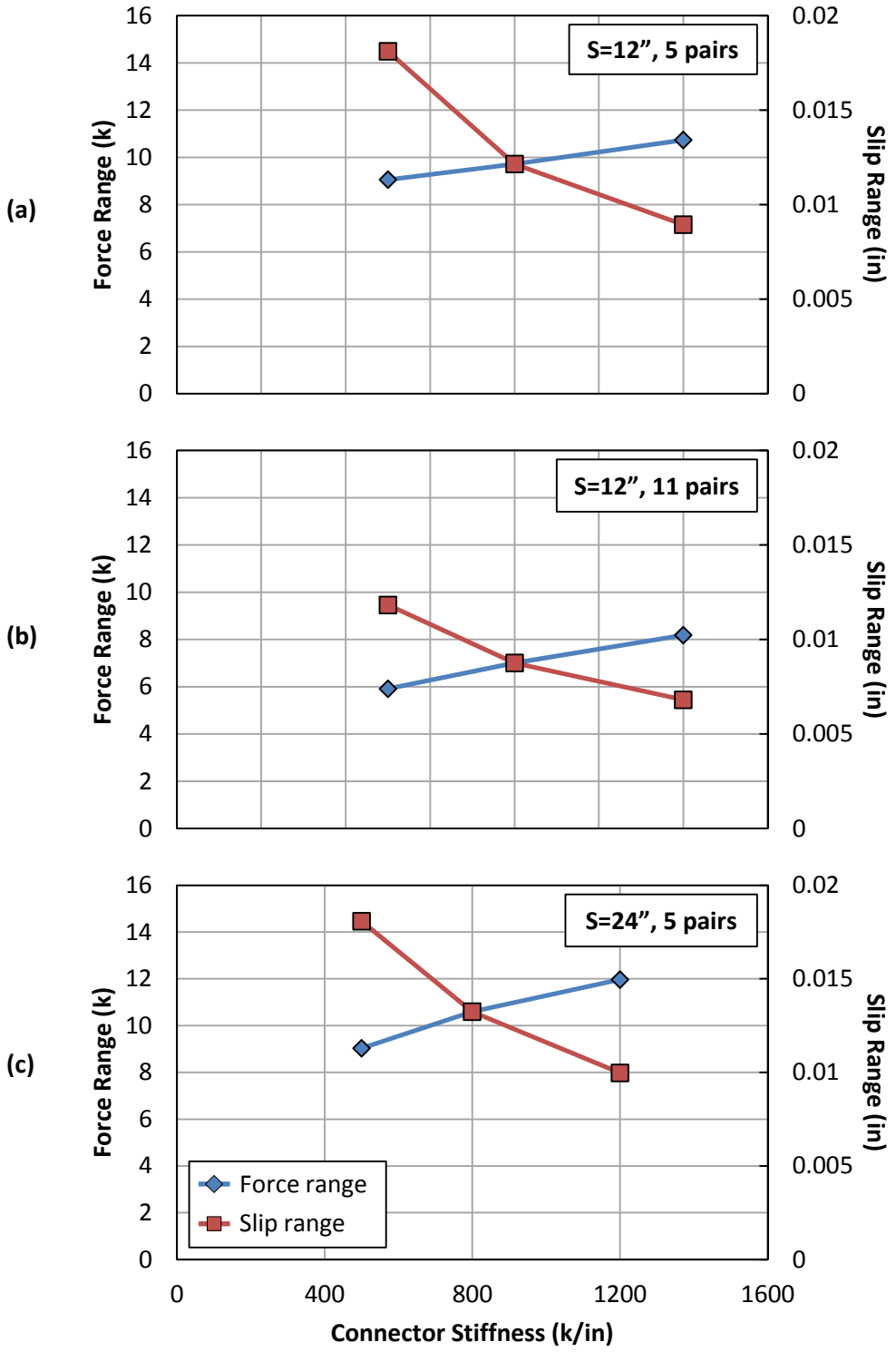

Figure 7.4 Effect of Location of Connector Groups

7.3.3 Variation of Connector Group Location

The location of the connector groups was found to be the most important factor that affects the connector slip and force demand. Figure 7.5 shows the variation of the maximum force range in any connector along the partially composite girder as a function of α, the normalized distance from the first connector pair to the interior support in each span. This graph was produced using a connector stiffness of 800 kips per inch. Although the trend is not linear and varies with different values of connector spacing and number of connectors, the force range tends to be minimized when α is 0.15 for most cases. The exception to this observation occurs when many connectors are provided at large spacing, for which a value of α of 0.1 results in the lowest force range.

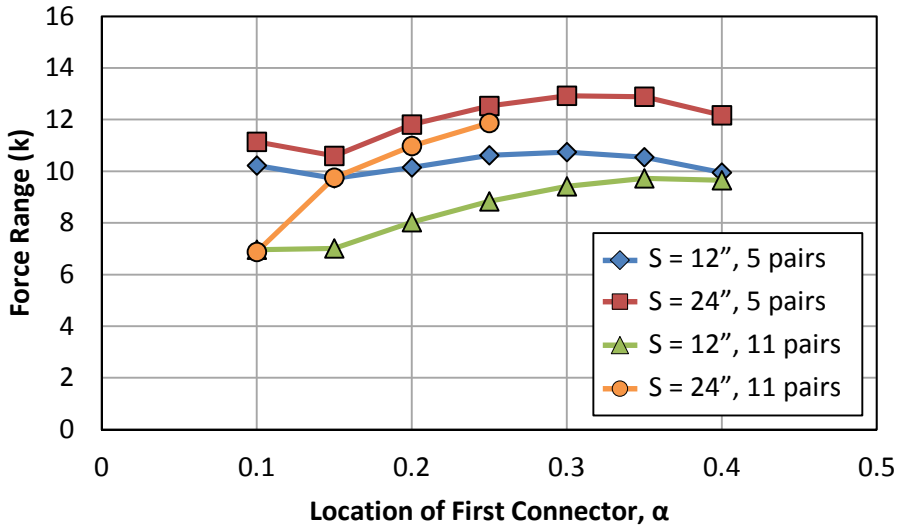

Figure 7.5 Effect of Location of Connector Groups

The reason that a value of α of approximately 0.15 results in the lowest demand on the connectors is that the distribution of forces between connectors in a single group is the most even in this configuration. This is illustrated for a particular case in Figure 7.6(a), which compares the force range for α values of 0.15 and 0.3 for all connectors located in one half of the bridge length. Note that due to symmetry, the results on the other half of the bridge are symmetric. For the case of α = 0.15, the connectors on both ends of each interior group are subjected to similar force ranges, indicating a more even distribution of forces within the group. However, for the case of α = 0.3, there is a vast discrepancy between the force range of the end connectors in each of the interior groups, indicating that the location is inefficient because of the very uneven distribution of forces within the group.

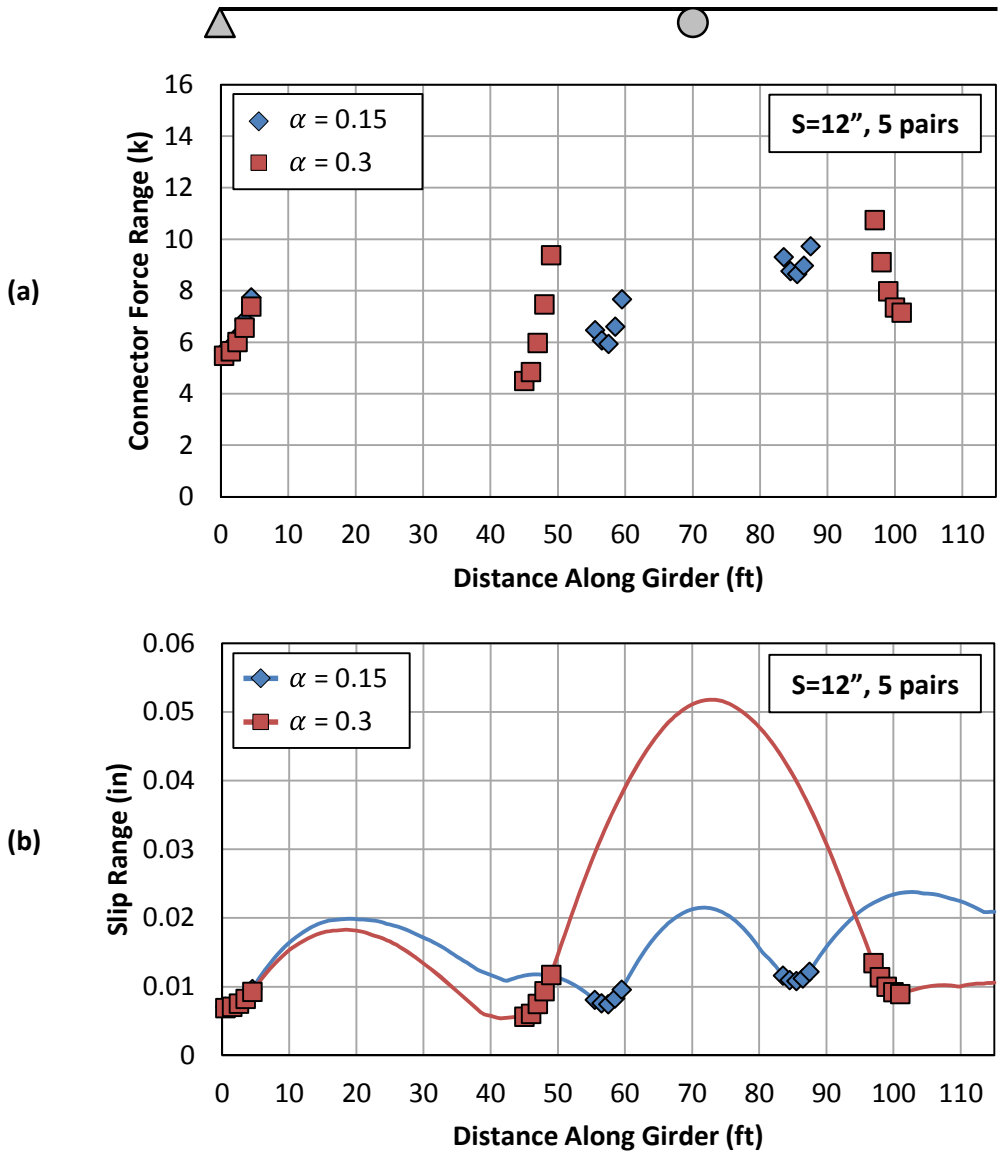

Figure 7.6 Comparison of Connector Group Locations – (a) Connector force range and (b) Profile of interface slip range

The cause of these trends is illustrated in Figure 7.6(b), which plots the slip range along the entire length of one half of the girder. The points shown on the graph represent the slip range at locations of connectors, while the lines represent the slip range between the concrete deck and steel beam at locations with no connectors. Note that the slip range at the connector locations is proportional to the connector force range shown in Figure 7.6(a) by the connector stiffness of 800 kips per inch. While the same trends within the interior connector groups are observed for the slip range as for the force range, of more interest in this plot is the slip profile over the regions of the girder between the connector groups. For the case of α = 0.15, the maximum slip range between connector groups is approximately even along the girder. However, for the case of α = 0.3, the maximum slip range near the interior pier is much larger than that in the exterior or interior spans. It appears that a more even distribution of slip of the girder between the connector

groups leads to a more efficient shear connector layout and improved elastic behavior of the connectors.

7.3.4 Variation of Connector Spacing

In most cases, larger values of connector spacing resulted in higher force and slip ranges, as shown in Figure 7.7, which also uses a connector stiffness of 800 kips per inch. However, the increase in demand with larger spacing values tends to be less significant when a smaller number of connectors are located using a value of α of 0.15. This is illustrated as the relatively flat line in the figure representing a case falling into this particular category. Practically, this means that if the connectors are located well and the composite ratio is low, a convenient spacing can be chosen for constructability without a significant impact on performance. With larger numbers of connectors or connectors that are not well-located, however, increasing the spacing tends to have a more significant effect on the maximum force and slip range demand for the connectors, a trend that is also illustrated in Figure 7.7. In this case, less flexibility on the connector spacing may be available in the design to account for field conditions and constraints.

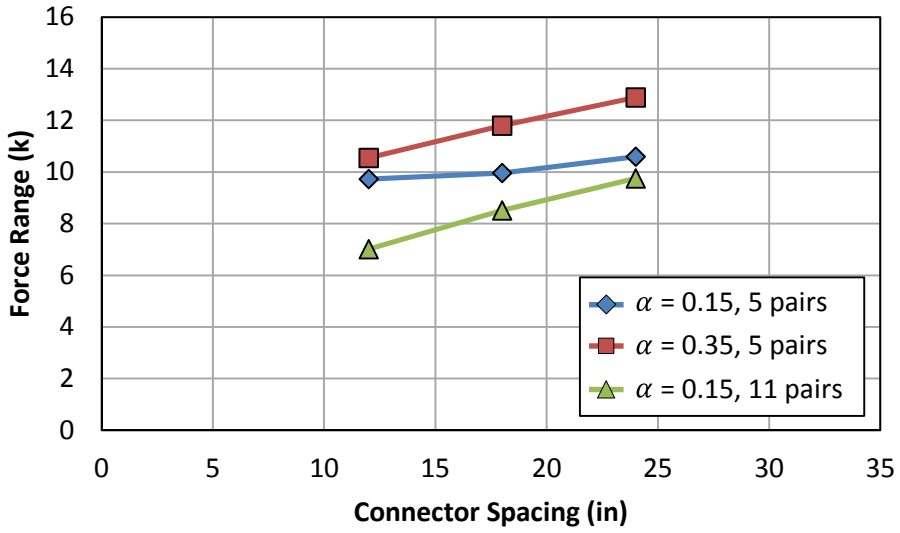

Figure 7.7 Effect of Connector Spacing

7.3.5 Variation of Composite Ratio

From an intuitive standpoint, increasing the composite ratio by providing additional connectors in each group should decrease the demand on each connector. However, because of the complexities in the mechanics of partial-composite behavior, this is not necessarily the case. The results of these studies indicate that increasing the composite ratio tends to decrease the maximum force and slip demand only if the groups are located with a value of α around 0.15 and thus have a fairly even distributions of force demand within each group. Otherwise, adding more connectors to a group does not have a significant effect on the maximum demand placed on the connectors along the girder. Furthermore, as more and more connectors are added to a group, diminishing returns are gained. For example, an increase from 5 pairs to 8 pairs causes more reduction in demand than increasing from 8 pairs to 11 pairs. Both of these trends are illustrated in Figure 7.8, in which a connector stiffness of 800 kips per inch was used.

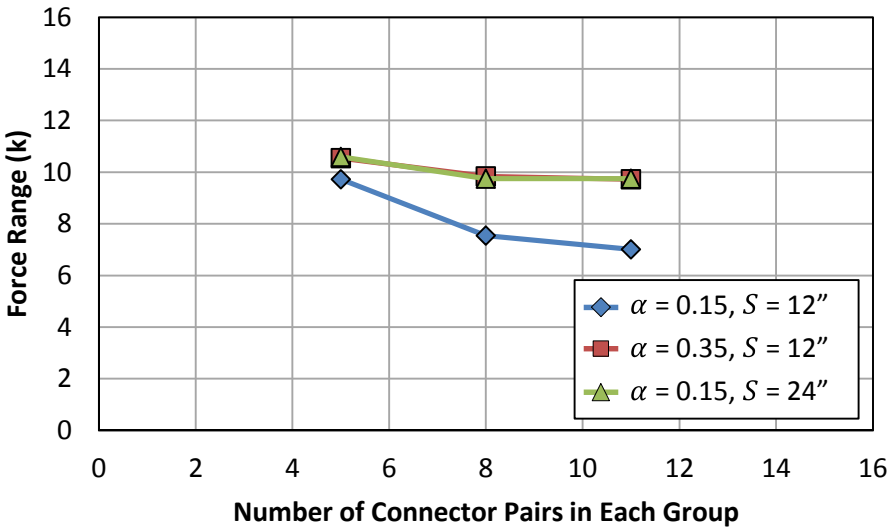

Figure 7.8 Effect of Number of Connectors per Group

7.4 Summary

A set of parametric studies consisting of 488 total analyses was carried out to investigate the effect of the shear connector layout on the elastic behavior of a strengthened bridge girder, with particular emphasis on the fatigue demands placed on the connectors. These studies were conducted using the analytical method described in Appendix A, which has been corroborated by finite element modeling in SAP2000 and ANSYS.

The results of the study indicate that the most important factor in minimizing the force and slip demand on the connectors is to locate the connector groups such that a reasonably even force distribution occurs amongst the connectors in a single group. For the girder geometries and connector layouts considered in this study, this typically corresponds to placing the interior connector groups such that the connector pair closest to the interior pier is approximately 15% of the span length away from that pier. For a large number of connectors or a wide connector spacing, the first connector should be placed closer to the interior pier to minimize the demand.

Furthermore, the results showed that increasing the composite ratio by providing additional shear connectors in a group only reduces the demand on individual connectors if the groups are well-located. The spacing of the connectors in a group also affects the maximum demand on the connectors, with larger values of spacing corresponding to higher demand. However, this effect is less significant with low composite ratios and well-located connectors.

Increasing the stiffness of the connectors tends to decrease the slip range and increase the force range, although specific trends were difficult to discern. For this reason, it is recommended to choose an average stiffness value and be consistent throughout the analysis and design process, as the stiffness may affect the results in an unexpected manner. The span length and exterior-to-interior span length ratio of the three-span girders did not significantly affect the observed trends with all other variables. As expected, larger connector slip and force ranges resulted in the longer spans under the same loading conditions.

Chapter 8. Summary, Conclusions, and Design Recommendations

8.1 Summary

This study investigated the behavior of non-composite bridge girders strengthened with post-installed shear connectors composed of adhesive anchors. Inelastic moment redistribution was also considered to address strength deficiencies in negative bending and to increase the overall capacity of the bridge. The primary objectives were to explore the performance of strengthened girders and to develop design recommendations for implementing such strengthening measures in existing non-composite continuous steel girder bridges. A variety of theoretical, analytical, and experimental tasks were completed as part of this investigation.

First, a survey of existing non-composite bridges in Texas was conducted and strengthening concept studies were carried out on several of these bridges. The typical geometry and other features of the bridges from the survey provided a basis for the later analytical and experimental tasks, while the concept studies demonstrated the existing strength deficiencies of these bridges and confirmed the feasibility for strengthening using the proposed method.

Next, a series of small-scale direct-shear fatigue tests were conducted to better characterize the fatigue strength of the post-installed adhesive anchor shear connector. In addition to conventional unidirectional loading, these tests also investigated the effects of stress reversal, or the condition in which the force on the connector changes sign during the loading cycle.

Finally, large-scale testing was conducted on a representative bridge girder strengthened with post-installed shear connectors. The comprehensive test program included elastic loading, fatigue loading, large repeated loads requiring moment redistribution, and monotonic loading to failure. A series of parametric studies aimed at determining the optimal locations to install the connectors for elastic behavior followed.

Key conclusions from all of these tasks are presented in this chapter, followed by preliminary strengthening design recommendations and connector installation procedures. The design process is illustrated in Appendix B, which provides detailed calculations throughout the strengthening process for a sample bridge.

8.2 Conclusions

The findings of this research indicate that strengthening continuous non-composite steel girder bridges with post-installed shear connectors and moment redistribution is a feasible and efficient method of extending the useful service life of a bridge. The following points summarize the major conclusions from this research:

- Many existing non-composite steel girder bridges in Texas have a significantly lower load-carrying capacity than is required by current design standards. Strengthening of these bridges may be necessary or desired to maintain safety or to avoid load posting.
- Significant strength gains can be achieved by post-installing shear connectors and allowing for moment redistribution in continuous bridges. Increases of more than 60% in the load rating of bridges from the survey were attained by strengthening to a composite ratio of only 30%. Most of the bridges in the survey require a

composite ratio of 30% and minimal to no moment redistribution to reach a load-carrying capacity exceeding that required by current design standards.

- Adhesive anchor shear connectors have improved fatigue performance over conventional welded studs. This allows for partially composite design to be used in the strengthening process, as the fatigue limit state is not likely to greatly control the number of connectors required. Stress reversal does not seem to have an adverse effect on the fatigue life, even at stress ranges as high as 35 ksi.
- As tested in the laboratory, a strengthened bridge girder exhibited resilient structural performance under service, fatigue, and strength limit states. The ultimate strength and shakedown load of the partially composite girder were well-predicted by simple plastic analysis. The application of 2 million cycles of fatigue loading did not reduce the strength of the girder at the shakedown or ultimate strength limit states.
- Interface slip should be considered when determining the force demand on shear connectors in a partially composite girder. The slip reduces the loads required to be transferred by the shear connection, oftentimes to a very large extent. This can be done analytically using the spreadsheet-based calculation method described in detail in Appendix A, or computationally using simple 3D models.
- Concentrating the post-installed shear connectors in groups near points of low moment demand increases the ductility and performance of the partially composite girder at strength limit states. To reduce the force demand on the connectors under elastic-level loads, these groups should be located as close as possible to exterior supports, and so that the connectors closest to the interior supports are approximately 15% of the span length away from those supports. The most efficient configuration of a connector group results in the most evenly distributed demand amongst all connectors in the group.

8.3 Recommended Strengthening Design Procedure

The recommended design procedure for strengthening existing bridges with post-installed shear connectors and moment redistribution is summarized in Figure 8.1. This procedure was developed for bridge girders primarily governed by flexural strength requirements and fatigue considerations. Shear strength and the behavior of other bridge components are not explicitly included here, but should be checked as well. For more details and sample calculations, refer to the design example in Appendix B.

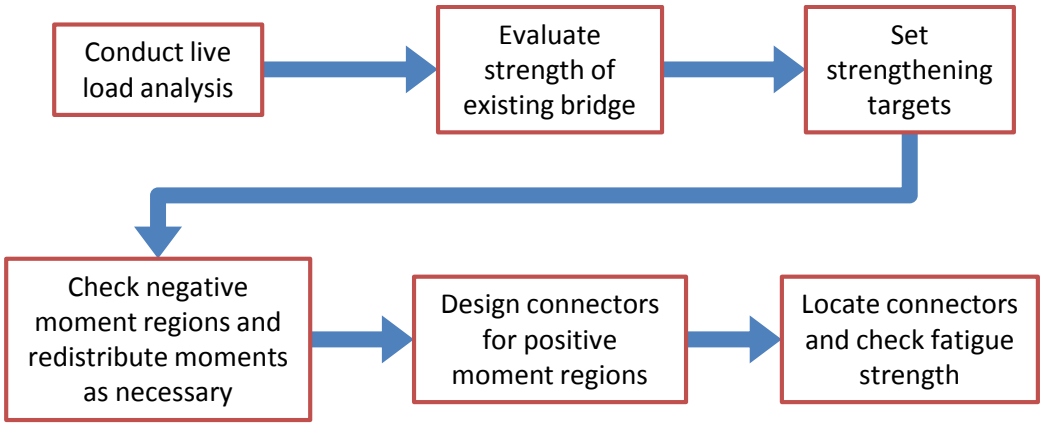

Figure 8.1 Design Procedure

8.3.1 Live Load Analysis

The first step that should be taken is to conduct a structural analysis on the bridge under the live load that will be used to evaluate the existing bridge and design the strengthened girders. This loading pattern can be chosen to meet the needs of a particular bridge or situation, allowing for flexibility in the procedure for a variety of cases. In this research project, an AASHTO HS 20 load was generally used to be consistent with the Load Factor Design and Rating methods.

The moving load analysis can be conducted in any manner desired by the designer. For the purposes of determining the live load moment envelopes, researchers have found that a simple line element analysis using a constant value of flexural stiffness along the entire length of the girder adequately represents the distribution of forces in both the non-composite existing bridge as well as the partially composite strengthened bridge for typical straight girder bridges with a fairly symmetric span layout. The appropriate distribution factors should be applied for interior and exterior girders.

Alternatively, a more rigorous live load analysis can be conducted using software with 3D modeling capabilities, such as SAP2000, which can explicitly model the steel beams, concrete deck, and shear connectors (CSI 2011). This type of analysis may be particularly useful for bridges with complex geometries. However, it requires that an initial guess of the number and layout of the shear connectors is made, leading to an iterative design procedure. It is recommended to run separate analyses for the non-composite existing bridge and for the partially composite strengthened bridge, because the moment envelopes may vary based on the location of the shear connectors. This may be especially true for asymmetric span layouts in which the composite ratio varies greatly along the length of the strengthened bridge. In any 3D model, it is recommended to represent the adhesive anchor shear connectors as linear elastic springs with a stiffness of 900 kips per inch.

8.3.2 Evaluation of Existing Bridge

Using the results from the live load analysis, the strength of the existing bridge can be determined. For the purposes of this research project, the Load Factor Rating method was used, as specified in the *AASHTO Manual for Bridge Evaluation* (AASHTO 2011). Limit states of Overload and Maximum Load were both considered in the load rating process. The Overload limit state prevents excessive permanent deformations of the bridge under typical levels of load and corresponds to the Service II limit state in the *AASHTO LRFD Bridge Design Specifications*

(AASHTO 2010). The Maximum Load limit state is a reflection of the maximum carrying capacity of the bridge and corresponds to the Strength I limit state in the LRFD specifications when only considering gravity loads.

Fatigue was not considered in the evaluation of existing bridges discussed in this report, but can be if desired. The *Manual for Bridge Evaluation* provides guidelines on evaluating the remaining fatigue life for critical details of existing bridges (AASHTO 2011). Recently proposed revisions to these guidelines are available through research conducted by the National Cooperative Highway Research Program (NCHRP 2012).

8.3.3 Targets for Strengthened Bridge

Once the existing bridge has been evaluated, targets for the strength and remaining life of the strengthened bridge should be set before beginning the design process. These targets can be chosen to accommodate any particular case, but it is recommended that both strength and fatigue limit states are considered. For fatigue purposes, a projected average daily truck traffic in a single lane ($(ADTT)_{SL}$) of the bridge over the expected remaining life should be estimated.

A strengthening target of attaining an inventory load rating of HS 20 was chosen by the researchers as an upper bound of the strengthening requirements that a bridge owner might consider. A bridge with an inventory rating of HS 20 has a load-carrying capacity meeting the design requirements for a new bridge designed with the Load Factor Design method from the *AASHTO Standard Specifications for Highway Bridges* (AASHTO 2002). No specific strengthening targets for fatigue were consistently used by the researchers. This will vary depending on the desired remaining bridge life and the projected truck traffic over that bridge life for the particular bridge of interest.

8.3.4 Check Negative Moment Regions and Redistribute Moments

To begin the design of the strengthened bridge, the first step is to check the negative moment regions around the interior piers. If the capacity of the existing non-composite girder exceeds the demand from the moment envelope at all pier locations, the negative moment regions can be deemed acceptable in terms of strength, and the design can proceed to the positive moment regions.

Otherwise, if the demand from the moment envelope at any of the pier locations exceeds the capacity of the existing non-composite girder, inelastic moment redistribution is required. It is recommended that the provisions of Appendix B6 of the AASHTO LRFD specifications be used for moment redistribution. These provisions require that the bridge is straight with no more than a 10° skew, and that the interior pier sections are well-braced, meet fairly unrestrictive slenderness limits, and have bearing stiffeners. Based on the results from the bridge survey, these provisions are generally already satisfied in most existing bridges with the exception of the support skew angle limit and the bearing stiffener requirement. In many cases, bearing stiffeners will need to be added to the bridge as part of the strengthening process.

The provisions also limit the amount of moment redistribution to 20% of the elastic moment, a requirement that does not seem to be restrictive for strengthening the surveyed bridges. By following the procedure outlined in the specifications, the “redistribution moment diagram” can be drawn. These redistribution moments are then added to the design moment envelope for the remainder of the design. Note that inelastic moment redistribution can occur at both the Overload and Maximum Load limit states, although the capacities and moment

envelopes will be different between the two cases. This process is illustrated in detail in the sample calculations provided in Appendix B.

8.3.5 Design Connectors for Positive Moment Regions

The next step in the design is focused on strengthening the positive moment regions near the middle of the spans by adding shear connectors and creating composite action. To begin this process, the required strength in these regions is determined from the design moment envelope, including the redistribution moments if applicable. Simple plastic cross-sectional analysis is then used to determine the number of connectors needed to attain the required strength, as described in Section 2.2.2 and illustrated in Appendix B. The following equation was recommended by Kwon et al. (2009) for the design strength of a single post-installed shear connector (Q_n):

$$Q_n = 0.5\, A_{sc} F_u \qquad \textit{Equation 8.1}$$

where A_{sc} is the effective shear area of the connector, taken as 80% of the nominal area for the threaded rod adhesive anchor connectors, and F_u is the specified nominal tensile strength of the connector material.

Note that the maximum strength of a composite girder is ultimately controlled by the properties of the steel girder and concrete deck, rather than the shear connectors. If the required strength in any of the positive moment regions exceeds the fully composite cross-section strength, adding more shear connectors will not result in any further strength gain. Along with the 20% limit on moment redistribution, the strength of the fully composite section places an upper limit on the potential strength increase that can be achieved for a particular bridge.

8.3.6 Locate Connectors along Bridge

After the strength design is complete, the connectors must be laid out along the girders before the fatigue limit state can be checked. The following preliminary recommendations for connector layout, illustrated in Figure 8.2, are made based on analytical and experimental investigation from the present research and from previous research (Kwon et al. 2007, 2009):

- Connectors should be placed in pairs, with one on either side of the web at every location. It is recommended that general AASHTO requirements regarding clear cover, edge distance, and minimum transverse spacing are followed. A transverse spacing of approximately 6 inches was used in all laboratory testing for beams with 10- to 11-inch wide flanges.
- It is recommended that connectors are concentrated near points of zero or low moment, rather than distributed uniformly through the positive moment regions, to improve the ductility of the strengthened girders.
- A longitudinal spacing of approximately 12 inches is recommended between pairs of concentrated connectors, although analysis indicates that the behavior is not significantly affected by slight changes in spacing, provided that the connectors are still effectively concentrated near points of low moment. All laboratory testing was conducted with a 12-inch spacing. Choosing a connector spacing that is a multiple of the transverse rebar spacing will help avoid bars during construction.
- At the ends of continuous units, the connector group should be located as close as possible to the end of the steel beam. The minimum longitudinal distance from the

centerline of the support to the first connector pair used in the experimental testing was 6 inches.

- The most efficient location for interior connector groups is typically when the connector closest to the interior support is located approximately 15% of the span length away from that support.
- Constructability and accessibility in the field should be considered when choosing a connector layout. If possible, the site should be visited to identify potential problems that may arise during connector installation. The use of a rebar locator is highly recommended to choose a layout that avoids reinforcing bars.

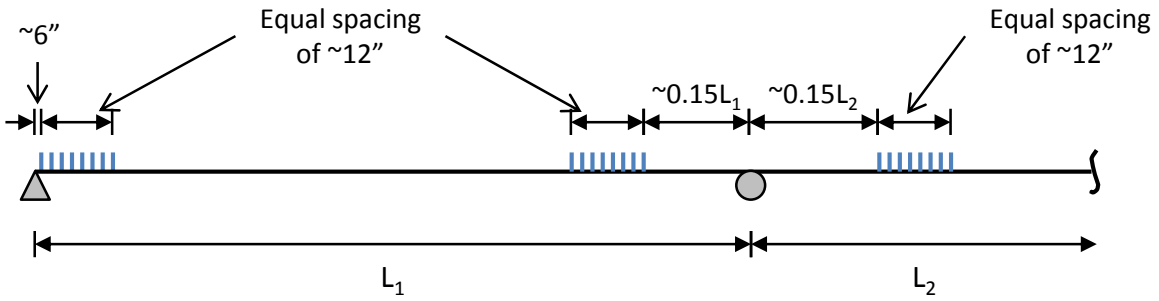

Figure 8.2 Recommended Connector Layout

8.3.7 Check Fatigue Strength of Connectors

Once a connector layout has been chosen, an analysis is conducted under fatigue loading and the connectors are checked at the fatigue limit state. The following proposed fatigue design provisions for post-installed adhesive anchor shear connectors are provided in a parallel format to those in the AASHTO LRFD specifications for conventional welded shear studs described in Section 2.4.1. The main differences between the two sets of provisions are that the expected remaining life of a strengthened bridge is likely much less than the 75-year design life of a new bridge, and that post-installed shear connectors have significantly better fatigue strength than welded studs.

For adhesive anchor connectors, the Fatigue I load combination is used to design for infinite fatigue life if the projected $(ADTT)_{SL}$ over the expected remaining bridge life in years (Y) exceeds a limiting value ($(ADTT)_{SL\ limit}$). This limit is determined by equating the infinite life and finite life fatigue shear resistances, accounting for the different load factors in the two load combinations:

$$(ADTT)_{SL\ limit}\left(\frac{trucks}{day}\right) = \frac{22600}{Y\ (years)} \qquad \textit{Equation 8.2}$$

If the $(ADTT)_{SL}$ is less than this limiting value, the Fatigue II load combination is used to design for finite life over a computed number of truck passages (N). The following equations define the fatigue shear resistance in kips (Z_r) for adhesive anchor connectors:

For infinite life and the Fatigue I load combination:

$$Z_r = 9.4d^2 \qquad \textit{Equation 8.3}$$

For finite life and the Fatigue II load combination:

$$Z_r = (63.5 - 8.5\log(N))d^2 \qquad \textit{Equation 8.4}$$

$$N = (365)(Y)n(ADTT_{SL}) \qquad \textit{Equation 8.5}$$

where d is the nominal diameter of the connector and n is the number of stress cycles on the connector for a single truck passage. For continuous bridges with span lengths greater than 40 feet, n is taken as 1.0 for all connectors located more than one-tenth of the span length away from an interior support. For connectors located within one-tenth of the span length from an interior support, n is taken as 1.5.

For all connectors on a bridge, the factored force range in kips under fatigue loading (ΔF) using the appropriate load combination cannot exceed the corresponding fatigue shear resistance (Z_r):

$$\Delta F \leq Z_r \qquad \textit{Equation 8.6}$$

In these design equations, the fatigue shear resistance for infinite life (Equation 8.3) corresponds to the endurance limit of 15 ksi that was observed during the small-scale testing discussed in Chapter 5. The fatigue shear resistance for finite fatigue life (Equation 8.4) is derived directly from Equation 5.1 using the effective area to convert from stress range to force range. It is important to note that these design equations were determined empirically from testing of 7/8-inch diameter adhesive anchor shear connectors. Slightly higher fatigue strength was observed in a few tests conducted on 3/4-inch diameter connectors in previous research (Kayir 2006). Caution should be used in applying these design equations to connectors smaller than 3/4 inches or larger than 7/8 inches in diameter.

The fatigue analysis should be conducted using the procedure adopted for the parametric studies in Chapter 7 and described in Appendix A. This procedure explicitly considers the slip at the steel-concrete interface in partially composite girders, which can significantly reduce the force demand on the connectors. While this analysis is more complex than the typical approach to designing shear connectors, it will provide more realistic connector forces for design and is easily programmed in a simple spreadsheet. Additionally, the analysis can be done computationally through reasonably simple 3D models that discretely represent the shear connectors as spring elements. In this case, the force range in the connectors can be determined directly from the forces in the spring elements. A spring stiffness of 900 kips per inch is recommended for a single shear connector in a 3D model.

8.4 Recommended Connector Installation Procedure

The adhesive anchor shear connectors, shown in Figure 1.2, are composed of 7/8-inch diameter ASTM A193 B7 threaded rods. A two-part structural adhesive (Hilti HIT-HY 150-MAX or 200-R) was used in all of the experimental testing. The connectors are installed with the following procedure, illustrated in Figure 8.3:

1. Drill a 1-inch diameter hole through the top flange of the steel beam at the connector location (Figure 8.3(a)). This can be done using a portable drill with a magnetic base.
2. Through the hole in the flange, drill a 15/16-inch diameter hole into the concrete deck to the desired depth (Figure 8.3(b)). This can be done using a rotary hammer drill. A 2-inch cover to the top of the concrete deck was maintained in all laboratory testing, leaving an embedment depth of 4.5 inches into the deck.

3. Clean the hole with a wire brush and compressed air, as specified by the adhesive installation procedures (Figure 8.3(c)).
4. Inject the adhesive into the hole using the appropriate dispenser (Figure 8.3(d)). Take care that the hole is filled from the top down so that no air bubbles are present. The Hilti adhesive was viscous enough to not run downwards out of the hole after injection.
5. Place the threaded rod into the hole using a twisting motion so the adhesive fills the threads (Figure 8.3(e)). The Hilti adhesive was able to hold the connector in place immediately after installation and has a 9-minute working time at 70°F.
6. Allow the adhesive to cure. The Hilti adhesive has a 1-hour cure time at 70°F.
7. Tighten the nut to the torque specified by the adhesive (Figure 8.3(f)). The Hilti adhesive specifies a torque of 125 foot-pounds for 7/8-inch diameter rods.
8. Strike the exposed threads below the nut with a grinder. Although it is unlikely to occur, this will prevent any nuts that inadvertently loosen over time from potentially falling onto traffic or pedestrians passing under the bridge.

Figure 8.3 Connector Installation

Generally, this procedure follows the installation process recommended by the Hilti adhesive product with a few exceptions, namely the use of a 15/16-inch diameter hole in the deck instead of the prescribed 1-inch diameter. Due to the slightly enlarged head of the hammer drill bits, a 1-inch bit does not fit through the 1-inch diameter hole in the top flange. To minimize the oversized hole in the flange, a 15/16-inch diameter bit was used for the hole drilled into the deck.

8.5 Recommendations for Future Research

The following recommendations are made for future research conducted on strengthening existing non-composite steel girder bridge with post-installed shear connectors:

- Additional fatigue testing conducted on large-scale girder specimens may help to relax the fatigue design requirements for the post-installed adhesive anchor shear connector. The design equations recommended in this report are based primarily on experimental results from small-scale direct-shear tests on individual shear connectors. Results from minimal girder fatigue tests indicate that the small-scale test results provide a lower bound for fatigue strength and that any fatigue issues may actually be "self-correcting" through degradation of the adhesive.
- Further study is warranted to simplify the procedure to estimate the force demand on shear connectors in partially composite girders with significant interface slip. While the iterative process described in Appendix A can be easily conducted using a spreadsheet, simple hand calculations are more desirable for design purposes.
- Conducting additional finite element modeling studies can expand the laboratory test results to a wider range of parameters. Particularly, investigating the effects of skewed supports and curved girders on moment redistribution behavior would widen the range of bridges that can be strengthened in this manner.
- Implementing the concepts described in this report to strengthen an existing bridge would provide cost information, and feedback from the engineers and contractors involved would aid in improving the design and installation process for future use.

References

AASHO 1961, *Specifications for Highway Bridges*, 8th edition, American Association of State Highway Officials, Washington, DC.

AASHO 1965, *Specifications for Highway Bridges*, 9th edition, American Association of State Highway Officials, Washington, DC.

AASHTO 1986, *Guide Specifications for Alternate Load Factor Design Procedures for Steel Beam Bridges Using Braced Compact Sections*, 1st edition, American Association of State Highway and Transportation Officials, Washington, DC.

AASHTO 1994, *AASHTO LRFD Bridge Design Specifications*, 1st edition, American Association of State Highway and Transportation Officials, Washington, DC.

AASHTO 2002, *Standard Specifications for Highway Bridges*, 17th edition, American Association of State Highway Officials, Washington, DC.

AASHTO 2004, *AASHTO LRFD Bridge Design Specifications*, 3rd edition, American Association of State Highway and Transportation Officials, Washington, DC.

AASHTO 2010, *AASHTO LRFD Bridge Design Specifications*, 5th edition, American Association of State Highway and Transportation Officials, Washington, DC.

AASHTO 2011, *The Manual for Bridge Evaluation*, 2nd edition, American Association of State Highway and Transportation Officials, Washington, DC.

AISC 2010, *Commentary on the Specification for Structural Steel Buildings*, American Institute of Steel Construction, Chicago, Illinois.

ASCE-WRC 1971, *Plastic Design in Steel: A Guide and Commentary*, 2nd edition, American Society of Civil Engineers and the Welding Research Council, New York, New York.

ASTM 1963, *ASTM Standards in Building Codes: Specifications, Methods of Test, Definitions*, 2nd edition, American Society for Testing and Materials, West Conshohocken, PA.

ASTM 2008, *Standard Specification for Carbon Structural Steel*, no. A 36/A 36M – 08, American Society for Testing and Materials, West Conshohocken, PA.

Barth, KE, Hartnagel, BA, White, DW & Barker, MG 2004, 'Recommended Procedures for Simplified Inelastic Design of Steel I-Girder Bridges', *Journal of Bridge Engineering*, vol. 9, no. 3, pp. 230-242.

Bergson, PM 1994, Shakedown and Ultimate Load Tests of a One-Third Scale Three-Span Composite Bridge, MS Thesis, University of Minnesota, Minneapolis, Minnesota.

Bleich, H 1932, 'Über die bemessung statisch unbestimmter stahltragwerke unter berücksichtigung des elastisch-plastischen verhaltens des baustoffes (The design of statically indeterminate steel frames considering the elastic-plastic behavior of the material)', *Bauingenieur*, vol. 13, pp. 261-267.

Carskadden PS 1980, *Autostress Design of Highway Bridges, Phase 3: Interior-Support Model Test*, Technical Report, United States Steel Corporation Research Laboratory, American Iron and Steel Institute (AISI) Project No. 188.

Chapman, JC & Balakrishnan, S 1964, 'Experiments on Composite Beams', *The Structural Engineer*, vol. 42, no. 11, pp. 369-383.

CSI 2011, *SAP2000*, Computers and Structures, Inc., Version 15, Walnut Cree, CA.

Culver, C & Coston, R 1961, 'Tests of Composite Beams with Stud Shear Connectors', *Journal of the Structural Division, Proceedings of the American Society of Civil Engineers*, vol. 87, no. ST1, pp. 1-17.

Daniels, JH & Fisher, JW 1968, *Fatigue Behavior of Continuous Composite Beams*, Research report no. 324, Fritz Engineering Laboratory, Lehigh University, Bethlehem, Pennsylvania.

Dionne, G, Picard, A, & Beaulieu, D 1997, "Development of Composite Action in Existing Non-Composite Bridges", *Conference Report: Composite Construction – Conventional and Innovative*, Innsbruck, Austria.

Eyre, DG & Galambos, TV 1970 , 'Shakedown Tests on Steel Bars and Beams', *Journal of the Structural Division, Proceedings of the American Society of Civil Engineers*, vol. 96, no. ST7, pp. 1287-1304.

Flemming, DJ 1994, *Experimental Verification of Shakedown Loads for Composite Bridges*, PhD Thesis, The University of Minnesota, Minneapolis, Minnesota.

Fukumoto, Y & Yoshida, H 1969, 'Deflection Stability of Beams Under Repeated Loads', *Journal of the Structural Division, American Society of Civil Engineers*, vol. 95, no. ST7, pp.1443-1458.

Gattesco, N & Giuriani, E 1996, 'Experimental Study on Study Shear Connectors Subjected to Cyclic Loading', *Journal of Constructional Steel Research*, vol. 38, no. 1, pp. 1-21.

Ghiami Azad, AR 2016 (expected), *Fatigue Behavior of Post-Installed Shear Connectors used to Strengthen Continuous Non-composite Steel Bridges*, PhD Dissertation, The University of Texas at Austin, Austin, Texas.

Gozum, AT 1954, *Experimental "Shakedown" of Continuous Steel Beams*, Research report no. 205G.1, Fritz Engineering Laboratory, Lehigh University, Bethlehem, Pennsylvania.

Grant Jr., JA, Fisher, JW, & Slutter, RG 1977, 'Composite Beams with Formed Steel Deck', *AISC Engineering Journal*, vol. 14, no. 1, pp. 24-43.

Grubb, MA & Carskaddan, PS 1979, *Autostress Design of Highway Bridges, Phase 3: Initial Moment-Rotation Tests*, Research Report 97-H-045(019-4), American Iron and Steel Institute (AISI), Project 188.

Grubb, MA & Carskaddan, PS 1981, *Autostress Design of Highway Bridges, Phase 3: Moment-Rotation Requirements*, Research Report 97-H-045(018-1), American Iron and Steel Institute (AISI), Project 188.

Grüning, M 1926, Die Tragfähigkeit statisch unbestimmter Tragwerke aus Stahl bei beliebig häufig wiederholter Belastung (The carrying capacity of statically indeterminate steel frames subjected to arbitrarily repeated loading), Julius Springer, Berlin, Germany.

Hansell, WG & Viest, IM 1971, 'Load Factor Design for Steel Highway Bridges', *AISC Engineering Journal*, vol. 8, no. 4, pp. 113-123.

Hartnagel, BA 1997, *Inelastic Design and Experimental Testing of Compact and Noncompact Steel Girder Bridges*, PhD Dissertation, University of Missouri-Columbia, Columbia, Missouri.

Hungerford, BE 2004, *Methods to Develop Composite Action in Non- Composite Bridge Floor Systems: Part II*, MS Thesis, The University of Texas at Austin, Austin, Texas.

Kayir, H 2006, *Methods to Develop Composite Action in Non-Composite Bridge Floor Systems: Fatigue Behavior of Post-Installed Shear Connectors*, MS Thesis, The University of Texas at Austin, Austin, Texas.

King, DC, Slutter, RG & Driscoll Jr., GC 1965, *Fatigue Strength of ½-Inch Diameter Stud Shear Connectors*, Paper 294, Fritz Laboratory Reports, Lehigh University, Bethlehem, Pennsyvania.

Klaiber, FW, Dedic, DJ, Dunker, KF & Sanders Jr., WW 1983, *Strengthening of Existing Single Span Steel Beam and Concrete Deck Bridges*, Engineering Research Institute, Iowa State University, Ames, Iowa.

Klöppel, K 1936, 'Contribution to the Question of Utilising Plasticity in Continuous Girders Subject to Repeated Stresses', *Second Congress Report of the International Association for Bridge and Structural Engineering*, pp. 77-81.

Kreitman, KL 2016 (expected), *Shakedown Behavior of Continuous Steel Bridges Strengthened with Post-Installed Shear Connectors*, PhD Dissertation, The University of Texas at Austin, Austin, Texas.

Kwon, G 2008, *Strengthening Existing Steel Bridge Girders by the Use of Post-Installed Shear Connectors*, PhD Dissertation, The University of Texas at Austin, Austin, Texas.

Kwon, G, Engelhardt, M & Klingner, R 2009, *Implementation Project: Strengthening of a Bridge near Hondo, Texas using Post-Installed Shear Connectors*, Research report no. 5-4124-01-1, Center for Transportation Research, Austin, Texas.

Kwon, G, Hungerford, B, Kayir, H, Schaap, B, Ju, YK, Klingner, R & Engelhardt, M 2007, *Strengthening Existing Non-Composite Steel Bridge Girders Using Post-Installed Shear Connectors*, Research report no. 0-4124-1, Center for Transportation Research, Austin, Texas.

Mainstone, RJ & Menzies, JB 1967a, 'Shear Connectors in Steel-Concrete Composite Beams for Bridges, Part 1: Static and Fatigue Tests on Pushout Specimens', *Concrete*, vol. 1, no. 9, pp. 291-302.

Mainstone, RJ & Menzies, JB 1967b, 'Shear Connectors in Steel-Concrete Composite Beams for Bridges, Part 2: Fatigue Tests on Beams', *Concrete*, vol. 1, no. 9, pp. 291-302.

Massonnet, C 1953, 'Essais d'adaptation et de stabilization plastiques sur des poutrelles laminees (Plastic collapse and shake-down tests on small rolled beams)', *Publications of the International Association for Bridge and Structural Engineering*, vol. 13, pp. 239-282.

Melan, E 1936, 'Theorie statisch unbestimmter systeme aus ideal plastischen baustoff (The theory of statically indeterminate systems made of ideally plastic material)', *Sitzungsberichte der Akademie der Wissenschaften*, vol. 2a, no. 145, pp. 195-218.

Mertz, DR 2004, 'Service Limit State Control of Permanent Deflection for Steel Sections in Flexure', *Structures Congress 2000: Advanced Technology in Structural Engineering*, May 2000, Philadelphia, PA.

Moore, M & Grubb, MA 1990, 'Behavior of a Two-Span Continuous Plate Girder Bridge Designed by the Alternate Load Factor Method', *AISC Engineering Journal*, vol. 27, no. 4, pp. 132-149.

Nakajima, A, Saiki, I, Kokai, M, Doi, K, Takabayashi, Y & Ooe, H 2003, 'Cyclic Shear Force-Slip Behavior of Studs under Alternating and Pulsating Load Condition', *Journal of Engineering Structures*, vol. 25, pp. 537-545.

National Cooperative Highway Research Program (NCHRP) 2012, *Fatigue Evaluation of Steel Bridges*, Report 721, Transportation Research Board, Washington, DC.

Neal, BG 1977, *The Plastic Methods of Structural Analysis*, 3rd (S.I.) edition, Chapman and Hall, New York, New York.

Newmark, NM, Seiss, CO & Veist, IM 1951, 'Tests and analysis of composite beams with incomplete interactions,' *Proceedings of the Society for Experimental Stress Analysis*, vol. 4, no. 1, pp. 75-92.

Oehlers, DJ & Bradford, MA 1995, *Composite Steel and Concrete Structural Members: Fundamental Behavior*, 1st edition, Elsevier Science Inc., Tarrytown, New York.

Patel, HV 2013, Strengthening of Noncomposite Steel Girder Bridges with Post-Installed Shear Connectors: Fatigue Behavior of the Adhesive Anchor, MS Thesis, The University of Texas at Austin, Austin, Texas.

PennDOT 2010, *BAR7 Bridge Analysis and Rating*, V7.13.0.0, Commonwealth of Pennsylvania Department of Transportation.

Proctor, MH 1963, Analytical and Experimental Study of Lightweight Concrete-Steel Composite Beams, MS Thesis, The University of Missouri, Columbia, Missouri.

Roeder, CW & Eltvik, L 1985, "An Experimental Evaluation of Autostress Design," *Transportation Research Record*, vol. 1044, pp. 35-42.

Schaap, BA 2004, Methods to Develop Composite Action in Non-Composite Bridge Floor Systems: Part I, MS Thesis, The University of Texas at Austin, Austin, Texas.

Seracino, R 1999, Partial-interaction behavior of composite steel-concrete bridge beams subjected to fatigue loading, PhD Dissertation, The University of Adelaide, Adelaide, Australia.

Seracino, R, Oehler, DJ & Yeo, MF 1999, *Reverse-Cycle Fatigue Tests on Stud Shear Connectors*, Research report no. R165, Department of Civil and Environmental Engineering, University of Adelaide, Adelaide, South Australia, Australia.

Seracino, R, Oehlers, DL & Yeo, MF 2001, "Partial-interaction flexural stresses in composite steel and concrete bridge beams," *Engineering Structures*, vol. 23, pp. 1186-1193.

Sherbourne, AN 1963, 'Some Preliminary Experiments on the Behavior of Ductile Structures Under Repeated Loads', *Experimental Mechanics*, vol. 3, no. 5, pp. 119-128.

Slutter, RG & Driscoll Jr., GC 1963, *The Flexural Strength of Steel and Concrete Composite Beams*, Paper 549, Fritz Laboratory Reports, Lehigh University, Bethlehem, Pennsylvania.

Slutter, RG & Fisher, JW 1966, *Fatigue strength of shear connectors*, Paper 214, Fritz Laboratory Reports, Lehigh University, Bethlehem, Pennsylvania.

Texas Highway Department (THD) 1951, *Standard Specifications for Road and Bridge Construction*, Texas Highway Department.

Thirugnanasundralingam, K 1991, *Continuous Composite Beams under Moving Loads*, PhD Dissertation, Monash University, Victoria, Australia.

Thurlimann, B 1959, 'Fatigue and Static Strength of Stud Shear Connectors', *Journal of the American Concrete Institute*, vol. 30, no. 12, pp. 1287-1302.

Toprac, AA 1965, 'Fatigue Strength of ¾-Inch Stud Shear Connectors', *Highway Research Record*, Highway Research Board, no. 103, pp. 53-77.

US Army Corps of Engineers (USACE) 2001, *Inspection, Evaluation, and Repair of Hydraulic Steel Structures*, Department of the Army, Washington, DC, pp. 7-22, <http://publications.usace.army.mil/publications/eng-manuals/EM_1110-2-6054/EM_1110-2-6054.pdf>

Weber, DC 1994, *Experimental Verification of Inelastic Load and Resistance Factor Design Limits*, MS Thesis, University of Missouri-Columbia, Columbia, Missouri.

Appendix A. Partial-Composite Beam Theory

Overview

Newmark et al. (1961) were the first researchers to propose a method of directly analyzing composite beams while considering slip at the steel-concrete interface. They used classical beam theory as a basis for deriving differential equations for shear flow at the interface of a composite beam, starting with simple equations that enforced equilibrium, displacement compatibility, and elastic material laws. Using several simplifying assumptions, these differential equations can be solved to yield the distribution of slip along the length of a composite girder for simple cases, such as a simply supported beam with a point load.

While many other researchers extended these concepts to further explore the theoretical behavior of partially composite beams with significant amounts of interface slip, of particular interest to this study is the work of Proctor (1963). The key difference between the two approaches is that while Newmark et al. assumed that the shear connection between the concrete slab and steel beam is continuous and uniform along the entire length of the girder, Proctor considered the existence of discrete shear connectors at particular locations. Although it was not directly considered by Proctor, this also allows for the use of inelastic load-slip behavior of each shear connector, rather than the elastic assumption made by Newmark et al. Proctor's method does not lead to closed form solutions for slip in a composite girder, and instead requires an iterative numerical solution. This appendix describes the derivation of Proctor's equations followed by a description of the iterative solution procedure used in the research reported here.

Derivation of Proctor's Equations

In deriving his equations, Proctor made the following assumptions:

1. The strain profile through the partially composite section is linear and has the same slope in both the concrete deck and steel beam, although there can be a strain discontinuity at the steel-concrete interface. A typical strain profile (ε) is shown in Figure A.1. Compressive strains are assumed to be negative while tensile strains are taken as positive values.
2. The concrete deck and the steel girder deflect the same amount at all points along the beam. Therefore, no uplift occurs along the length of the girder.
3. Neither bond nor friction is present at the interface, so that all of the interface force must be transmitted by the shear connectors, located at discrete points along the girder.
4. The concrete deck and steel beam behave according to linear elastic constitutive laws, with stress being proportional to strain. Thus, the following equation is true for both materials:

$$\phi = \frac{M}{EI} \qquad \textit{Equation A.1}$$

where ϕ is the curvature, M is the bending moment, E is the elastic modulus, and I is the moment of inertia.

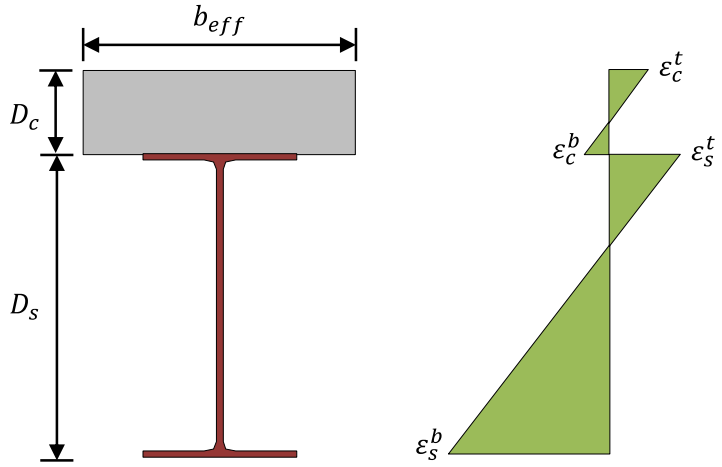

Figure A.1: Typical Strain Profile in a Partially Composite Beam

Figure A.2 illustrates the forces and moments on the steel beam and concrete deck over a distance of dx along the girder. In this figure, V refers to the vertical shear force, F represents the axial force, ΔF indicates the force carried by the shear connector, and s is the interface slip. The subscript 'c' refers to the concrete deck while the subscript 's' is associated with the steel beam.

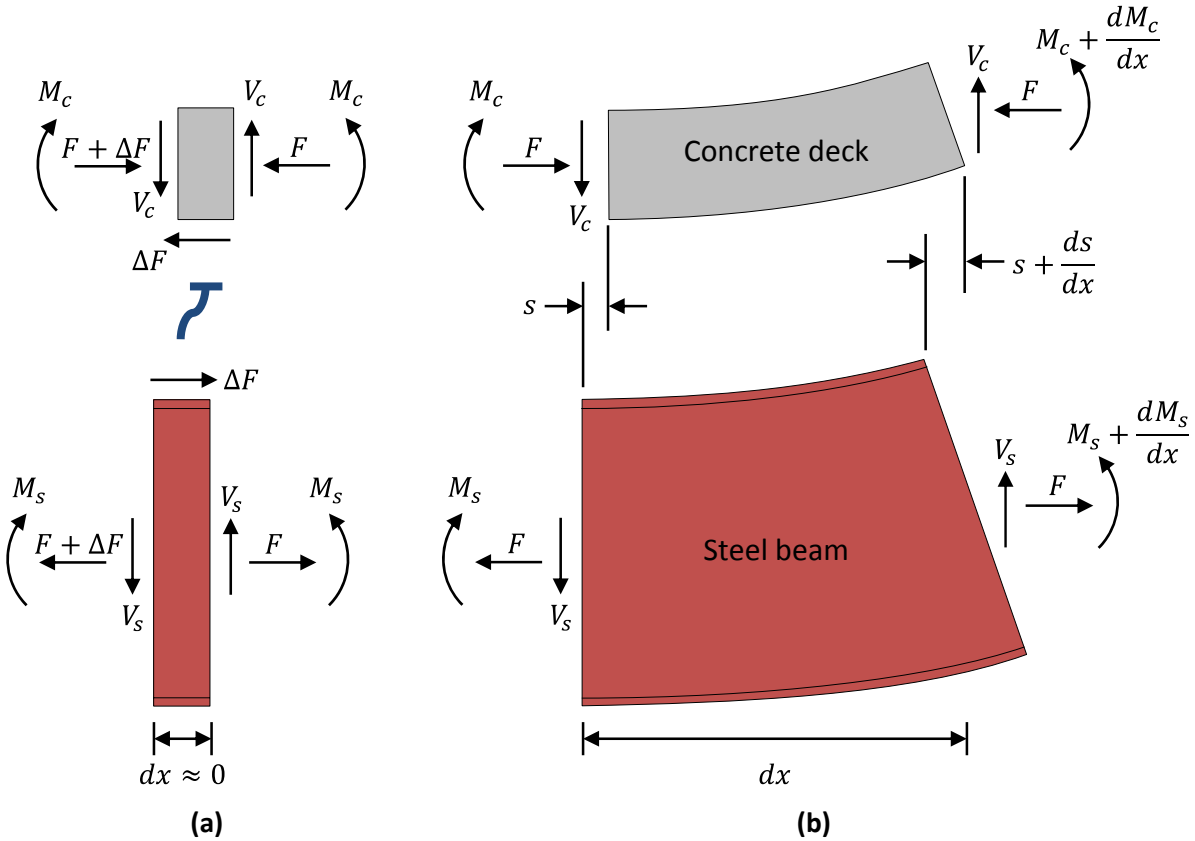

Figure A.2: Free Body Diagrams for Partial-Composite Analysis – (a) At the location of a connector and (b) With no connectors

To begin the derivation, Proctor's first assumption is stated in terms of curvature. In other words, the curvature, which is represented by the slope of the strain profile, is equivalent in the concrete deck and in the steel beam, as indicated in Equation A.2:

$$\phi = \frac{M_s}{E_s I_s} = \frac{M_c}{E_c I_c} \qquad \textit{Equation A.2}$$

The total moment (M) carried by the partially composite section consists of separate bending components in the deck and in the steel beam along with a force couple composed of the net axial force in deck and the steel beam. The total moment is obtained by adding these three components, as shown in Equation A.3, which enforces equilibrium of the internal forces in the cross section:

$$M = M_s + M_c + Fz \qquad \textit{Equation A.3}$$

where z is the vertical distance between the centroids of the concrete deck and steel beam. By rearranging and substituting Equation A.3 into Equation A.2 to eliminate M_c, Equation A.4 can be developed. Further manipulation yields Equation A.5, which defines the curvature of the section in terms of the moment, axial force, and geometric properties:

$$M_s \left[1 + \frac{E_c I_c}{E_s I_s}\right] = M - Fz \qquad \textit{Equation A.4}$$

$$\frac{M_s}{E_s I_s} = \phi = \left[\frac{M - Fz}{E_c I_c + E_s I_s}\right] \qquad \textit{Equation A.5}$$

Next, the rate of change of slip is defined as equal to the difference between the strain at the bottom of the concrete deck (ε_c^b) and the strain at the top of the steel beam (ϵ_s^t), as indicated in Equation A.6. This effectively enforces displacement compatibility at the interface. Equation A.7 and Equation A.8 define these interface strains, which have both pure bending and pure axial components, based on the strain profile shown in Figure A.1. Substituting these equations for strain into Equation A.6 and simplifying yields Equation A.9:

$$\frac{ds}{dx} = \varepsilon_c^b - \varepsilon_s^t \qquad \textit{Equation A.6}$$

$$\varepsilon_s^t = -\frac{1}{2} D_s \phi + \frac{F}{E_s A_s} \qquad \textit{Equation A.7}$$

$$\varepsilon_c^b = \frac{1}{2} D_c \phi - \frac{F}{E_c A_c} \qquad \textit{Equation A.8}$$

$$\frac{ds}{dx} = z\phi - F\left[\frac{1}{A_s E_s} + \frac{1}{A_c E_c}\right] \qquad \textit{Equation A.9}$$

The final step of the derivation is to substitute the curvature from Equation A.5 into Equation A.9 and simplify to arrive at Equation A.10. Integrating with respect to x yields Equation A.11, representing the slip between points x_1 and x_2 along the length of composite girder. Equation A.12 and Equation A.13 define the geometric variables of k_1 and k_2, respectively:

$$\frac{ds}{dx} = k_1 M - k_2 F \qquad \textit{Equation A.10}$$

$$s = k_1 \int_{x_1}^{x_2} M\, dx - k_2 \int_{x_1}^{x_2} F\, dx \qquad \textit{Equation A.11}$$

$$k_1 = \frac{z}{E_s I_s + E_c I_c} \qquad \textit{Equation A.12}$$

$$k_2 = \frac{z^2}{E_s I_s + E_c I_c} + \frac{1}{E_s A_s} + \frac{1}{E_c A_c} \qquad \textit{Equation A.13}$$

The variation in the axial force in the concrete deck and steel beam is a stepped function along the length of the girder because the discrete shear connectors are the only method of load transfer between the two materials. Thus, the second term of Equation A.11 can be written as the product of the axial force in the deck and the length of the increment ($\Delta x = x_2 - x_1$), as indicated in Equation A.14:

$$s = k_1 \int_{x_1}^{x_2} M \, dx - k_2 \, F \, \Delta x \qquad \textit{Equation A.14}$$

The force in each shear connector is computed based on the constitutive law chosen for the connectors and is a function of the slip at the location of each connector, thus requiring an iterative solution procedure, described in the following section.

Iterative Solution Procedure

Generally, the solution process is based on satisfying the boundary conditions in which no axial load is present in either the concrete deck or steel beam at the ends of the girder. The basic steps to the iterative procedure are as follows:

1. Determine all of the required geometric, material, and load parameters, as well as the constitutive law for the connectors in terms of a force-slip relationship.
2. Calculate the distribution of the bending moment along the girder by any method of structural analysis.
3. Divide the girder into increments of length for analysis. A new increment must begin at the location of every shear connector because the axial force in the deck changes at these locations.
4. Choose an arbitrary magnitude of slip at a single location along the girder. For simplicity, a zero slip can be defined at one end of the girder. Also define zero axial force at this end of the girder to satisfy the required boundary condition.
5. Starting at the end of the girder, calculate the slip accumulated at each increment along the length using Equation A.14. Additionally, calculate the associated forces in the shear connectors using the constitutive force-slip relationship to keep track of the axial force along the girder.
6. Iterate by changing the magnitude of the slip at the end of the girder and repeating step 5 until the axial force at the other end of the girder is zero.

The iterative calculations associated with determining the slip in a partially composite girder are well-suited for a spreadsheet application. Microsoft Excel was used for all of the analysis described in this report.

Appendix B. Sample Strengthening Calculations

Overview

The process for designing a strengthening scheme is illustrated in this appendix for a sample bridge. The symmetric three-span, four-girder bridge has geometry and material properties representative of bridges in the survey. For simplicity and clarity, only the interior girders will be considered in this design. However, the same process would be followed for the exterior girders as well. Figure B.1 shows half elevation, half plan, and full cross-section views of the bridge used in this example.

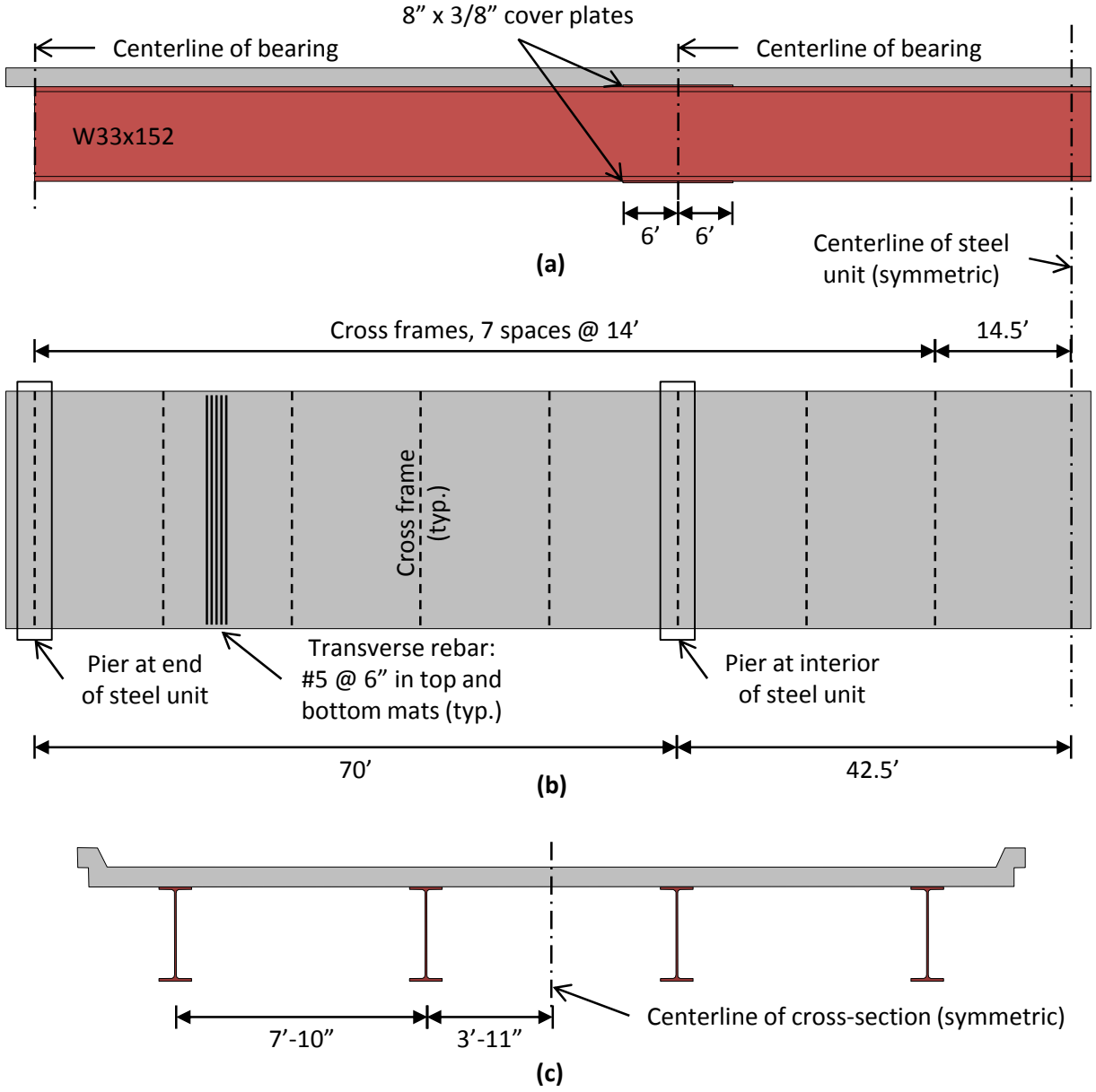

Figure B.1: Geometry of Sample Bridge – (a) Elevation, (b) Plan, and (b) Cross-section views

The following geometric and material properties are defined for the W33x152 steel beams comprising the sample bridge:

- Flange width, $b_f = 11.6\ in$
- Flange thickness, $t_f = 1.06\ in$
- Total depth, $d = 33.5\ in$
- Web thickness, $t_w = 0.635\ in$
- Area, $A_s = 44.9\ in^2$
- Moment of inertia (strong axis), $I_s = 8160\ in^4$
- Elastic section modulus, $S = 487\ in^3$
- Plastic section modulus, $Z = 559\ in^3$
- Young's modulus, $E = 29000\ ksi$
- Yield stress, $F_y = 33\ ksi$
- Web depth, $D = d - 2t_f = 33.5\ in - 2(1.06\ in) = 31.4\ in$
- Depth of web in compression under elastic loads, $D_c = \frac{D}{2} = \frac{31.4\ in}{2} = 15.7\ in$
- Depth of web in compression at plastic moment, $D_{cp} = D_c = 15.7\ in$
- Girder spacing, $S_{gird} = 94\ in$

The following geometric properties have been calculated for the W33x152 steel beam with 8"x3/8" cover plates welded to the top and bottom flanges near the interior piers:

- Total depth, $d = 34.25\ in$
- Area, $A_s = 50.9\ in^2$
- Moment of inertia (strong axis), $I_s = 9881\ in^4$
- Elastic section modulus, $S = 577\ in^3$
- Plastic section modulus, $Z = 661\ in^3$

The following geometric and material properties are defined for the concrete deck of the sample bridge:

- Effective width for interior girders, $b_{eff} = S_{gird} = 94\ in$
- Thickness, $t_{deck} = 6.5\ in$
- 28-day compressive strength of concrete, $f_c' = 3\ ksi$
- Area, $A_{deck} = b_{eff} t_{deck} = (94\ in)(6.5\ in) = 611\ in^2$
- Moment of inertia, $I_{deck} = \frac{b_{eff} t_{deck}^3}{12} = \frac{(94\ in)(6.5\ in)^3}{12} = 2151\ in^4$

- Young's modulus, $E_c(ksi) = 57\sqrt{f_c'(psi)} = 57\sqrt{3000\ psi} = 3122\ ksi$

The following geometric and material properties are defined for the post-installed adhesive anchor shear connectors, which are composed of ASTM A193 B7 threaded rods:

- Nominal diameter, $d_{sc} = \frac{7}{8} in$
- Ultimate tensile strength, $F_{u\,sc} = 125\ ksi$

Conduct Live Load Analysis

The first step in the strengthening process is to conduct a structural analysis on the bridge using the appropriate live load for the evaluation and design. In this case, the Load Factor Design and Rating methods will be used with an HS 20 live load as defined in the AASHTO *Standard Specifications for Highway Bridges* (AASHTO 2002). Because this bridge has straight, symmetric geometry, a simple line girder analysis will suffice for both the existing non-composite bridge and the strengthened composite bridge.

The software program BAR7 was used to conduct the analysis to obtain the unfactored dead load moments and live load moment envelope, which includes the appropriate dynamic impact factors and distribution factors for the interior girders (PennDOT 2010). Although the primary function of the software is conducting load rating analysis of bridges, it can also be used to easily determine the unfactored moments from an HS 20 live load. The graph in Figure B.2 plots these unfactored moments along the length of the bridge for a single interior girder. The moments at the critical points for load rating are given in Table B.1. Because of symmetry and simplicity of the girder geometry, the only critical locations are at the maximum positive moment in both the outer and middle spans, and at the maximum negative moment at the interior support. In addition to the moments at the three critical sections, the moments at the brace points in the unbraced lengths adjacent to the interior pier sections may also be necessary if inelastic moment redistribution is required. These brace point moments are also given in Table B.1.

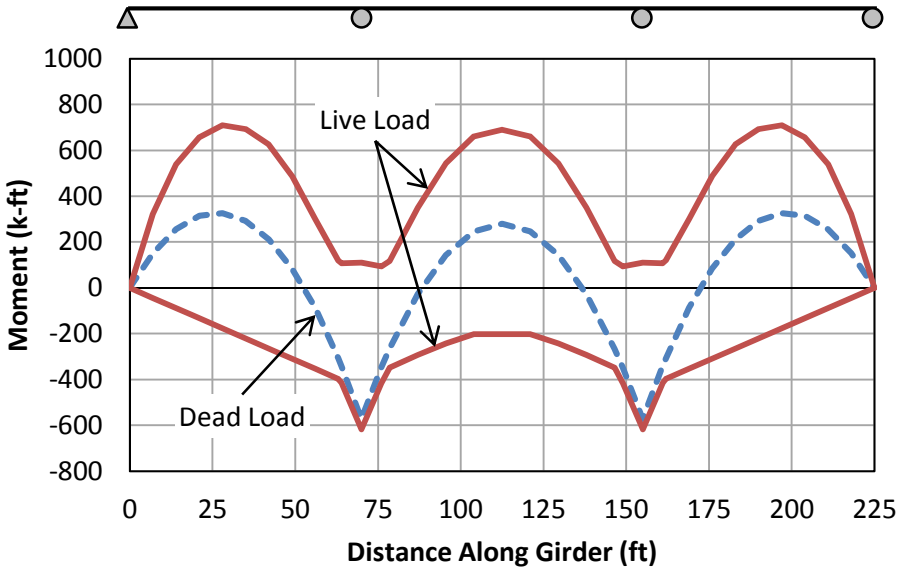

Figure B.2: Moments from Analysis of Existing Structure under HS 20 Load

Table B.1: HS 20 Moments at Critical Sections and Brace Points near Interior Piers

Distance (ft)	Unfactored Moment (k-ft)	
	Dead Load	Live Load
28	326	709
56	-88	-353
70	-572	-618
84	-111	-313
112.5	280	691

Note that in general, any section transitions, including the termination of cover plates, should also be considered as critical locations in a load rating. However, for simplicity, evaluation of the section transitions is not included in this example, as they do not control the load rating. Transition locations should be checked in both positive and negative bending in the same manner as for the other critical sections illustrated in this example.

Evaluate Existing Structure

Once the moment envelopes have been computed, the strength of the existing bridge is evaluated. This step can be carried out in any manner desired by the bridge owner. For the purposes of this example, the Load Factor Rating method will be used, as described in Section 4.4 of this report and in the AASHTO *Manual for Bridge Evaluation* (AASHTO 2011). Both the Overload and Maximum Load limit states from the *AASHTO Standard Specifications for Highway Bridges* will be considered in the rating (AASHTO 2002), and only inventory load ratings will be considered. The inventory load rating corresponds directly to design loads that are safe to be repeatedly applied to the bridge, while the operating load rating, which is not considered in this example, represents the maximum live load the bridge can be subjected to. Fatigue will not be considered in the evaluation of the existing bridge. Additionally, only gravity loads are considered in the evaluation, which is limited to flexural behavior only. This procedure inherently assumes that the flexural capacity of the girders controls the strength of the bridge. Other limit states and bridge components should be checked as well, including shear forces in the girders and capacity of the substructure elements.

For load rating purposes, the capacity (C) at each of the critical sections depends on the limit state considered. For the Overload limit state, the maximum stress in the steel beam is limited to 80% of the yield stress for non-composite sections. This is equivalent to limiting the moment in the girder to 80% of the yield moment (M_y) for this case, in which the short-term and long-term section moduli are the same. For the Maximum Load limit state, the capacity is simply the nominal moment strength (M_n) of the section. Because this bridge has compact steel girders and is well braced, the nominal moment capacity is equal to the plastic moment that can be developed in the steel (M_p). The capacities for both limit states are:

W33x152, no cover plates:

$$C_{Overload} = 0.8M_y = 0.8SF_y = 0.8(487\ in^3)(33\ ksi)\left(\frac{1\ ft}{12\ in}\right) = 1071\ k.ft$$

$$C_{Max\ Load} = M_p = ZF_y = (559\ in^3)(33\ ksi)\left(\frac{1\ ft}{12\ in}\right) = 1537\ k.ft$$

W33x152 with cover plates:

$$C_{Overload} = 0.8M_y = 0.8SF_y = 0.8(577\ in^3)(33\ ksi)\left(\frac{1\ ft}{12\ in}\right) = 1269\ k.ft$$

$$C_{Max\ Load} = M_p = ZF_y = (661\ in^3)(33\ ksi)\left(\frac{1\ ft}{12\ in}\right) = 1818\ k.ft$$

Once the capacities are defined, the rating factor (RF) is computed for each critical section using Equation 4.1, and the load factor rating (LFR) is obtained by multiplying the rating factor by 20, since an HS 20 load was used in the structural analysis. The following calculations summarize this process:

$$RF_{Overload}\ at\ 28' = \frac{(1071\ k.ft) - (1.0)(326\ k.ft)}{\left(\frac{5}{3}\right)(709\ k.ft)} = 0.63\ \rightarrow\ LFR = HS\ 12.6$$

$$RF_{Max\ Load}\ at\ 28' = \frac{(1537\ k.ft) - (1.3)(326\ k.ft)}{(2.17)(709\ k.ft)} = 0.72\ \rightarrow\ LFR = HS\ 14.5$$

$$RF_{Overload}\ at\ 70' = \frac{(1269\ k.ft) - (1.0)(572\ k.ft)}{\left(\frac{5}{3}\right)(618\ k.ft)} = 0.68\ \rightarrow\ LFR = HS\ 13.5$$

$$RF_{Max\ Load}\ at\ 70' = \frac{(1818\ k.ft) - (1.3)(572\ k.ft)}{(2.17)(618\ k.ft)} = 0.80\ \rightarrow\ LFR = HS\ 16.0$$

$$RF_{Overload}\ at\ 112.5' = \frac{(1071\ k.ft) - (1.0)(280\ k.ft)}{\left(\frac{5}{3}\right)(691\ k.ft)} = 0.69\ \rightarrow\ LFR = HS\ 13.7$$

$$RF_{Max\ Load}\ at\ 112.5' = \frac{(1537\ k.ft) - (1.3)(280\ k.ft)}{(2.17)(691\ k.ft)} = 0.78\ \rightarrow\ LFR = HS\ 15.6$$

Thus, ***the interior girders of the existing bridge have an inventory load factor rating of HS 12.6***, which is the lowest rating calculated from all critical sections. The rating is controlled by the Overload limit state in the positive moment region of the outer span (at 28').

Set Strengthening Targets

Any desired strengthening target can be chosen by the bridge owner. For the purposes of this example, an inventory load factor rating of HS 20 will be targeted for strength limit states. This target represents the required strength of a new bridge designed using the load factor design method in the AASHTO *Standard Specifications for Highway Bridges* (AASHTO 2002). For the fatigue limit state, a target of 20 additional years of fatigue life (Y) is set. The projected single lane average daily truck traffic ($(ADTT)_{SL}$) over the next 20 years is 300 trucks per day.

Because the target rating of HS 20 is the same as the live load used in the structural analysis of the existing bridge, the moments in Table B.1 are also valid for the strengthening design. If a different magnitude of HS loading is chosen as a target, the moments from Table B.1 should be adjusted proportionally. If a different type of live load is targeted for the strengthened bridge, a new structural analysis should be conducted using that live load.

Check Negative Moment Regions and Redistribute Moments

To begin the design of the strengthened bridge, the non-composite negative moment regions are first checked for strength at the Overload and Maximum Load limit states to determine if any inelastic moment redistribution is necessary. The capacity at both limit states remains the same as in the evaluation of the existing structure. The factored elastic moments at the interior pier section (at 70') are:

$$M_{u\ Overload} = (1.0)(572\ k.ft) + \left(\frac{5}{3}\right)(618\ k.ft) = 1602\ k.ft$$

$$M_{u\ Max\ Load} = (1.3)(572\ k.ft) + (2.17)(618\ k.ft) = 2085\ k.ft$$

At the Overload limit state, the factored moment (1602 k-ft) at the interior pier section is greater than the capacity (1269 k-ft). Similarly, at the Maximum Load limit state the factored moment (2085 k-ft) at the interior pier section also exceeds the capacity (1818 k-ft). This indicates that inelastic moment redistribution is required from the interior piers for both limit states.

Inelastic moment redistribution should be accounted for using the provisions in Appendix B6 of the AASHTO *LRFD Bridge Design Specifications* (AASHTO 2010). To begin, the bridge geometry and cross section at the pier must meet several requirements, as stated in section B6.2 of the LRFD specifications:

1. The bridge must be straight with supports not skewed more than 10° $\rightarrow\ OK$
2. The specified minimum yield stress does not exceed 70 ksi $\rightarrow\ OK$
3. Holes in the tension flange may not be present within a distance of twice the web depth from each interior pier section from which moments are redistributed $\rightarrow\ OK$
4. The web proportions cannot violate the following requirements:

   $$\frac{D}{t_w} \leq 150\ \rightarrow\ \frac{31.4\ in}{0.635\ in} \leq 150\ \rightarrow\ 49 \leq 150\ \rightarrow\ OK$$

   $$\frac{2D_c}{t_w} \leq 6.8\sqrt{\frac{E}{F_y}}\ \rightarrow\ \frac{2(15.7\ in)}{0.635\ in} \leq 6.8\sqrt{\frac{29000\ ksi}{33\ ksi}}\ \rightarrow\ 49 \leq 202\ \rightarrow\ OK$$

   $$D_{cp} \leq 0.75D\ \rightarrow\ 15.7\ in \leq 0.75(31.4\ in)\ \rightarrow\ 15.7\ in \leq 23.6\ in\ \rightarrow\ OK$$

5. The compression flange proportions cannot violate the following requirements:

   $$\frac{b_f}{2t_f} \leq 0.38\sqrt{\frac{E}{F_y}}\ \rightarrow\ \frac{11.6\ in}{2(1.06\ in)} \leq 0.38\sqrt{\frac{29000\ ksi}{33\ ksi}}\ \rightarrow\ 5.47 \leq 11.3\ \rightarrow\ OK$$

   $$b_f \geq \frac{D}{4.25}\ \rightarrow\ 11.6\ in \geq \frac{31.4\ in}{4.25}\ \rightarrow\ 11.6\ in \geq 7.4\ in\ \rightarrow\ OK$$

   For simplicity here, the cover plates are ignored in the compression flange proportion calculations.

6. There cannot be any section transitions within the unbraced length of the interior pier section → OK

   Note that this design assumes that termination of the cover plates within the unbraced length of the interior pier is not considered to be a section transition. This is not directly specified in the AASHTO specifications, but will be assumed for the design. However, when making this assumption, it is important to ensure that the steel section at the location of cover plate termination is not expected to yield prior to the section with cover plates at the location of the interior pier under the specified loads. If the critical section for flexural strength at any limit state including moment redistribution is located at the termination of the cover plates, this requirement should be considered violated and no moment redistribution should be allowed.

7. The compression flange must be adequately braced to prevent lateral-torsional buckling and allow the section to achieve enough plastic rotation to adequately redistribute moments:

   $$L_b \leq \left[0.1 - 0.06\left(\frac{M_1}{M_2}\right)\right]\frac{r_t E}{F_y}$$

   Because the unbraced length is the same on both sides of the interior pier, the critical ratio of the factored brace point moments (M_1 and M_2) is the most positive value that can be obtained from either side of the interior pier. By observation, this occurs in the unbraced length in the outer span (between 56' and 70'). Note that because both load factors for the Maximum Load limit state are exactly 30% greater than the two load factors for the Overload limit state, the moment ratios will always be the same for the two limit states:

   $$\left(\frac{M_1}{M_2}\right)_{Overload} = \frac{(1.0)(88\ k.ft) + \left(\frac{5}{3}\right)(353\ k.ft)}{(1.0)(572\ k.ft) + \left(\frac{5}{3}\right)(618\ k.ft)} = 0.42$$

   $$\left(\frac{M_1}{M_2}\right)_{Max\ Load} = \frac{(1.3)(88\ k.ft) + (2.17)(353\ k.ft)}{(1.3)(572\ k.ft) + (2.17)(618\ k.ft)} = 0.42$$

   The effective radius of gyration (r_t) is defined in Appendix A6 of the AASHTO LRFD specifications (again, ignoring the cover plates):

   $$r_t = \frac{b_f}{\sqrt{12\left(1 + \frac{1}{3}\frac{D_c t_w}{b_f t_f}\right)}} = \frac{11.6\ in}{\sqrt{12\left(1 + \frac{1}{3}\frac{(15.7\ in)(0.635\ in)}{(11.6\ in)(1.06\ in)}\right)}} = 2.97\ in$$

   So the unbraced length is checked as follows:

   $$(14\ ft)\frac{(12\ in)}{(1\ ft)} \leq [0.1\ in - (0.006\ in)(0.42)]\frac{(2.97\ in)(29000\ ksi)}{(33\ ksi)}$$

   $168\ in \leq 254\ in\ \rightarrow\ OK$

8. Bearing stiffeners must be present at the interior pier locations → $NOT\ OK$

Thus, bearing stiffeners must be added to the girders to allow for inelastic moment redistribution. These stiffeners should be designed according to the provision in Article 6.10.11.2 in the AASHTO LRFD specifications. These provisions require double-sided stiffeners that extend over the full depth of the web and as close to the outer edges of the flanges as is practical. Thus, choose a stiffener width of 5 inches and calculate the minimum thickness using the following equation from the AASHTO LRFD specifications:

$$b_t \leq 0.48 t_p \sqrt{\frac{E}{F_y}} \rightarrow t_p \geq \frac{b_t}{0.48}\sqrt{\frac{F_y}{E}} \rightarrow t_p \geq \frac{(5\ in)}{0.48}\sqrt{\frac{33\ ksi}{29000\ ksi}} \rightarrow t_p \geq 0.35\ in$$

Choose a thickness of 3/8 inches so that ***double-sided 5-inch by 3/8-inch bearing stiffeners should be installed at the interior pier sections***. Strength considerations for the bearing stiffeners can be addressed by investigating the effects of the concentrated reaction force at the interior piers. Equations for the strength of the stiffeners can also be found in Article 6.10.11.2.

Because the girder and interior pier sections satisfy the requirements for inelastic moment redistribution, pending the addition of the bearing stiffeners, the design process can continue. Note that if these conditions are not met, moment redistribution cannot be allowed and the maximum load rating that can be achieved through the strengthening process may be limited by the existing strength at the interior pier sections.

The flexural capacity of the interior pier regions when considering moment redistribution is the effective plastic moment (M_{pe}), which accounts for the slenderness of the section to ensure that enough plastic rotation capacity exists at the pier section to adequately redistribute moments at both the Overload and Maximum Load limit states. The interior pier section is considered to have "enhanced moment-rotation characteristics" because the web satisfies the below requirement and is thus considered to be "ultracompact." The effective plastic moment for both limit states is calculated below. Note that because the section is compact and well-braced, the nominal moment capacity (M_n) is equal to the plastic moment capacity (M_p). Again, for simplicity in the calculations, the cover plates are not included in any terms involving slenderness or aspect ratios.

$$\frac{2D_{cp}}{t_w} \leq 2.3\sqrt{\frac{E}{F_y}} \rightarrow \frac{2(15.7\ in)}{0.635\ in} \leq 2.3\sqrt{\frac{29000\ ksi}{33\ ksi}} \rightarrow 49.5 \leq 68.2 \rightarrow OK$$

$$M_{pe\ Overload} = M_n = M_p = ZF_y = (661\ in^3)(33\ ksi)\left(\frac{1\ ft}{12\ in}\right) = 1818\ k.ft$$

$$M_{pe\ Max\ Load} = \left(2.78 - 2.3\frac{b_f}{t_f}\sqrt{\frac{F_y}{E}} - 0.35\frac{D}{b_f} + 0.39\frac{b_f}{t_f}\sqrt{\frac{F_y}{E}}\frac{D}{b_f}\right)M_n \leq M_n$$

$$= \left(2.78 - 2.3\left(\frac{11.6\ in}{1.06\ in}\right)\sqrt{\frac{33\ ksi}{29000\ ksi}} - 0.35\left(\frac{31.4\ in}{11.6\ in}\right)\right.$$

$$\left. + 0.39\left(\frac{11.6\ in}{1.06\ in}\right)\sqrt{\frac{33\ ksi}{29000\ ksi}}\left(\frac{31.4\ in}{11.6\ in}\right)\right)(1818\ k.ft) \leq 1818.ft$$

$$\rightarrow\ M_{pe\ Max\ Load} = 1818\ k.ft$$

Once the capacity has been calculated, it is compared to the factored moments, which were calculated previously, to determine how much moment redistribution is required at each limit state. The difference between the capacity and the factored moment at each interior pier is called the "redistribution moment" (M_{rd}), which is limited to 20% of the factored moment at each pier:

$$M_{rd\ Overload} = M_{u\ Overload} - M_{pe\ Overload} = 1602\ k.ft - 1818\ k.ft = -216\ k.ft$$

$$M_{rd\ Max\ Load} = M_{u\ Max\ Load} - M_{pe\ Max\ Load} = 2085\ k.ft - 1818\ k.ft = 267\ k.ft$$

$$\frac{M_{rd\ Max\ Load}}{M_{u\ Max\ Load}} \leq 20\% \rightarrow \frac{267\ k.ft}{2085\ k.ft} \leq 20\% \rightarrow 13\% \leq 20\% \rightarrow OK$$

Because the capacity exceeds the factored moments at the Overload limit state, no actual moment redistribution is necessary, indicated by the negative redistribution moment. This is because of the significant increase in capacity from the $0.8M_y$ limit to the full plastic moment capacity (M_p). For the Maximum Load limit state, moment redistribution is required, as the factored moment exceeds the capacity at the interior pier section. The redistribution moment is 13% of the factored elastic moment, which is below the maximum of 20% allowed by the specifications. The redistribution moment diagram for Maximum Load is shown in Figure B.3, along with the same dead load and live load moments from Figure B.2. Table B.2 summarizes the value of the redistribution moment at each of the critical sections, along with the same dead and live load moments from Table B.1. The redistribution diagram is constructed by first plotting the redistribution moments calculated at each of the interior piers, and then connecting them by straight lines, with zero moment at the end of the girder. For the remainder of the design, the redistribution moments will be added to the dead and live load moments for the Maximum Load limit state. Note that the redistribution moments have a load factor of 1.0 in all load combinations.

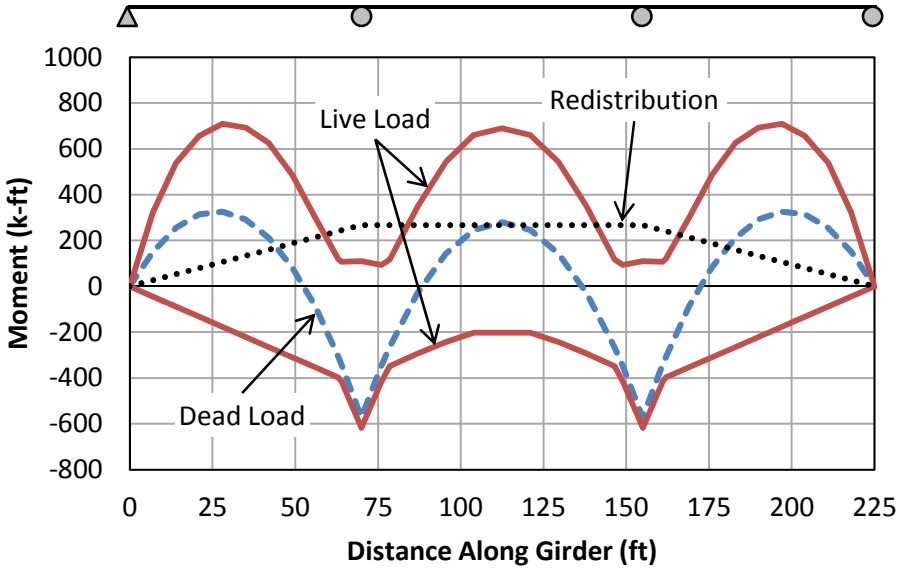

Figure B.3: Dead Load, Live Load and Redistribution Moments from Initial Analysis of Strengthened Structure under HS 20 Load

Table B.2: HS 20 and Residual Moments at Critical Sections

Distance (ft)	Unfactored Moment (k-ft)		
	Dead Load	Live Load	Redistribution
28	326	709	107
70	-572	-618	267
112.5	280	691	267

Design Post-Installed Shear Connectors for Positive Moment Regions

Now that the redistribution moments are known, the partially composite positive moment regions can be designed and checked at both the Overload and Maximum Load limit states. For this bridge, a different design needs to be conducted for the outer span, which has a critical section at 28', and for the middle span, which has a critical section at 112.5'. The design can be completed first for the Overload limit state and then checked at the Maximum Load limit state, or vice versa. In this case, the Maximum Load limit state will be investigated first.

Design for the Maximum Load Limit State

The factored moments, including redistribution moments, for each of these critical sections at the Maximum Load limit state are:

$$M_{u\ Max\ Load}\ at\ 28' = 1.3(326\ k.ft) + 2.17(709\ k.ft) + 1.0(107\ k.ft) = 2069\ k.ft$$

$$M_{u\ Max\ Load}\ at\ 112.5' = 1.3(280\ k.ft) + 2.17(691\ k.ft) + 1.0(267k.ft) = 2130\ k.ft$$

The capacity at the Maximum Load limit state is the nominal moment capacity of the section (M_n). This will usually be equal to the plastic moment of the partially composite cross section, because the deck typically provides continuous lateral support for the top flange of the

girder to prevent lateral torsional buckling, and little to none of the steel section is required to resist large compressive forces, so local buckling is unlikely to control. First, the fully composite section is analyzed to determine the number of connectors required for full-composite action as well as the strength and stiffness of the fully composite section, indicated by the subscript "FC". The number of connectors needed is simply the compression force in the deck (C_f) divided by the strength of a single connector (Q_n), given by Equation 2.12. Simple plastic cross-sectional analysis, as described in Section 2.2.2, is then used to determine the properties of the fully composite section.

$$C_{f\,FC} = min\begin{Bmatrix} 0.85f_c' A_{deck} \\ A_s F_y \end{Bmatrix} = min\begin{Bmatrix} 0.85(3\ ksi)(611\ in^2) \\ (44.9\ in^2)(33\ ksi) \end{Bmatrix} = min\begin{Bmatrix} 1558\ k \\ 1482\ k \end{Bmatrix} = 1482\ k$$

$$Q_n = 0.5A_{sc}F_{u\,sc} = 0.5\left(0.8\left(\frac{\pi d_{sc}^2}{4}\right)\right) = 0.5\left(0.8\left(\frac{\pi\left(\frac{7}{8}in\right)^2}{4}\right)\right)(125\ ksi) = 30.1\ k$$

$$N_{FC} = \frac{C_{f\,FC}}{Q_n} = \frac{1482\ k}{30.1\ k} = 49.2$$

Generally, the number of connectors in a design should be rounded up to the next even number, as they are installed in pairs. However, since the final design is unlikely to be fully composite, the number of connectors required for a fully composite girder can remain as a decimal at this point. Also, because the second term in the equation for C_f is the smallest, the plastic neutral axis will be in the concrete deck.

The stress distribution at the plastic moment capacity is shown in Figure B.4. Force resultants, which act at mid-height of the corresponding stress block, are indicated by filled arrowheads and bold labels. The unknown distance "a" represents the depth of the concrete deck that is in compression and can be solved for using the known compressive force in the deck ($C_{f\,FC}$). Because the concrete is assumed to resist no tensile stresses, the only forces in the system are the tensile force in the steel and the compressive force in the deck. Summing forces in the horizontal direction is trivial due to the definition of the compressive force in the deck. The plastic moment capacity (M_p) is calculated by summing moments on the section. For simplicity, the moment is calculated using the force couple of T_s and $C_{f\,FC}$:

$$T_s = A_s F_y = (44.9\ in^2)(33\ ksi) = 1482\ k$$

$$C_{f\,FC} = 0.85f_c' b_{eff} a \ \rightarrow\ a = \frac{C_{f\,FC}}{0.85f_c' b_{eff}} = \frac{1482\ k}{0.85(3\ ksi)(94\ in)} = 6.18\ in$$

$$M_{p\,FC} = \Sigma M_{interface} = T_s\left(\frac{d}{2} + \left(t_{deck} - \frac{a}{2}\right)\right) = (1482\ k)\left(\frac{33.5\ in}{2} + \left(6.5\ in - \frac{6.18\ in}{2}\right)\right)$$

$$= (29877\ k.in)\left(\frac{1\ ft}{12\ in}\right) = 2490\ k.ft$$

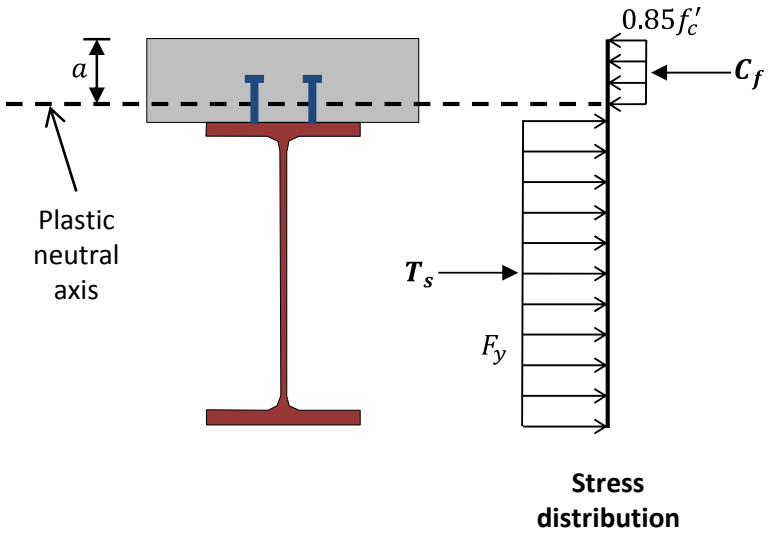

Figure B.4: Stress Distribution at Plastic Moment of Fully Composite Section

The transformed moment of inertia (I_{tr}) and elastic section modulus to the extreme bottom fiber of the steel beam (S_{tr}) of the fully composite section can also be calculated using basic concepts of mechanics of materials, along with locating the elastic neutral axis (at a distance of y_{NA} below the interface). Two sets of calculations follow, one of which corresponds to the short-term composite section and the other of which corresponds to the long-term composite section. The short-term composite section properties, indicated by the subscript "*ST*", are calculated using the short-term modular ratio of n while the long-term composite section properties, indicated by the subscript "*LT*", are calculated using the long-term modular ratio of $3n$:

Short-term section:

$$n = \frac{E_s}{E_c} = \frac{29000\ ksi}{3122\ ksi} = 9.3$$

$$y_{NA\ ST} = \frac{A_s\left(\frac{d}{2}\right) - \frac{A_{deck}}{n}\left(\frac{t_{deck}}{2}\right)}{A_s + \frac{A_{deck}}{n}} = \frac{(44.9\ in^2)\left(\frac{33.5\ in}{2}\right) - \frac{(611\ in^2)}{9.3}\left(\frac{6.5\ in}{2}\right)}{(44.9\ in) + \frac{(611\ in^2)}{9.3}} = 4.87\ in$$

$$I_{tr\ ST} = I_s + A_s\left(\frac{d}{2} - y_{NA}\right)^2 + \frac{I_{deck}}{n} + \frac{A_{deck}}{n}\left(\frac{t_{deck}}{2} + y_{NA}\right)^2$$

$$= 8160\ in^4 + (44.9\ in^2)\left(\frac{33.5\ in}{2} - 4.87in\right)^2 + \frac{(2151\ in^4)}{9.3}$$

$$+ \frac{(611\ in^2)}{9.3}\left(\frac{6.5\ in}{2} + 4.87\ in\right)^2 = 19060\ in^4$$

$$S_{tr\ ST} = \frac{I_{tr\ ST}}{d - y_{NA}} = \frac{19060\ in^4}{(33.5\ in) - (4.87\ in)} = 666\ in^3$$

Long-term section:

$$3n = 3(9.3) = 27.9$$

$$y_{NA\,LT} = \frac{A_s\left(\frac{d}{2}\right) - \frac{A_{deck}}{3n}\left(\frac{t_{deck}}{2}\right)}{A_s + \frac{A_{deck}}{3n}} = \frac{(44.9\ in^2)\left(\frac{33.5\ in}{2}\right) - \frac{(611\ in^2)}{27.9}\left(\frac{6.5\ in}{2}\right)}{(44.9\ in) + \frac{(611\ in^2)}{27.9}} = 10.2\ in$$

$$I_{tr\,LT} = I_s + A_s\left(\frac{d}{2} - y_{NA}\right)^2 + \frac{I_{deck}}{3n} + \frac{A_{deck}}{3n}\left(\frac{t_{deck}}{2} + y_{NA}\right)^2$$

$$= 8160\ in^4 + (44.9\ in^2)\left(\frac{33.5\ in}{2} - 10.2\ in\right)^2 + \frac{(2151\ in^4)}{27.9}$$

$$+ \frac{(611\ in^2)}{27.9}\left(\frac{6.5\ in}{2} + 10.2\ in\right)^2 = 14130\ in^4$$

$$S_{tr\,LT} = \frac{I_{tr\,LT}}{d - y_{NA}} = \frac{14130\ in^4}{(33.5\ in) - (10.2\ in)} = 606\ in^3$$

Now that the analysis of the fully composite section is complete, the iterative process of designing the partially composite section can be done. Since the plastic strength of the fully composite section (2490 k-ft) is greater than the factored moments in both the outer and middle spans (2069 k-ft and 2130 k-ft, respectively) at the Maximum Load limit state, the girder can be strengthened to the target level using partial-composite design. To begin, choose an approximate composite ratio, and calculate the number of connectors required and the strength of the partially composite section, indicated by a subscript "PC." Recall that because the connectors are installed in pairs, the number of connectors should be rounded up to the nearest even number. The strength calculations are conducted in the exact same manner as for the fully composite section, except the interface shear ($C_{f\,PC}$) will now be controlled by the strength of the partially composite shear connection. This means that the plastic neutral axis will always be located in the steel beam.

For this example, a composite ratio (η) of approximately 30% will be chosen to start. Composite ratios smaller than 30% are not recommended. The first step is to compute the number of connectors corresponding to the desired composite ratio and calculate the compressive force in the deck ($C_{f\,PC}$):

$$N_{PC} = \eta\, N_{FC} = (0.3)(49.2) = 14.76 \rightarrow N_{PC} = 16 = 8\ pairs$$

$$\eta_{actual} = \frac{N_{PC}}{N_{FC}} = \frac{16}{49.2} = 0.325$$

$$C_{f\,PC} = min\begin{Bmatrix} 0.85f_c'A_{deck} \\ A_sF_y \\ N_{PC}Q_n \end{Bmatrix} = min\begin{Bmatrix} 0.85(3\ ksi)(611\ in^2) \\ (44.9\ in^2)(33\ ksi) \\ (16)(30.1\ k) \end{Bmatrix} = min\begin{Bmatrix} 1558\ k \\ 1482\ k \\ 482\ k \end{Bmatrix} = 482\ k$$

Next, determine whether the plastic neutral axis is located in the top flange or in the top portion of the web of the steel beam. If the plastic neutral axis is in the web of the steel beam, the net force in the top and bottom flanges will cancel out, since the section is doubly symmetric. Thus, the plastic neutral axis can only be in the web of the steel beam if the maximum plastic force that can be developed in the web ($P_{y\,web}$) is greater than the compressive force in the slab ($C_{f\,PC}$), which is the case here. Otherwise, the plastic neutral axis would be located in the top flange of the steel beam:

$$P_{y\,web} = A_{web}F_y = \left(A_s - 2A_f\right)F_y = \left(A_s - 2b_f t_f\right)F_y$$
$$= \left(44.9\ in^2 - 2(11.6\ in)(1.06\ in)\right)(33\ ksi) = 670\ k$$

$$670\ k > 482\ k\ \rightarrow\ P_{y\,web} > C_{f\,PC}\ \rightarrow\ Plastic\ neutral\ axis\ is\ in\ the\ web$$

The stress distribution for this partially composite case is shown in Figure B.5. For simplicity, an equivalent stress distribution, shown in the far right portion of the figure, will be used for the calculations. Using the equivalent stress distribution helps to simplify the calculations while keeping the same net stresses on the section. In this equivalent stress distribution, the top half of the steel is shown under the yield stress in compression, while the bottom half of the steel is subjected to the yield stress in tension. This stress distribution creates two equal and opposite force resultants that form a force couple with the same magnitude as the plastic moment of the steel section ($M_{p\,steel}$). The portion of the steel above mid-depth of the beam and below the plastic neutral axis is also under a tensile stress of twice the yield stress. The unknown distance "z" represents the height of the web above mid-depth of the steel section but below the plastic neutral axis, and can be solved for by summing forces on the section. Again, the depth of the concrete compression block is denoted "a":

$$a = \frac{C_{f\,PC}}{0.85f_c' b_{eff}} = \frac{482\ k}{0.85(3\ ksi)(94\ in)} = 2.01\ in$$

$$T_s = zt_w\left(2F_y\right) = (z)(0.635\ in)\left(2(33\ ksi)\right) = \left(41.9\frac{k}{in}\right)(z)$$

$$M_{p\,steel} = Z\,F_y = (559\ in^3)(33\ ksi) = 18447\ k.in$$

$$\Sigma F = 0\ \rightarrow\ T_s - C_{f\,PC} = 0\ \rightarrow\ \left(41.9\frac{k}{in}\right)(z) - 482\ k = 0\ \rightarrow\ z = 11.5\ in$$

$$M_{p\,PC} = \Sigma M_{interface} = T_s\left(\frac{d}{2} - \frac{z}{2}\right) + C_{f\,PC}\left(t_{deck} - \frac{a}{2}\right) + M_{p\,steel}$$
$$= \left(\left(41.9\frac{k}{in}\right)(11.5\ in)\right)\left(\frac{(33.5\ in)}{2} - \frac{(11.5\ in)}{2}\right)$$
$$+ (482\ k)\left(6.5\ in - \frac{2.01\ in}{2}\right) + 18447\ k.in = (26396\ k.in)\left(\frac{1\ ft}{12\ in}\right)$$
$$= 2200\ k.ft$$

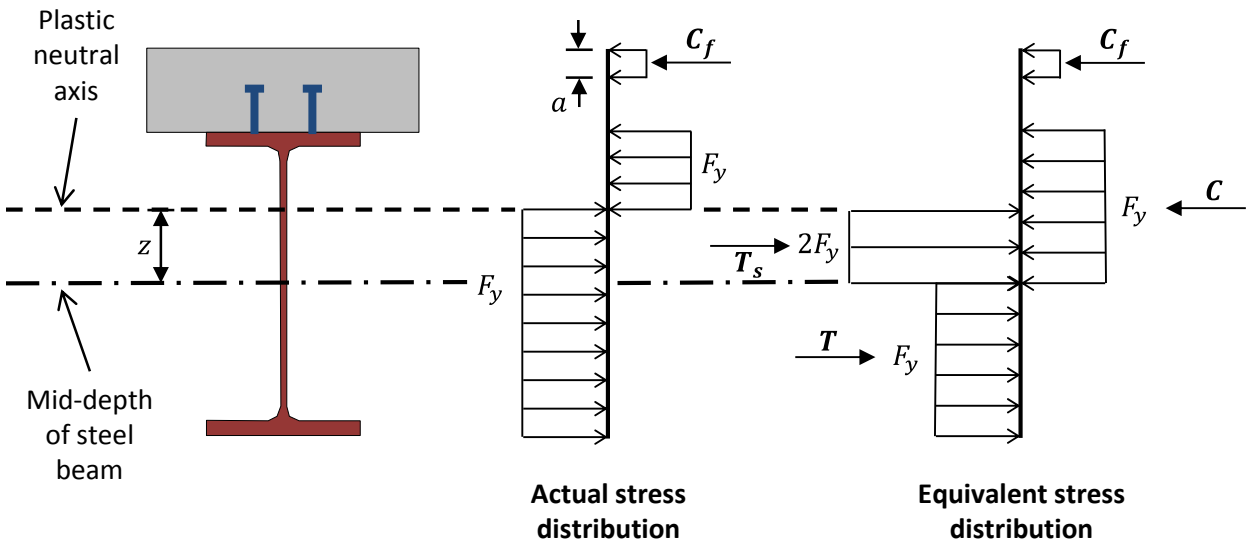

Figure B.5: Stress Distribution at Plastic Moment of Partially Composite Section

The plastic moment capacity of the approximately 30% partially composite section (2200 k-ft) exceeds both the maximum factored moment in the middle span (2130 k-ft) and the maximum factored moment in the outer spans (2069 k-ft). Because 30% is the minimum recommended composite ratio, choose $N_{PC} = 16$ for both the middle and outer spans in this design, to satisfy the requirements of the Maximum Load limit state.

Check the Design at the Overload Limit State

Next, check the Overload limit state with $N_{PC} = 16$ in both the middle and outer spans. Computing the stress in the steel portion of any composite section due to bending moments resulting from different types of load generally consists of using several different values of the section modulus for the different load types. For bridges strengthened with post-installed shear connectors, all dead load present prior to the installation of the connectors is applied to the non-composite section. Any dead load applied after the connectors are installed, such as an overlay of the driving surface, is applied to the long-term composite section, along with any redistribution moments. The long-term composite section properties are determined using the long-term modular ratio of $3n$. The live load is applied to the short-term composite section, in which the section properties are computed using the short-term modular ratio of n. The short- and long-term effective elastic moduli of the partially composite section (S_{eff}) are calculated using the relationship given in Equation 2.5, by substituting "*S*" for "*I*". Note that because there are no redistribution moments at the Overload limit state, the long-term effective elastic section modulus will not be used in any calculations:

$$S_{eff\ ST} = S_s + \sqrt{\eta_{actual}}(S_{tr\ ST} - S_s) = (487\ in^3) + \sqrt{0.325}\big((666\ in^3) - (487\ in^3)\big)$$
$$= 589\ in^3$$

$$S_{eff\ LT} = S_s + \sqrt{\eta_{actual}}(S_{tr\ LT} - S_s) = (487\ in^3) + \sqrt{0.325}\big((606\ in^3) - (487\ in^3)\big)$$
$$= 555\ in^3$$

The following factored stresses are calculated at the Overload limit state in regions of positive bending:

$$\sigma_{u\ Overload}\ at\ 28' = 1.0\left(\frac{326\ k.ft}{487\ in^3}\right)\left(\frac{12\ in}{1\ ft}\right) + \left(\frac{5}{3}\right)\left(\frac{709\ k.ft}{589\ in^3}\right)\left(\frac{12\ in}{1\ ft}\right) = 32.1\ ksi$$

$$\sigma_{u\ Overload}\ at\ 112.5' = 1.0\left(\frac{280\ k.ft}{487\ in^3}\right)\left(\frac{12\ in}{1\ ft}\right) + \left(\frac{5}{3}\right)\left(\frac{691\ k.ft}{589\ in^3}\right)\left(\frac{12\ in}{1\ ft}\right) = 30.4\ ksi$$

For a composite section, the extreme stress in the steel beam is limited to 95% of the yield stress at the Overload limit state. Note that this requirement applies to only fully composite sections in the AASHTO specification, which does not currently allow for partial-composite design. The difference in stress limits between non-composite (80%) and fully composite (95%) sections is primarily due to the vast difference in the ratio of nominal moment capacity (M_n) to yield moment (M_y) for the two types of sections. Even with low composite ratios, partially composite sections have nominal moment-to-yield moment ratios much closer to fully composite sections than to non-composite sections; therefore, the 95% stress limit is recommended for use with partially composite strengthened girders. Thus, the capacity, or maximum allowed stress (σ_{max}), at the Overload limit state is calculated as:

$$\sigma_{max} = 0.95F_y = 0.95(33\ ksi) = 31.4\ ksi$$

This maximum allowed stress (31.4 ksi) is exceeded by the factored stresses in the outer spans (32.1 ksi), but not in the middle span (30.4 ksi). Thus, using $N_{PC} = 16$ in the middle span satisfies the Overload limit state as well as the Maximum Load limit state, and the design of this span is complete. However, more shear connectors are needed to satisfy the requirements of the Overload limit state in the outer spans. The required short-term elastic section modulus can be calculated to limit the stress from the factored loads to the maximum allowed stress in both the outer and middle spans. Then, the required composite ratio can be calculated, along with the required number of connectors. Note that this calculation becomes more complicated if there are also redistribution moments or any other loads applied to the long-term composite section:

$$\sigma_{max} \geq (1.0)\left(\frac{M_{dead\ load}}{S_s}\right) + \left(\frac{5}{3}\right)\left(\frac{M_{live\ load}}{S_{eff\ ST}}\right) \rightarrow S_{eff\ ST} \geq \frac{\left(\frac{5}{3}\right)M_{live\ load}}{\sigma_{max} - (1.0)\left(\frac{M_{dead\ load}}{S_s}\right)}$$

$$S_{eff\ ST} = S_s + \sqrt{\eta}(S_{tr\ ST} - S_s) \rightarrow \eta = \left(\frac{S_{eff\ ST} - S_s}{S_{tr\ ST} - S_s}\right)^2$$

$$S_{eff\ ST\ req'd}\ at\ 28' = \frac{\left(\frac{5}{3}\right)(709\ k.ft)\left(\frac{12\ in}{1\ ft}\right)}{(31.4\ ksi) - (1.0)\left(\frac{(326\ k.ft)\left(\frac{12\ in}{1\ ft}\right)}{487\ in^3}\right)} = 607\ in^3$$

$$\eta_{req'd}\ at\ 28' = \left(\frac{(607\ in^3) - (487\ in^3)}{(666\ in^3) - (487\ in^3)}\right)^2 = 0.45$$

$$N_{req'd}\ at\ 28' = \eta_{req'd}N_{FC} = (0.45)(49.2) = 22.1 \rightarrow N_{PC}\ at\ 28' = 24 \rightarrow \eta_{actual}\ at\ 28' = \frac{N_{PC}\ at\ 28'}{N_{FC}} = \frac{24}{49.2} = 0.488$$

Thus, to satisfy the requirements of the Overload limit state, $N_{PC} = 24$ connectors must be provided in the outer spans, corresponding to a composite ratio of nearly 50%. This design will also satisfy the Maximum Load limit state, since the flexural capacity of the partially composite sections will be greater than the required 30% composite section chosen previously. The design of the middle span is not controlled by the Overload limit state, so $N_{PC} = 16$ connectors must be provided to satisfy the Maximum Load limit state and maintain a composite ratio not less than 30%.

In summary, to satisfy the requirements of the strength limit states considered (Overload and Maximum Load), ***use $N_{PC} = 24$ in the outer spans and $N_{PC} = 16$ in the middle span***. Note that N is the number of shear connectors required between points of zero and maximum moment. Thus, the two outer spans will each contain two sets of 24 connectors, while the middle span will contain two sets of 16 connectors, resulting in ***a total of 128 connectors along a single interior girder line***.

Layout Connectors

Before checking the fatigue behavior of the post-installed shear connectors, a connector layout must be chosen. Based on the recommendations given in Chapter 8, the layout in Figure B.6 is proposed. Because the girder is symmetric, only the left half is shown in the figure. Within a group, the connectors are spaced at 12 inches, which is equal to the transverse rebar spacing in the deck. The connector nearest to the end of the girder is located 6 inches away from the centerline of the support, while the connectors nearest to the interior support are located a distance of approximately $0.15L$ from that support.

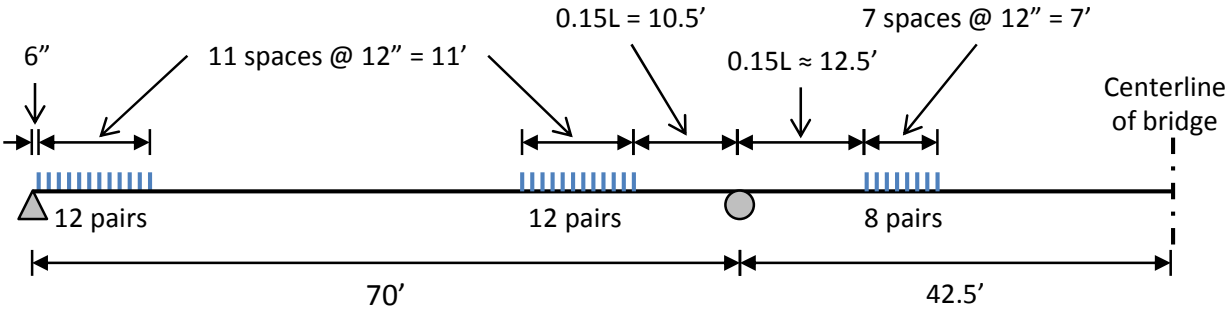

Figure B.6: Proposed Connector Layout

In addition to the recommendations provided for locating the connectors, it is important to consider constructability and field conditions when choosing a connector layout, paying particular attention to the accessibility of the locations along the girder in which the connectors are to be installed. Because small changes in the connector layout will likely not significantly affect the behavior, some adjustments can be made in the field when necessary. It is highly recommended to use a rebar locator to find the transverse deck reinforcement in the locations where the connectors will be installed. Once the bars are located, modify the connector layout so that the connectors are installed approximately halfway between reinforcing bars and use a connector spacing equal to a multiple of the bar spacing. This should prevent conflicts with reinforcing bars when drilling into the deck to install the connectors.

Check Fatigue Limit State

The first step in checking the connectors for fatigue is to determine which load combination from the AASHTO LRFD specifications is to be used. As described in Chapter 8, the Fatigue I load combination controls whether the projected average daily truck traffic in a single lane ($(ADTT)_{SL}$) is greater than or equal to the limiting value ($(ADTT)_{SL\ limit}$) calculated with Equation 8.2. Otherwise, the Fatigue II load combination is to be used for finite fatigue life over a number of cycles (N) calculated using Equation 8.5. The Fatigue II load combination controls in this case, so the appropriate fatigue shear resistance is calculated using Equation 8.4:

$$(ADTT)_{SL\ limit}\left(\frac{trucks}{day}\right) = \frac{22600}{Y\ (years)} = \frac{22600}{20\ years} = 1130\frac{trucks}{day}$$

$$(ADTT)_{SL} = 300\frac{trucks}{day} < 1130\frac{trucks}{day} \rightarrow use\ Fatigue\ II\ load\ combination$$

$$N = (365\ )Y\ n\ (ADTT)_{SL} = \left(365\frac{days}{year}\right)(20\ years)\left(1.0\frac{cycle}{truck}\right)\left(300\frac{trucks}{day}\right)$$
$$= 2{,}190{,}000\ cycles$$

$$Z_r = (63.5 - 8.5\,log(N))d^2 = (63.5 - 8.5\,log(2{,}190{,}000))\left(\frac{7}{8}in\right)^2 = 7.35\ k$$

Next, the fatigue analysis is conducted using the method described in Appendix A. This method explicitly considers the interface slip between the steel beam and concrete deck, which is restricted by linear elastic springs that represent the shear connectors. The stiffness of these springs used in the analysis is 900 kips per inch for a single shear connector. Note that because the connectors are installed in pairs with one on either side of the web in a cross section, the stiffness of a connector pair will be 1800 kips per inch.

The calculations were carried out in Microsoft Excel in a similar manner to that described in Chapter 7. An AASHTO HS 20 fatigue truck, with the appropriate load, dynamic impact, and distribution factors for the Fatigue II load combination and bridge geometry, was moved along the bridge in 4-foot increments in both directions to determine the force range that each connector is subjected to under fatigue loading. Figure B.7 shows the force range for the connectors under fatigue loading. Again, because of symmetry, only connectors on one half of the bridge are shown.

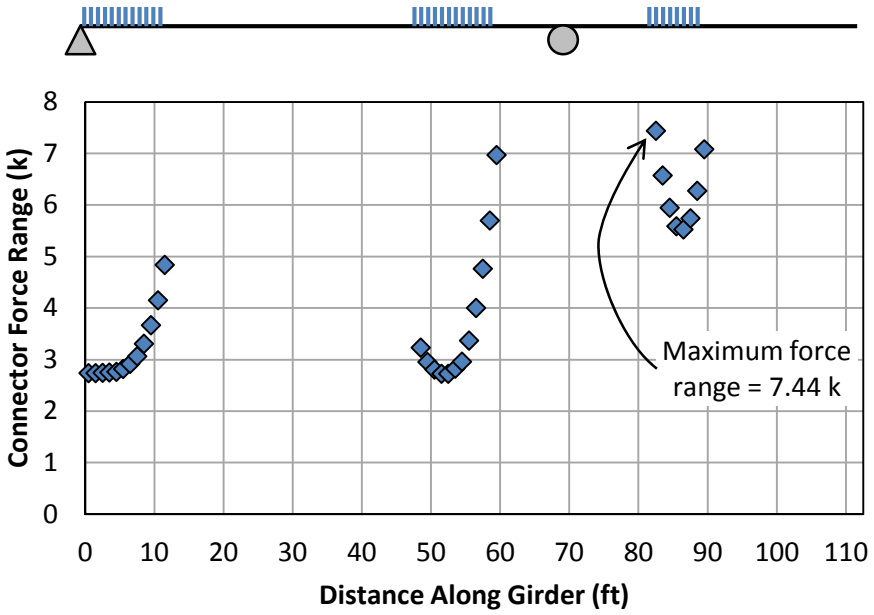

Figure B.7: Results from Fatigue Analysis

The maximum force range (ΔF) that a connector undergoes during fatigue loading is 7.44 kips. As shown in Figure B.7, the critical connector is the closest connector to the interior support in the middle span. This maximum connector force range is greater than the fatigue resistance of a single connector (7.35 kips), indicating that the fatigue behavior for this connector layout is slightly inadequate for the desired life of the strengthened bridge. Thus, the connector layout must be modified or additional connectors must be added to reduce the fatigue demands.

The most efficient way to modify the connector layout to reduce the force demands is to shift the interior connector groups along the length of the girder to find a balanced layout for which the connectors on either end of the group are subjected to approximately the same force range. This is accomplished by moving the connector groups in the direction of the connector in the group subjected to the largest force range. It is most important to find this balanced layout for the connector group with the largest force range, but shifting the non-critical connector groups towards a balanced layout can also help reduce the demand on more critical connectors. Exterior connector groups should remain as close as practical to the ends of the girder.

In this case, because the critical connector group (in the middle span) is already very balanced, try shifting the connector group closest to the interior support in the outer span. However, take care that the first connector is not located closer than one-tenth of the span length from the interior support, as this increases the number of cycles of load on the connector per truck passage (N) from 1 to 1.5, leading to a significant reduction in the fatigue resistance. Figure B.8 shows the results of the fatigue analysis of a slightly modified connector layout in which the connector group in the outer span closest to the interior support is shifted 3.5 feet towards that support. As can be seen in the figure, the force ranges are more evenly distributed between the connectors in that particular group. Additionally, the maximum force range in all connector groups in the modified layout is reduced from the initial layout. The maximum force range (7.17 kips) is now less than the fatigue resistance (7.35 kips), indicating that the connectors have adequate fatigue life to satisfy the design requirement of 20 years of remaining life. Thus,

the design of the post-installed shear connectors is complete, as it satisfies both strength and fatigue limit states.

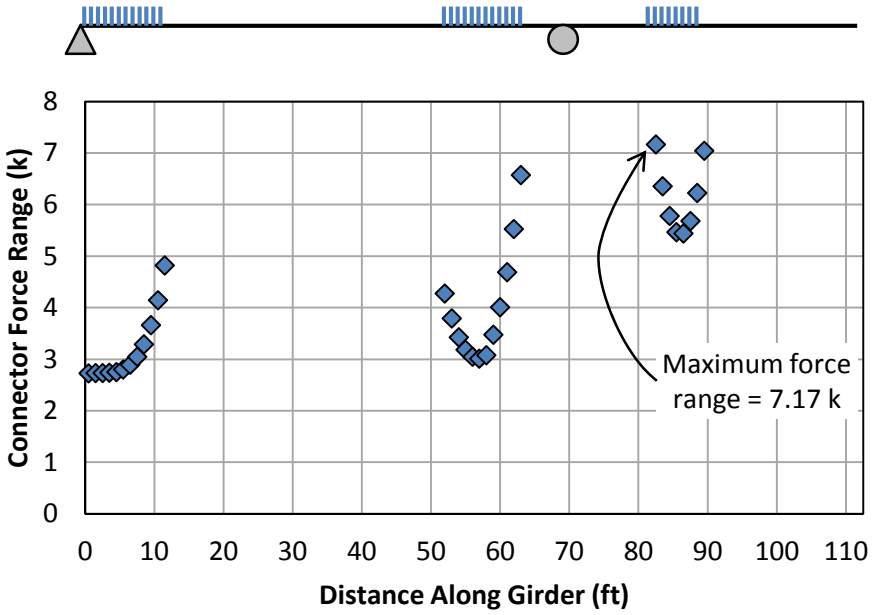

Figure B.8: Results from Fatigue Analysis with Modified Connector Layout – Outer Span Connector Group near Interior Support Shifted 3.5 Feet Towards that Support

Although it is not necessary for this example, more connectors can also be added to reduce the fatigue demands on each connector. It is important to note that additional connectors are most effective in reducing the demand when the connectors are in a balanced layout. Figure B.9 shows the results from the fatigue analysis with a connector layout that has been further modified to have 10 pairs of connectors in the groups in the middle span ($N_{PC} = 20$), rather than 8 pairs ($N_{PC} = 16$). To maintain the already balanced layout, one pair of connectors was added on either side of the group. This further reduces the maximum force range in that group to 6.50 kips.

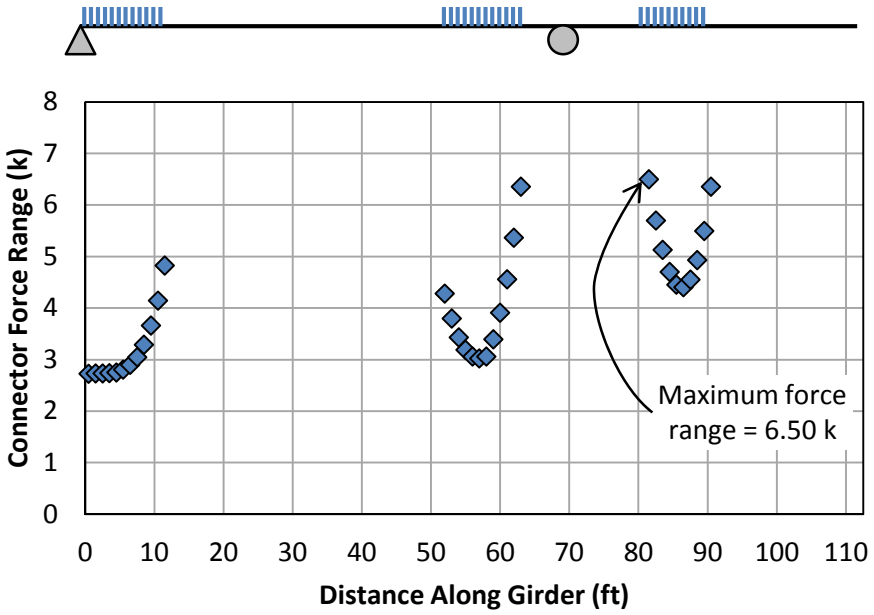

Figure B.9: Results from Fatigue Analysis with Further Modified Connector Layout – Added Two Pairs of Connectors to Groups in Middle Span

Summary of Design

The design procedure for strengthening an existing non-composite bridge with post-installed shear connectors and inelastic moment redistribution was illustrated for a sample three-span, four-girder bridge. For simplicity, the process was only shown for the interior girders. To complete the design, analysis should also be conducted for the exterior girders in the same manner. The existing and strengthened girders were analyzed primarily using the load factor design method from *AASHTO Standard Specifications for Highway Bridges*, but provisions from the *AASHTO LRFD Bridge Design Specifications* were used for moment redistribution and fatigue evaluation (AASHTO 2002, AASHTO 2010). For strength limit states, both the Overload and Maximum Load limit states were considered.

The interior girders of the existing bridge were found to have inventory load rating of HS 12.6, indicating that the load-carrying capacity is less than two-thirds of that of a new bridge designed using the load factor method with an HS 20 live load. A strengthening target of an HS 20 inventory load rating was chosen, which represents strengthening the bridge to meet current design standards for new bridges designed by the load factor method. Reaching this strengthening target corresponds to nearly a 60% increase in the load rating. Additionally, a remaining life of 20 years was targeted, over which an $(ADTT)_{SL}$ of 300 trucks per day was projected.

This target was achieved using a combination of inelastic moment redistribution to address strength deficiencies in the negative moment regions at the interior piers, and post-installed shear connectors to create composite action and increase the strength and stiffness of the positive moment regions near the middle of the spans. Redistribution of 13% of the elastic moment at the interior piers was required to satisfy the Maximum Load limit state. For the Overload limit state, no actual redistribution was necessary after removing the stress limits at the interior piers and allowing those sections to reach the effective plastic moment capacity. The

existing non-composite steel girder satisfies all of the prescribed provisions for moment redistribution except for the presence of bearing stiffeners at the interior piers. Thus, double-sided bearing stiffeners of at least 5 inches wide and 3/8 inches thick need to be added at the interior pier sections.

A total of 128 post-installed shear connectors must be installed on a single girder line in the layout shown in Figure B.10, which was slightly modified from that shown in Figure B.6 to improve the fatigue performance. This layout may need to be modified to account for field conditions and accessibility. If it is necessary to make significant changes to the layout or if fatigue behavior is of particular concern, additional connectors can be installed to ensure adequate fatigue strength. A rebar locator should be used to find the transverse deck reinforcing bars so that they can be avoided during connector installation.

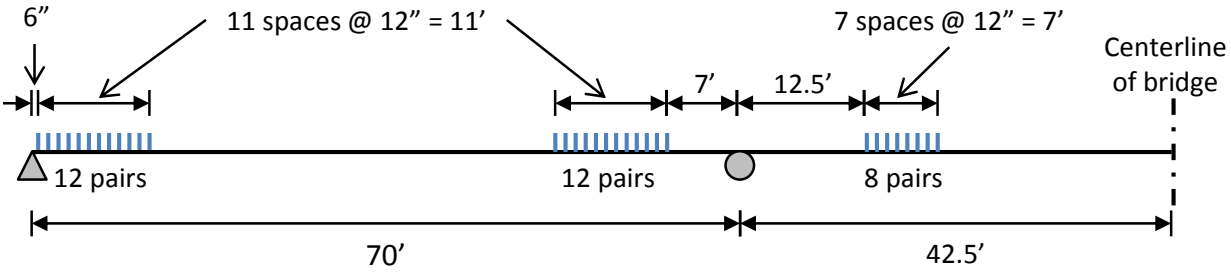

Figure B.10: Final Connector Layout

Figure B.11 shows the recommended positioning of the shear connectors in a cross section, abiding by the provisions for conventional welded studs in the AASHTO LRFD specifications.

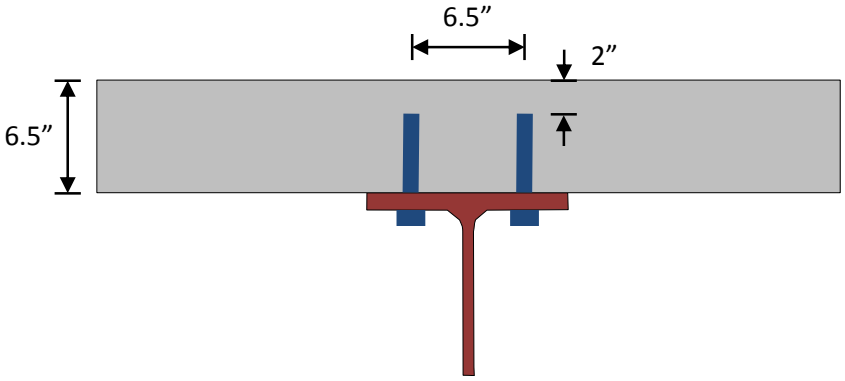

Figure B.11: Cross Sectional Connector Layout

Note that while the process shown here focused on the flexural strength of the girders and the fatigue behavior of the post-installed connectors, there are many other components and limit states that may ultimately control the strength and behavior of a bridge. These include but are not limited to the shear strength of the girders, the strength of the substructure, and the fatigue life of other critical details. When strengthening a bridge, all possible limit states should be considered in all components of the structure.